



ARISTOTLE UNIVERSITY OF THESSALONIKI
FACULTY OF ENGINEERING
SCHOOL OF ELECTRICAL & COMPUTER ENGINEERING

Design and Implementation of a Battery Management System for Lithium-Ion Batteries suitable for Automotive Applications

Diploma Thesis

Georgios Darikas

Supervisor: Dr. Christos Mademlis
Associate Professor at Aristotle University of Thessaloniki

Thessaloniki, May 2018



ΑΡΙΣΤΟΤΕΛΕΙΟ ΠΑΝΕΠΙΣΤΗΜΙΟ ΘΕΣΣΑΛΟΝΙΚΗΣ
ΠΟΛΥΤΕΧΝΙΚΗ ΣΧΟΛΗ
ΤΜΗΜΑ ΗΛΕΚΤΡΟΛΟΓΩΝ ΜΗΧΑΝΙΚΩΝ & ΜΗΧΑΝΙΚΩΝ Η/Υ

Σχεδιασμός και Υλοποίηση Συστήματος Διαχείρισης
Μπαταριών για Μπαταρίες Ιόντων Λιθίου Κατάλληλου για
Εφαρμογές Ηλεκτρικών Αυτοκινήτων

Διπλωματική Εργασία

Γεώργιος Δαρίκας

Επιβλέπων: Χρήστος Μαδεμλής
Αναπληρωτής Καθηγητής Α.Π.Θ

Θεσσαλονίκη, Μάιος 2018

To my father,

Acknowledgements

I would like to express my appreciation to my supervisor, Dr. Christos Mademlis for his guidance and support throughout this thesis project.

My coworkers at hofer eds GmbH deserve my gratitude for all their contribution and interest in the project. I would especially like to thank Mr. Juergen Kohn for believing in my abilities and allowing me to take on such an interesting and demanding task, as well as Mr. Matthias Buerchl for his advice and technical expertise.

I would also like to express my gratitude to Mr. Fotios Panteliadis, for introducing me to the people of hofer eds GmbH. Without his contribution this collaboration would not be possible.

My sincere gratitude also goes to the PhD candidates of the Electrical Machines Laboratory, for their continuous support and constructive criticism throughout the years. Mr. Nektarios Karakasis and Mr. Nikolaos Jabbour, who introduced me to embedded systems, and guided me through my first battery management system project. Mr. Evangelos Tsioumas, whose advice and support extended far beyond engineering, and helped me evolve to the person I am today.

Finally, I would like to take the opportunity to thank my family and friends for their love and support. I would not have been able to complete this work without their sustained encouragement.

George Darikas

Thessaloniki, May 2018

Abstract

The use of sustainable energy is becoming increasingly important in today's world. Therefore, electric vehicles are currently the best choice for the environment in terms of public and personal transportation. Because of its high energy and power density, lithium-ion batteries are widely used in electric and hybrid vehicles. Nevertheless, this battery technology can be dangerous if not operated within its safe operating range. Therefore, a control system, commonly referred as battery management system, must be used in every lithium-ion battery system, especially in those used in electric vehicle applications.

The scope of this thesis is the design and implementation of a battery management system for lithium-ion batteries, suitable for automotive applications. This includes the definition of the system requirements, the development of the system's architecture, the design of the hardware, taking into consideration the automotive industry standards, and the implementation of a sample test component of the system for the evaluation of its functionality.

The first two chapters cover a literature review, about battery technologies and their use in automotive applications. Chapter 3 describes in detail the purpose, functions and topologies of battery management systems. Then, in Chapter 4, the developed battery management system architecture is introduced along with its major features and advantages. The basic component of the system, the module management unit, is presented in detail, and its components and design solutions are elaborately explained. Chapter 5, provides a thorough description of the hardware design, including the schematics and PCB layout, while Chapter 6 presents the software architecture of the system. The experimental results of the testing hardware are depicted in Chapter 7. Finally, Chapter 8 concludes the thesis work, containing the conclusions from the experiments and possible future improvements for the system.

The project was carried out in collaboration with hofer eds GmbH. The overall design procedure was co-supervised by the people in hofer eds GmbH, which also funded the manufacturing and material costs of the test hardware. The testing process took place in the hofer eds GmbH facilities in Lenting, Germany, in the electronics laboratory, which was equipped with all the necessary equipment for the experiments. Aside from the equipment and funding, hofer eds GmbH provided valuable technical expertise and experience, which contributed significantly to the completion of the project.



Περίληψη

Η χρήση ανανεώσιμων και ενναλακτικών μορφών ενέργειας γίνεται ολοένα και πιο σημαντική στον σύγχρονο κόσμο. Επομένως, τα ηλεκτρικά οχήματα είναι προς το παρόν η καλύτερη επιλογή για το περιβάλλον τόσο για δημόσια όσο και για προσωπικά μέσα μεταφοράς. Λόγω της υψηλής πυκνότητας ενέργειας και ισχύος, οι μπαταρίες ιόντων λιθίου χρησιμοποιούνται ευρέως σε ηλεκτρικά και υβριδικά οχήματα. Παρόλα αυτά, η συγκεκριμένη τεχνολογία μπορεί να γίνει επικίνδυνη έαν δεν χρησιμοποιείται εντός της προδιαγεγραμένης περιοχής ασφαλούς λειτουργίας της. Επομένως, ενα σύστημα ελέγχου, το οποίο συνήθως αναφέρεται ως σύστημα διαχείρησης μπαταριών πρέπει να χρησιμοποιείται σε κάθε σύστημα μπαταριών ιόντων λιθίου, και ειδικότερα σε εκείνα που προορίζονται για εφαρμογές ηλεκτρικών οχημάτων.

Ο σκοπός της παρούσας εργασίας είναι ο σχεδιασμός και η υλοποίηση ενός συστήματος διαχείρησης μπαταριών για μπαταρίες ιόντων λιθίου, κατάλληλου για εφαρμογές αυτοκινήτων. Στα πλαίσια της εργασίας περιλαμβάνεται ο καθορισμός των απαιτήσεων του συστήματος, η ανάπτυξη της αρχιτεκτονικής του, ο σχεδιασμός του υλικού, λαμβάνοντας υπ'όψιν τις απαιτήσεις της αυτοκινητοβιομηχανίας, και η υλοποίηση ενός τμήματος του συνολικού συστήματος για την αξιολόγηση και επιβεβαίωση της λειτουργικότητας του.

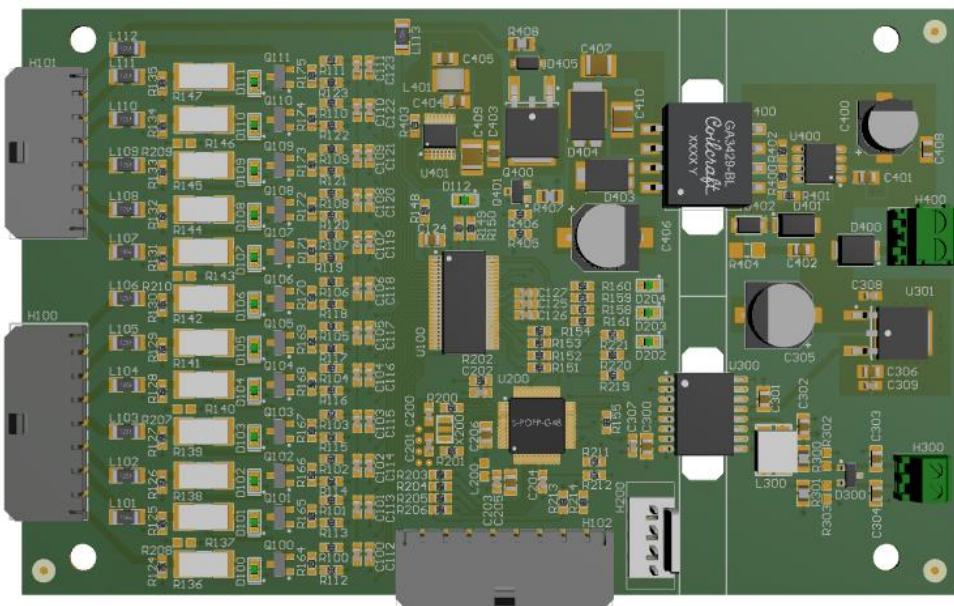
Το σύστημα αναπτύχθηκε με βάση την διανεμημένη αρχιτεκτονική, καθώς αυξάνει την ευελιξία του και διευκολύνει την υλοποίηση του. Πιο συγκεκρίμενα, η αρχιτεκτονική αυτή ορίζει δυο ξεχωριστές μονάδες, καθεμία από τις οποίες μπορεί να θεωρηθεί ως ξεχωριστό σύστημα, και διαμοιράζει τις λειτουργίες του σε αυτές. Η πρώτη είναι η μονάδα διαχείρησης μπαταριών, η οποία είναι η μονάδα ελέγχου του συστήματος, και έχει την δυνατότητα να λαμβάνει αποφάσεις που αφορούν τη λειτουργία του σύστηματος. Η δεύτερη είναι η μονάδα παρακολούθησης μπαταριών, η οποία είναι υπεύθυνη για την συλλογή δεδομένων από τα κελιά, όπως είναι η τάση τους και η θερμοκρασία τους. Οι δύο αυτές μονάδες συνδέονται μεταξύ τους μέσω διαύλου επικοινωνίας CAN, ο οποίος αποτελεί και την πιο διαδεδομένη επιλογή στα συστήματα αυτοκινήτων.

Στα πλαίσια της εργασίας, μελετήθηκε και σχεδιάστηκε λεπτομερώς η μονάδα παρακολούθησης μπαταριών, καθώς περιλαμβάνει όλες τις βασικές λειτουργίες που είναι απαραίτητες για την λειτουργία ενός συστήματος διαχείρησης μπαταριών. Η κάθε τέτοια μονάδα είναι ικανή να μετρά την τάση 12 κελιών μπαταριών ιόντων λιθίου, και την θερμοκρασία τους, μέσω 4 εισόδων για αισθητήρες θερμοκρασίας. Επίσης, στην μονάδα αυτή βρίσκεται ενσωματωμένο ένα κύκλωμα εξισσορόπησης των κελιών, βασισμένο στην “passive” τεχνική. Η επιλογή της τεχνικής αυτής έγινε λόγω της απλής της λειτουργίας, του χαμηλού της κόστους, και του μικρού αριθμού στοιχείων που απαιτεί. Το σύστημα δέχεται τροφοδόσια από εξωτερική πηγή, αλλά περιέχει την επιλογή τροφοδόσιας από τα κελιά τα οποία παρακολουθεί. Τέλος, η μονάδα διαθέτει γαλβανική απομόνωση, η οποία είναι απαραίτητη για την προστασία του συστήματος από σφάλματα που μπορεί να παρουσιαστούν στις μπαταρίες, που κατά κανόνα αποτελούν σύστημα υψηλής τάσης και ισχύος.

Στα αρχικά κεφάλαια της εργασίας, περιεχέται μια βιβλιογραφική αναφορά σχετικά με τις διάφορες τεχνολογίες μπαταριών και της χρήσης τους σε συστήματα αυτοκινήτων. Το κεφάλαιο 3, αναφέρεται με λεπτομέρεια στα συστήματα διαχείρησης μπαταριών, αναλύοντας το σκοπό τους, τις λειτουργίες και τις τοπολογίες τους. Στο κεφάλαιο 4 ξεκινά η παρούσιαση του συστήματος που αναπτύχθηκε στα πλαίσια αυτής της διπλωματικής εργασίας. Το κεφαλαίο

παρουσίαζει την αρχιτεκτονική τους συστήματος που επιλέχθηκε, και δίνει ιδιαίτερη έμφαση στο βασικό κομμάτι του, τη μονάδα διαχείρησης των κελιών. Η περιγραφή του υλικού γίνεται στο κεφάλαιο 5 ενώ η παρουσίαση του λογισμικού που αναπτύχθηκε για την λειτουργία του συστήματος περιέχεται στο κεφάλαιο 6. Τα πειραματικά αποτελέσματα που προέκυψαν από τις πειραματικές δοκιμές του συστήματος παρουσιάζονται στο κεφάλαιο 7. Η εργασία ολοκληρώνεται με το κεφάλαιο 8, στο οποίο εξάγονται τα συμπεράσματα από την ανάπτυξη και λειτουργία του συστήματος και γίνονται προτάσεις για περαιτέρω βελτίωση του στο μέλλον.

Η εργασία πραγματοποιήθηκε σε συνεργασία με την εταιρία hofer eds GmbH. Η συνολική διαδικάσια σχεδιασμού και ανάπτυξης του συστήματος έγινε υπό την επίβλεψη της εταιρίας, η οποία επίσης χορήγησε το κόστος των υλικών και της κατασκευής τους συστήματος. Τα πειράματα διεξήχθησαν στις εγκαταστάσεις της εταιρίας, στο Lenting της Γερμανίας, στο εργαστήριο ηλεκτρονικής, το οποίο διέθετε τον απαραίτητο εξοπλισμό για την διεξαγωγή των πειραμάτων. Πέρα από τον εξοπλισμό και την χρηματοδότηση, η hofer eds GmbH παρείχε σημαντική τεχνογνωσία και εμπειρία πάνω στο αντικείμενο, πράγμα που συνέβαλε σημαντικά στην ολοκλήρωση της εργασίας.



hofer
powertrain

Contents

Acknowledgements	i
Abstract	iii
Περίληψη.....	v
Contents	vii
List of Figures.....	xi
List of Tables.....	xiii
1 Battery Technology.....	1
1.1 Components of Cells and Batteries	1
1.2 Classification of Cells and Batteries.....	1
1.3 Cell Electrical Properties.....	2
1.4 Battery Terminology	3
1.5 Traditional Battery and Cell Chemistries.....	4
1.6 Types of Cell Construction.....	8
2 Batteries in Automotive Applications.....	10
2.1 Introduction.....	10
2.2 Classification of Various Hybrid Vehicles.....	10
2.3 Battery Technologies and Automotive Applications	12
2.4 Choice of a battery type for Electric Vehicles.....	14
2.5 Automotive Battery System Design.....	15
2.6 Battery Safety	16
2.6.1 Voltage Levels.....	17
2.6.2 Battery Management	17
2.6.3 Thermal Management.....	18
3 Battery Management Systems	19
3.1 Introduction.....	19
3.2 Functions of the Battery Management System.....	20
3.3 Architecture of the Battery Management System	21
3.4 Design of the Battery Management System	21
3.4.1 Module Management Unit.....	22
3.4.2 Battery Management Unit.....	30
3.5 Data Communication.....	32
3.5.1 CAN Communication	32

3.5.2	Data Communication Topologies	34
3.6	Battery Management Requirements.....	36
4	Battery Management System Concept	37
4.1	General Description.....	37
4.2	System Requirements.....	39
4.3	Block Diagram.....	41
4.4	Component Description	43
4.4.1	Battery Monitoring IC.....	43
4.4.2	Microcontroller.....	48
4.4.3	Isolated Flyback Converter	50
4.4.4	Step-Down Regulator	58
4.4.5	CAN Transceiver	63
4.4.6	Power Supply Switch	64
5	Hardware Description.....	67
5.1	Schematic Layout.....	67
5.1.1	Monitoring & Balancing Circuit	67
5.1.2	Microcontroller Circuitry	67
5.1.3	Power Management Circuitry	67
5.1.4	CAN-bus Circuitry	67
5.2	PCB Layout.....	68
5.2.1	PCB Technical Description	68
5.2.2	PCB Design Methodology	68
5.3	Circuit Board Presentation	69
6	Software Description.....	70
6.1	Function Summary.....	70
6.2	Software Architecture	70
6.2.1	Operation Modes	70
6.2.2	Scheduling	71
6.2.3	LTC6811 Firmware.....	72
6.2.4	uController Functionalities	76
7	Experimental Results.....	82
7.1	Hardware Testing	82
7.1.1	Isolated Flyback Converter	82

7.1.2	Step-Down Regulator	83
7.1.3	Power Supply Switch	84
7.2	Balancing Experiments	86
7.2.1	Experimental Setup	86
7.2.2	Commanded Balancing.....	88
7.2.3	Autonomous Balancing.....	90
8	Conclusions and Future Work	93
	References	94
	Appendix A Module Management Unit Schematics	97
	Appendix B Microcontroller Software.....	101

x

List of Figures

Figure 1.1 Lithium Ion Battery Cell Structure	6
Figure 1.2 Cell Types: Cylindrical, Prismatic, Pouch	9
Figure 2.1 Electric Vehicle Energy and Power Demand	11
Figure 2.2 Battery Technologies Specific Power - Energy Comparison	14
Figure 2.3 Automotive Battery System Example.....	16
Figure 3.1 Resistance Divider Measurement Scheme	22
Figure 3.2 Relay Switching Measurement Scheme	23
Figure 3.3 Forward - Flyback Converter Equalization Method.....	26
Figure 3.4 Shared Converter - Half Bridge Converter Equalization Method	27
Figure 3.5 Switching Capacitors Equalization Method.....	28
Figure 3.6 Energy Dissipative Equalization Method	29
Figure 3.7 Open Loop Hall Current Sensor	31
Figure 3.8 Closed Loop Hall Current Sensor	31
Figure 3.9 CAN-bus Structure	33
Figure 3.10 Electric Vehicle CAN network	34
Figure 3.11 Parallel Independent CAN modules	35
Figure 3.12 Parallel Modules with CAN gateway	35
Figure 3.13 Series Modules with CAN gateway.....	36
Figure 4.1 Battery Management System Proposed Architecture	37
Figure 4.2 Module Management Unit Block Diagram.....	42
Figure 4.3 Linear Technology LTC6811-2 Block Diagram	44
Figure 4.4 LTC6811-2 Operation State Diagram.....	45
Figure 4.5 LTC6811-2 Cell Balancing Circuit	47
Figure 4.6 LTC6811-2 External Temperature Probe Reading	48
Figure 4.7 ST Microelectronics STM8AF5288 Block Diagram.....	49
Figure 4.8 Linear Technology LT8302 Block Diagram.....	50
Figure 4.9 Flyback Converter Snubber Circuit	53
Figure 4.10 Isolated Flyback Converter Topology	56
Figure 4.11 Isolated Flyback Converter LTspice Simulation Model.....	57
Figure 4.12 Isolated Flyback Converter Simulation Results	57
Figure 4.13 Linear Technology LT3990 Block Diagram.....	58
Figure 4.14 Step-Down Regulator Topology.....	61
Figure 4.15 Step-Down Regulator LTspice Simulation Model	62
Figure 4.16 Step-Down Regulator Simulation Results - 1.....	62
Figure 4.17 Step-Down Regulator Simulation Results - 2.....	63
Figure 4.18 Analog Devices AD3054 Block Diagram.....	63
Figure 4.19 Load Switch Simplified Topology.....	64
Figure 4.20 P-channel MOSFET Load Switch Circuit.....	64
Figure 4.21 Power Supply Switch Circuit	65
Figure 4.22 Power Supply Switch Pspice Simulation Model	66
Figure 4.23 Power Supply Switch Simulation Results.....	66
Figure 5.1 Module Management Unit PCB Board	69
Figure 6.1 Software Scheduling	72

Figure 6.2 Serial Peripheral Interface (SPI) Configuration.....	73
Figure 6.3 Address Command Format.....	73
Figure 6.4 Write Command Format.....	73
Figure 6.5 Read Command Format.....	73
Figure 6.6 LTC6811-2 ADC Measurement Method	75
Figure 6.7 uController Software Flowchart	76
Figure 6.8 power_supply_monitor() Routine Flowchart.....	77
Figure 6.9 cell_monitoring() Routine Flowchart	78
Figure 6.10 cell_management() Routine Flowchart.....	79
Figure 6.11 Commanded Balancing Algorithm Flowchart.....	80
Figure 6.12 Autonomous Balancing Algorithm Flowchart	81
Figure 7.1 Isolated Flyback Converter Experimental Results	82
Figure 7.2 Step-Down Regulator Experimental Results - 1	83
Figure 7.3 Step-Down Regulator Experimental Results - 2	83
Figure 7.4 Power Supply Switch Experimental Results - 1	84
Figure 7.5 Power Supply Switch Experimental Results - 2	85
Figure 7.6 Power Supply Switch Experimental Results - 3	85
Figure 7.7 Power Supply Switch Updated Topology	86
Figure 7.8 Module Management Unit Experimental Setup - 1	87
Figure 7.9 Module Management Unit Experimental Setup - 2	87
Figure 7.10 ST Visual Studio Graphical User Interface (GUI).....	88
Figure 7.11 Commanded Balancing Experiment – Individual Cell Voltages.....	89
Figure 7.12 Commanded Balancing Experiment – Cell Voltages.....	90
Figure 7.13 Commanded Balancing Experiment – Board Temperature.....	90
Figure 7.14 Autonomous Balancing Algorithm - Individual Cell Voltages	91
Figure 7.15 Autonomous Balancing Algorithm - Cell Voltages.....	92
Figure 7.16 Autonomous Balancing Algorithm - Board Temperature.....	92

List of Tables

Table 1 Battery Technology Characteristics Comparison.....	7
Table 2 Energy Non-Dissipative Equalization Methods Comparison	28
Table 3 Energy Dissipative vs Non-Dissipative Equalization Methods Comparison.....	30
Table 4 LTC6811-2 ADC Mode Options Comparison.....	46
Table 5 ST Microelectronics STM8AF5288 General Characteristics.....	48
Table 6 LTC6811-2 Configuration Register Group	74

1 Battery Technology

1.1 Components of Cells and Batteries

An electric battery is a device consisting of one or more electrical cells with external connections provided to power up external devices. While the term “battery” is often used, the basic electrochemical unit being referred to is the “cell”. A battery consists of one or more of these cells, connected in series or parallel, or both, depending on the desired output voltage and capacity.

A battery cell consists of three major components:

1. The anode, or negative electrode which gives up electrons to the external circuit and is oxidized during the electrochemical reaction.
2. The cathode or positive electrode which accepts electrons from the external circuit and is reduced during the electrochemical reaction.
3. The electrolyte which provides the medium for transfer of charge, as ions, inside the cell between the anode and the cathode.

The most advantageous combinations of anode and cathode materials are that they will provide a high cell voltage and capacity. In practical systems, the anode is selected based on efficiency as a reducing agent, high coulombic output (Ah/g), conductivity, stability as well as ease of fabrication and low cost. Metals are mainly used as anode materials, with Zinc and Lithium being the most popular examples. On the other hand, the cathode must be an efficient oxidizing agent, have a useful working voltage and remain stable, when in contact with the electrolyte. Most of the common cathode materials are metallic oxides. As for the electrolyte, the needed properties are good ionic but not electric conductivity, nonreactivity with the electrode materials, little change in its properties over temperature and low cost. Most electrolytes are aqueous solutions, but there are important exceptions, as for example in thermal and lithium anode batteries [1].

Physically the anode and cathode electrodes are electronically isolated in the cell to prevent internal short-circuiting but are surrounded by the electrolyte. In practical cell designs a separator material is used to separate the anode and cathode electrodes mechanically, while the separator is permeable to the electrolyte in order to maintain the desired ionic conductivity. The cell itself can be built in many shapes and configurations – cylindrical, prismatic, pouch – and the cell components are designed specifically to accommodate the particular cell shape. The cells are sealed in a variety of ways to prevent leakage and dry-out [1].

1.2 Classification of Cells and Batteries

Electrochemical cells and batteries are identified as primary (non-rechargeable) or secondary (rechargeable), depending on their capability of being electrically recharged. Within this classification, other classifications are used to identify particular structures or designs [1].

Primary Cells – Batteries - These batteries are not capable of being easily or effectively recharged electrically and, hence, are discharged once and discarded. The primary battery is a convenient,

usually inexpensive, lightweight source of packaged power with good shelf life, high energy density at low to moderate discharge rates [1].

Secondary Cells – Batteries - These batteries can be recharged electrically, after discharge, to their original condition by passing current through them in the opposite direction to that of the discharge current. The recharge process can be repeated for hundreds or thousands of times depending on the battery type and quality. They are storage devices for electric energy and are known also as “storage batteries” or “accumulators” [1].

The applications of secondary batteries fall into two main categories:

Those applications in which the secondary battery is used as an energy-storage device, being electrically connected to and charged by a prime energy source and delivering its energy to the load on demand. Examples are automotive and aerospace systems, standby (UPS) power sources and hybrid electric vehicles [1].

Those applications in which the secondary battery is used or discharged essentially as primary battery but recharged after use rather being discarded. Secondary batteries are used in this manner in portable consumer electronics, power tools and electric vehicles.

Secondary batteries are characterized by high power density, high discharge rate and flat discharge curves, while their energy densities are generally lower than those of primary batteries.

1.3 Cell Electrical Properties

Some terms which are essential to express the electrical characteristics of batteries, are presented in the following section.

Voltage: The standard potential of the cell is determined by the type of active materials contained in the cell. The standard potential can be calculated from the standard electrode potentials as follows:

$$\text{anode(oxidation potential)} + \text{cathode(reduction potential)} = \text{standard cell potential}$$

Capacity: The capacity of a cell is determined by the amount of active materials in the cell. It is expressed as the total quantity of electricity involved in the electrochemical reaction and is defined in terms of coulombs or ampere-hours.

Energy: The capacity of a cell can also be considered on an energy (watthour) basis by taking both the voltage and the quantity of electricity into consideration. This theoretical energy value is the maximum value that can be delivered by a specific electrochemical system.

Energy Density (Wh/kg): The nominal battery energy per unit mass, sometimes referred to as the gravimetric energy density. Specific energy is a characteristic of the battery chemistry and packaging.

Specific Power – Power Density (W/kg): The maximum available power per unit mass. Specific power is a characteristic of the battery chemistry and packaging. It determines the battery weight required to achieve a given performance target.

In summary, the maximum energy that can be delivered by an electrochemical system is based on the types of active materials that are used (this determines the voltage) and on the

amount of the active materials that are used (this determines ampere-hour capacity). In practice, only a fraction of the theoretical energy of the battery is realized. This is due to the need for electrolyte and nonreactive components (containers, separators, electrodes) that add to the weight and volume of the battery. Another contributing factor is that the battery does not discharge at the theoretical voltage (thus lowering the average voltage), nor is it discharged completely to zero volts (thus reducing the delivered ampere-hours). All these factors reduce significantly the specific energy. Experimental data has shown that the actual energy that is available from a battery under practical, but close to optimum, discharge conditions is only about 25 to 35 percent of the theoretical energy of the active materials [1].

1.4 Battery Terminology

Some terms are essential to understanding the performance and characteristics of batteries and are explained in the following paragraphs.

Battery Condition - This section describes some of the variables used to describe the present condition of a battery [2].

1. **Open-Circuit Voltage:** This refers to the voltage between the positive and the negative electrodes when there is no load on the battery. The open-circuit voltage depends on the battery state of charge, increasing with state of charge.
2. **Working Voltage:** This is also called terminal or closed-circuit voltage and refers to the voltage between the positive and the negative electrodes when there is a load connected on the battery. Working voltage varies with SOC and discharge/charge current.
3. **Discharge Rate (C-rate):** In describing batteries, discharge current is often expressed as a C-rate in order to normalize against battery capacity, which is often very different between batteries. A C-rate is a measure of the rate at which a battery is discharged relative to its maximum capacity. A 1C rate means that the discharge current will discharge the entire battery in 1 hour. The discharge rate can be used to evaluate the power output ability.
4. **Depth of Discharge (DOD):** This refers to the percentage of battery capacity that has been discharged expressed as a percentage of maximum capacity. A discharge of at least 80% DOD is referred to as a deep discharge.
5. **State of Charge (SoC):** An expression of the present battery capacity as a percentage of maximum capacity. SOC is generally calculated using current integration to determine the change in battery capacity over time.
6. **State of Health (SoH):** In general, SOH refers to the current state of health of the battery as compared to its beginning of life measurement. In other words, SOH is intended to indicate how long the battery will take to reach its end of life. In essence, it is a measure of internal resistance, capacity, voltage, self-discharge, the battery's ability to accept charge and the total number of charge-discharge cycles that the battery has completed at that point in time.
7. **Internal Resistance:** This is the total resistance of a battery between its two electrodes, including the resistance from current collectors, electrode and active materials, separators, and electrolytes. Usually, the smaller the internal resistance, the better the performance that will be achieved. It is also dependent on the state of charge/discharge

- of a battery. When the internal resistance increases, the battery efficiency decreases, and thermal stability is reduced, as more of the charging energy is converted into heat.
8. **Self-discharge:** This is a phenomenon in a battery in which internal chemical side reactions reduce the stored capacity of the battery without any connection between the electrodes. Self-discharge decreases the shelf life of batteries and causes them to initially have less than a full charge when actually put to use.

Battery Technical Specifications - This section explains the specifications you may see on battery technical specification sheets, and are used to describe battery cells, modules, and packs [2].

1. **Nominal Voltage:** This refers to the average voltage during the total discharge process of a battery at the rate of 0.2C. Also thought as the reported – “normal” - voltage of the battery.
2. **Cut-off Voltage:** This is the final voltage between two electrodes of a battery reached during a charge or discharge process. This is the minimum allowable voltage, and it generally defines the “empty” state of the battery.
3. **Discharge Curve:** This refers to the change of voltage with time during a discharge process.
4. **Nominal Capacity (Ah for a specific C-rate):** This refers to the total capacity available when the battery is discharged at a certain discharge current, specified as a C-rate (e.g. 0.2 C). Capacity is calculated by multiplying the discharge current (in Amps) by the discharge time (in hours) and decreases with increasing C-rate.
5. **Nominal Energy (Wh for a specific C-rate):** This refers to the “energy capacity” of the battery, the total energy available when the battery is discharged at a certain discharge current specified as a C-rate (e.g. 0.2 C). Energy is calculated by multiplying the discharge power (in Watts) by the discharge time (in hours). Like capacity, energy decreases with increasing C-rate.
6. **Cycle Life:** This is the number of times that a rechargeable battery can be cycled (charged and discharged) before it loses its ability to accept charge. Cycle life is estimated for specific charge and discharge conditions. It is dependent on battery type, chemical composition, depth of discharge, cell design and it is affected by other conditions such as temperature and humidity.
7. **Maximum Continuous Discharge Current:** The maximum current at which the battery can be discharged continuously. This limit is usually defined by the battery manufacturer in order to prevent excessive discharge rates that would damage the battery or reduce its capacity.

1.5 Traditional Battery and Cell Chemistries

There is a wide range of different cell chemistries that offer different voltages, power and energy performances. Lithium-ion cells have considerably greater energy density than previous chemistries, making them particularly suitable for automotive applications. They are also considered safer, less toxic and are more energy efficient with significantly longer cycle life. Some of the most popular chemistries are presented in the following section.

Lead-Acid (Pb) - Lead-acid batteries are composed of a Lead-dioxide cathode, a sponge metallic Lead anode and a Sulphuric acid solution electrolyte. This heavy metal element makes them toxic and improper disposal can be hazardous to the environment. The typical cell voltage is 2 Volts.

Lead acid is a popular low-cost secondary battery, available in large quantities and in a variety of sizes and designs, has good high-rate performance, moderately good low and high temperature performance, easy state of charge indication and good charge retention for intermittent charge applications. Cell components are easily recycled. Because of the irreversible physical changes in the electrodes, failure occurs between several hundred and 2,000 cycles. The main drawbacks of these batteries are their comparatively low energy density, long charging time and the need for careful maintenance [3].

It is widely used in battery power for energy storage, emergency power, earlier generations of electric and hybrid vehicles and for engine starting, vehicle lighting, and engine ignition (SLI). It still dominates the stop-start battery and e-bike battery market. With continuous improvement and the development of the advanced Lead acid battery, it will remain competitive.

Nickel Cadmium (NiCd) - These cells use nickel hydroxide Ni(OH)_2 for the cathode, cadmium Cd as the anode and an alkaline potassium hydroxide for the electrolyte. Standard Ni-Cd cells use an aqueous chemical impregnation process for the fabrication of the electrodes. It has been used for storing electrical energy in spacecraft since the beginning of space exploration. It has a long cycle life, good low-temperature and high-rate performance capability, long shelf life in any state of charge and rapid recharge capability. Memory effect is one of its biggest drawbacks, as is a fairly high rate of self-discharge at high temperature. As cadmium is highly toxic, its use in batteries is now banned, with the exception of medical and some military applications [3].

Nickel Metal Hydride (NiMH) - These cells use nickel hydroxide Ni(OH)_2 for the cathode. Hydrogen is used as an active element in a hydrogen-absorbing anode. This electrode is made from a metal hydride, usually alloys of lanthanum and rare earths that serve as a solid source of reduced hydrogen that can be oxidized to form protons. The electrolyte is alkaline, usually potassium hydroxide.

Nickel Metal Hydride cells have higher energy density than nickel-cadmium cells, rapid recharge capability, long cycle life and long shelf life in any state of charge. There are minimal environmental problems. However, its high-rate performance is less than that of nickel-cadmium. The poor charge retention, memory effect and higher cost anodes are the drawbacks. It has been used in computers, cellular phones and other consumer electronic applications, with the possible exceptions of high-drain power tools and applications where low battery cost is the major consideration. It was the main choice for hybrid electric vehicles. However, lithium-ion batteries are gradually taking the market [3].

Lithium-Ion - Lithium is attractive due to its low equivalent weight and high standard potential and has been used in rechargeable batteries to provide over three times the energy density of traditional rechargeable batteries. The field has seen significant advances in solid state chemistry in effort to improve performance further. This includes a drive for increased energy density, rate capability and the ability to provide high power, as well as long cycle life and thermal stability for increased safety. Attention has also focused on fast charge capability as well as cost reduction, through the use of inexpensive raw materials synthetic processes and using materials of low toxicity and environmental banality [3].

Research and development has focused on many aspects of cell chemistry to improve overall performance. However, large attention has been placed on positive cathode materials development as it has a large role to play in determining overall specific energy density. Depending on the electrolyte material choice, lithium-ion batteries can be separated into two categories, the liquid lithium-ion cells, which use liquid electrolytes, and the solid-state lithium-ion cells, which use inorganic or polymer electrolytes.

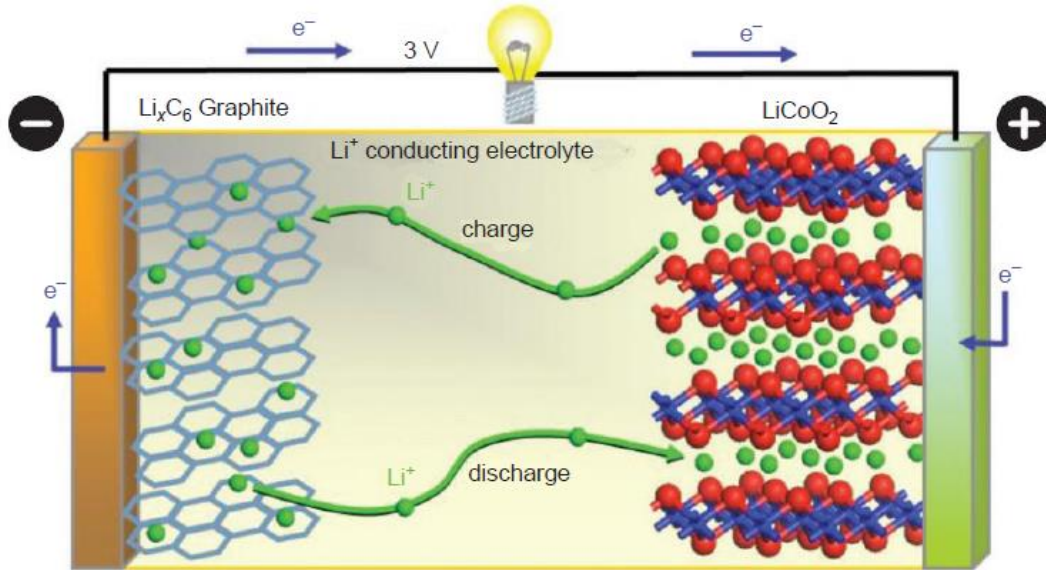


Figure 1.1 Lithium Ion Battery Cell Structure

There is a variety of lithium-ion cell chemistry each with unique features and properties.

Lithium Cobalt Oxide (LCO) - Lithium Cobalt Oxide has been the most widely used positive electrode material in lithium batteries for many years, being used for laptop, mobile phone and tablet batteries. LCO cells provide moderate cycle life (<500 cycles) and energy density. However, the chemistry is less thermally stable than other transition metal oxide or phosphate chemistries under extreme abuse conditions such as cell puncture or short circuit making them more susceptible to thermal runaway conditions [3]. These characteristics limit the use in Electric and Hybrid Vehicles.

Lithium Cobalt Aluminum Oxide (NCA) - Lithium Nickel Cobalt Aluminum Oxide offers high specific energy density and reasonably good power capabilities. NCA cells are considered somewhat safer than LiCoO_2 . NCA cells tend to have superior life characteristic to LCO and is more commonly available in some 18650 type cells than in large format automotive cells [3].

Lithium Iron Phosphate (LFP) - Phosphate-based technology lithium ion materials possess improved thermal and chemical stability than oxides and are generally perceived to be a safer cell chemistry than other Lithium-ion technologies and less susceptible to thermal runaway under abuse conditions. Automotive lithium ion cells are also durable and stable to long term cycling. Although Lithium iron phosphate batteries have lower energy density than Oxide systems they are typically able to support higher currents and thus suited to high power and longer life

applications. They are a significant improvement over lithium cobalt oxide cells in terms of cost, safety and toxicity [3].

Lithium Manganese Oxide Spinel (LMO) - Lithium Manganese Oxide Spinel provides a higher cell voltage than Cobalt-based chemistries and thermally is more stable. However, the energy density is typically 20% less. Manganese, unlike Cobalt, is a safe and more environmentally benign cathode material due to its low toxicity. Other benefits include lower cost and higher rate capability. However, they suffer from lower overall capacities as a result of their spinel structure and are unstable at higher temperatures in lithium-based electrolyte [3].

Lithium Nickel Cobalt Manganese Oxide (NCM) - Although no single cell chemistry currently ticks all the boxes of energy, power, cost, safety and life, the mixed metal oxide systems and in particular those based on NCM type chemistry can be optimized to give high specific energy and/or high specific power whilst being considered safer and more cost effective than LCO and LFP but with reasonable life expectation [3].

Lithium Titanate Oxide (LTO) - These cells replace the graphite negative electrode with lithium titanate. This negative electrode material is compatible with any of the above positive electrode materials but is commonly used in conjunction with Manganese-based materials. They offer superior rate capability and power combined with wide operating temperature range. They are considered a safer alternative to the graphite material due to higher potential vs Li/Li⁺ than conventional graphite and therefore have a degree of inbuilt overcharge protection. However, lithium titanate batteries tend to have a slightly lower energy density than graphite-based systems [3].

Application	Units	Lead-Acid	NiCd	NiMH	Li-Ion
Cell Voltage	Volts	2	1.2	1.2	2.4 – 3.8
Specific Energy	Wh/kg	30 – 40	35 – 80	55 – 110	100 – 300
Energy Density	Wh/l	50 – 90	50 – 70	160 – 420	125 – 600+
Power Density	W/kg	100 – 200	100 – 150	100 – 500	500 – 5000
Maximum Discharge	Rate	6 – 10C	20C	15C	80C
Useful Capacity	DOD %	50	50	50 – 80	>80
Charge Efficiency	%	60 – 80	60 – 80	70 – 90	>95
Self – Discharge	%/Month	3 – 4	15 – 20	15 – 30	2 – 3
Temperature Range	°C	-40 to 60	-20 to 70	-20 to 65	-30 to 70
Cycle Life	No. of Cycles	200 – 400	300 – 1000	500 – 1000	>2000
Memory Effect		No	Yes	Yes(<NiCd)	No
Robustness (Over/Under Voltage)		Yes	Yes	Yes	Needs BMS

Table 1 Battery Technology Characteristics Comparison [3]

Compared with the original state of lithium-ion batteries in the early 1990s, their performance has been improved significantly. Currently they have the following dominant advantages over other traditional rechargeable batteries [2]:

- High energy density: Specific energy density per volume and mass for a lithium-ion battery can be up to 500Wh/l and 230Wh/kg, respectively, which are continuously increasing with more research and development.
- High average output voltage (~3.6V): This is three times of that for the Ni-Cd or Ni-MH rechargeable batteries.
- High output power: This can be up to 2000W/kg for a short time.
- Low self – discharge: This is less than 3% per month, which is less than half the rate of Ni-Cd and Ni-MH batteries.
- No memory effect: This differs from that of Ni-Cd and Ni-MH batteries, and leads to good cycling performance for lithium-ion batteries.
- Fast charging and discharging: Capacity can be up to 80% of its nominal capacity at the rate of 1C.
- Wide operating temperature range (from -25°C to +50°C): Current research is aimed at widening this range to -40°C to +70°C with improvements of electrolytes and electrode materials.
- Easy testing for the residual capacity since the discharge curve is not a completely horizontal plateau.
- Maintenance-free since side reactions are minimal compared to rechargeable batteries using aqueous electrolytes.
- Long cycling life: More than 1000 times can be achieved. More than 5000 times can be achieved of a shallow depth of charge and discharge is carried out.

It should be admitted that the current lithium-ion batteries also have some shortcomings, such as the following [2]:

- High cost: Mainly because of the high cost of the LiCoO₂ positive electrode material. Along with continuously developing positive electrode material technology, Li[Ni_xCo_yMn_{1-x-y}]O₂, LiFePO₄, and LiMn₂O₄ can be used as the positive electrode material to greatly reduce their cost.
- There must be special protection circuitry to avoid overcharging.
- Poor compatibility with ordinary rechargeable batteries: Only in the cases that need three ordinary batteries (about 3.6V), can lithium-ion batteries be used to replace them.

However, compared with its dominant advantages, these shortcomings are not a major problem, especially when they are used in some high-tech and high-value-added products. Therefore, lithium-ion batteries are considered a dominant technology, and will continue to have a very wide range of applications in the foreseeable future [2].

1.6 Types of Cell Construction

The energy storage materials and the overall cell chemistry has a large role to play in determining the overall cell performance. However, Lithium-Ion cells are available in a range of form factors where the cell engineering also has a role to play in influencing overall cell and therefore battery performance in the end application. The energy storage cells need engineered supports and retention systems to connect and retain them in the battery pack structure.

- **Cylindrical** - The most commoditized form of lithium ion cell is that of the small cylindrical cell type. The most common variant being the 18650 format, so called due to being 18mm in diameter and 65mm long, being the most mature and used in many forms of consumer applications including laptops, power tools and E-Bikes. A wide range of 18650s are available, optimized for power and/or energy against the target applications. The cells may contain internal safety features such as over-temperature and pressure cut off features [3].
- **Prismatic** - Aluminum or steel cans are typically used as housing of prismatic lithium-ion cells. The metal case ensures structural stability, mechanical robustness and humidity protection. In addition, it allows the use of safety features such as pressure relief vents, which are not possible to be used in pouch cells. In some cases, prismatic cells may allow packaging to be more efficient than cylindrical cells because of their form factor [3].
- **Pouch** - Pouch cells are cells where the internal electrode stack is contained within a soft plastic-aluminum package. Current collectors are welded internally to terminal tabs that protrude through seals to allow external connection [3].

The minimizing of cell packaging material makes pouch cells attractive over metal body prismatic cells but to potentially higher energy density for the same chemistry type but will typically require complex module structure in order to constrain and retain the cells in the pack structure. The large surface area may be beneficial for thermal management [3].

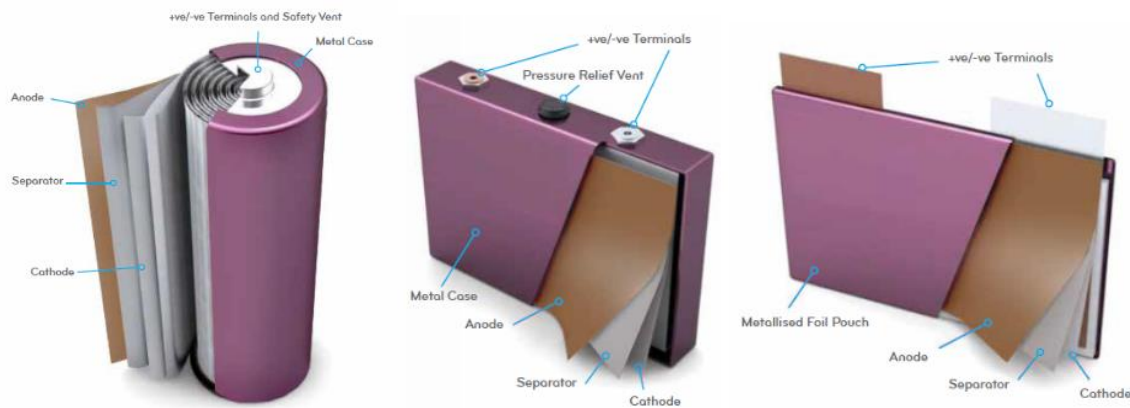


Figure 1.2 Cell Types: Cylindrical, Prismatic, Pouch

2 Batteries in Automotive Applications

2.1 Introduction

Modern electrified-vehicle concepts have a wide range of propulsion technologies. Micro-hybrid vehicle with a stop-start function and regenerative braking are in series production now. Further steps are mild or full-hybrid vehicles, powered with a conventional combustion engine with further additional electrification. These cars are not made for driving purely on electricity beyond some hundreds of meters, but they enable the shift of the energy operation close to the maximum-efficiency region. Full-electric vehicles without combustion engines are presented on the market or under development for the start of production in the coming months and years. A standard starting, lighting and ignition (SLI) battery is a part of all cars, either for cranking the combustion engine in conventional and micro-hybrid vehicles, or for supplying the 12V power supply system. The SLI battery typically is a lead-acid battery but concepts with lithium-ion batteries are also under development. The majority of the hybrid electric vehicles on the market today use nickel-metal hydride batteries, but it is expected that lithium-ion batteries will overtake this market segment in the following years. Full-electric vehicles use mainly lithium-ion batteries [4] [5].

A battery for electrified vehicles is always a compromise between a high-power performance, a high energy storage capability, a low weight, a small volume, a long lifetime and a low price. New propulsion concepts require improved battery systems. For each propulsion type a suitable battery system is needed. Despite the discussion on technical performance indicators, the price of the battery is the main challenge for market introduction. Batteries will be the most expensive part in full-electric vehicles. It is therefore essential for bringing electric cars to the market to select appropriate battery technologies, to size the battery optimally to the application needs and to design optimal batteries with the highest reliability, lifetime and safety [4] [5].

2.2 Classification of Various Hybrid Vehicles

Selection and sizing of a battery system depend on the requirements of the respective vehicles. The term 'hybrid vehicle' describes a wide range of vehicle concepts. In the following, various vehicle concepts are classified.

The used state-of-charge (SOC) region is specific to each vehicle concept. Related to this, a suitable battery type or a combination is chosen. This is of relevance because the number of cycles and the cycle depth are of the highest relevance to the battery lifetime. The number of achievable cycles increases strongly with decreasing depth of discharge. For several batteries, the SOC during operation is of relevance as well. Figure 2.1 compares all types of electrified vehicles with respect to the energy and power demand.

Micro-Hybrid Electric Vehicles - The first step of hybridization is a micro-hybrid vehicle. Vehicles with a conventional combustion engine are equipped with options for reducing CO₂ emissions. The stop-start function which has been available on the market for several years is widely known. The combustion engine is switched off during standing when the engine is in the idle state. During engine-off, the battery takes over all electric requirements. In most concepts the engine starts again when the driver presses the clutch. A further function is regenerative braking. In conventional cars, braking energy is lost by heat, while micro-hybrid vehicles use a part of this

energy for charging the battery (recuperation) via the existing reverse-operated power generator. Some researchers do not count micro-hybrid as hybrid vehicles because they do not support the engine. However, micro-hybrid vehicles extend the traditional functionality of the power system in vehicles significantly and they allow an accountable increase in fuel economy [4].

The challenge for the battery is a largely increased number of cranking events and a higher number of full cycle equivalents (due to the extra use of electrical power during stops). Regenerative braking can save fuel only when the dynamic charge acceptance is high, which is a challenge, especially for lead-acid batteries. Charge acceptance strongly depends on the SOC (which is better at low values) and the temperature (which is better at higher values). Furthermore, the battery needs to be capable of partial SOC operation.

Micro-hybrid vehicles are state of the art for many vehicle manufacturers. The batteries are sized to deliver appropriate cranking power but also to deliver sufficient energy, e.g. during long time parking for the remaining power consumption of various control units in the car (e.g. the alarm, wireless door opening and radio).

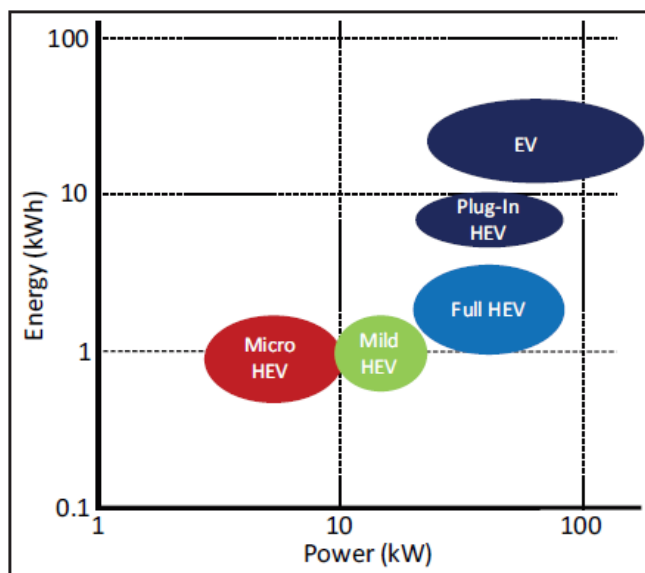


Figure 2.1 Electric Vehicle Energy and Power Demand [4]

Mild-hybrid electric vehicles - Mild-hybrid vehicles offer the same functions as micro-hybrid vehicles. In addition, they provide boosting as an extra function which is the electric motor assist for the drivetrain, especially during acceleration. As in micro-hybrid vehicles, the battery is charged only during driving. This can occur either when the vehicle's speed is reduced (regenerative braking) by the generator or when recharge energy is provided actively by the combustion engine. For the battery this is a high-power application. The battery is sized in such a way that it meets the power requirements appropriately [4].

Full-hybrid electric vehicles - Full-hybrid vehicles cover all functions of mild-hybrid vehicles. In addition, pure electric driving is possible as well as higher power assist during acceleration and regenerative braking. The battery system is used when a high power is needed or the efficiency of the combustion engine is low. In full-hybrid vehicles the battery is recharged only during driving by the internal-combustion engine or during regenerative braking. Therefore, the pure electric

driving range is very limited (typically below 1km). However, it is an interesting option for silent cruising in residential areas [4].

Plug-in Hybrid electric vehicles - Plug-in hybrid electric vehicles combine the characteristics of both a full-electric vehicle and a conventional vehicle with an internal combustion engine. For plug-in hybrid electric vehicles, charging is carried out during standing times when the car is plugged into the grid. Therefore, the pure electric driving range is higher than with full-hybrid vehicles. When the battery is at an SOC level of approximately 20%, the ICE works as the power source. From this point onwards, the car mainly behaves like a full-hybrid vehicle.

Generally, two different concepts can be realized to integrate the internal combustion engine (ICE). The parallel drivetrain design allows the ICE to transfer mechanical power via the gearbox directly to the wheels, and in addition it can recharge the battery to maintain the low SOC level. This is the concept used by full-hybrid vehicles as well. A variation of the parallel drivetrain is the power-split drivetrain (also called series-parallel hybrid drivetrain). The ICE and two electrical engines (one for powering and one for recuperation) are connected directly to the axle by a planetary gear set. From the battery's point of view, it does not make any difference whether a parallel or a power-split drivetrain is used. In series drivetrains the ICE is used only for powering the generator which is delivering electric power to the electric machine and for charging battery. The used SOC range of the battery is larger in a series drivetrain than in a parallel drivetrain [4].

Complete equipment with an ICE, an electric motor and a traction battery system, with each of the components designed to be able to drive the car alone, causes higher weight and rising costs. However, plug-in hybrid vehicles are operated with significantly smaller batteries than full-electric vehicles while at the same time having a maximum driving range due to the ICE.

Electric Vehicles - Electric vehicles are solely electrically driven and operate completely without an internal combustion engine. Brake energy recovery is installed as well.

The possible driving range of electric vehicles is lower than that of vehicles with conventional combustion engines. Larger driving ranges would require a larger battery but, since the costs and the weight would increase as well, equipping electric vehicles with larger batteries does not make sense economically. The need for machine maintenance is expected to be less for electric vehicles as the electric motor works almost without attrition. Thus, the traction battery system constitutes the main cost factor. However, even with slightly higher initial costs, electric vehicles can compete on the market with lower maintenance and lower fuel costs [4].

2.3 Battery Technologies and Automotive Applications

An overview on battery technologies and application for electric vehicles are presented in the following.

Lead-acid - Lead-acid batteries are by far the cheapest energy storage technology with regard to the raw material costs. Because of the low energy density, lead-acid batteries are the choice when operating distance and weight are less important. This is the case for micro-hybrid vehicles. The main drawbacks of this technology are the low energy density, the lifetime and the dynamic charge acceptance, e.g. during regenerative braking. The advantages are the low material costs, intrinsic safety and high recycling quotes [4] [5].

Today, in every car with a high voltage battery pack (e.g. electric vehicle) there is still a small lead-acid battery installed as well, e.g. for security reasons, as an SLI battery and to serve the 12V power system. In case of an accident, the high-voltage battery is disconnected from the electric system and the lead-acid battery provides the necessary power for the emergency systems.

Nickel-cadmium battery - Nickel-cadmium batteries show a slightly higher energy density than lead-acid batteries do and a significantly higher power density, but the specific battery costs are much higher. This battery type is technically mature and the possibility of using nickel-cadmium batteries in electric vehicles is similar to that of employing lead-acid batteries. However, it is not expected that nickel-cadmium batteries will play a major role in the future electrification of vehicles considering the energy density and costs [4] [5].

Nickel-metal hydride battery - Nickel-metal hydride batteries are a further development of nickel-cadmium batteries, with almost identical cell voltages, discharge and charge curves. However, nickel-metal hydride batteries achieve approximately double the energy density than nickel-cadmium batteries do, but it is especially the high-power density (greater than 1000 W/kg) and the sufficient lifetime that qualify the technology as the world market leader in hybrid electric vehicles.

Nickel-metal hydride batteries is a proven and mature technology for several years. However, at present, only a few experts expect to see this battery technology in full-electric vehicles or plug-in hybrid electric vehicles in large quantities owing to their high material costs. Nickel-metal hydride batteries do not seem to be competitive with lithium-ion batteries in the long term [4].

Lithium-ion batteries - “Lithium-ion batteries” is a general term for a variety of metal combinations used to form batteries. Their characteristics regarding the power, lifetime, low- and high- temperature performances and safety are very dependent on the material combination. This technology achieves the highest energy and power densities of all commercially available rechargeable batteries.

Today's material combinations for lithium-ion batteries do not offer a mechanism for overcharging that could take in current during overcharge without damaging the battery. Consequently, the energy efficiency is also very high compared with the other battery technologies. However, because of the missing internal overcharge process, lithium-ion battery cells must each be supervised individually to avoid overcharging of any cell as this would finally lead to the destruction of the cell. Another advantage of lithium-ion batteries is the high-capacity utilization even at high current rates. This is why lithium-ion batteries are especially suitable for applications with high currents, e.g. electric vehicles [4].

The availability of lithium, when the number of electric vehicles increases, is under controversial discussion. However, according to the current state of knowledge, there is sufficient lithium available to equip all vehicles in the world with large lithium-ion batteries.

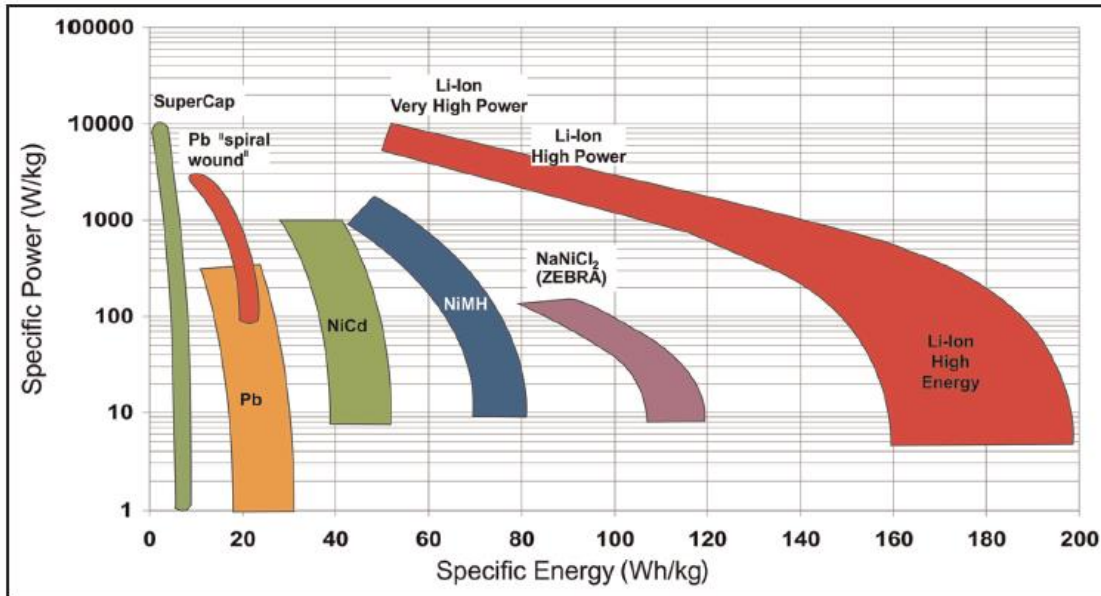


Figure 2.2 Battery Technologies Specific Power - Energy Comparison [4]

2.4 Choice of a battery type for Electric Vehicles

Li-ion batteries are capable of storing up to three times more energy per unit weight and volume than the conventional lead-acid and NiMH batteries. This is approximately three-times voltage level of 3.5V. Because of the high-energy characteristics, Li-ion batteries find widespread applications including aerospace, EV, and hybrid EV designs. However, the scaling of the consumer Li-ion cells is necessary.

While evaluating battery suitability for unique applications, it is important to understand a variety of battery characteristics, including the energy/power relationship, battery and cell impedance as a function of temperature, pulse discharge capability as a function of both temperature and load, and battery charge/discharge characteristics.

The self-discharge rate of the Li-ion battery is fairly low, <5% the capacity per month, compared to the 15% for the lead acid battery and 25% for NiMH battery. There is no memory effect in the solid-state Li-ion battery as is the case in the NiMH and lead-acid battery. The battery cycle life is superior to the NiMH and lead-acid batteries. In case of the NiMH battery, the cycle life typically drops to 80% of the rated capacity after 500 cycles at the 1C-rate. Li-ion batteries can achieve more than 1200 cycles before reaching 80% of their rated capacity. Li-ion batteries are efficient at charge-discharge rates other than the 1C-rate. In addition, the liquid Li-ion batteries are not suited for use in EVs owing to safety reasons while the solid-state batteries are well suited for high-rate applications. Solid-state Li-ion batteries allow for the development of virtually any size batteries. In addition, the batteries can be stacked into efficient multicell configurations. From a cost perspective, the solid-state Li-ion battery uses a relatively inexpensive metal oxide that is fabricated in sheet form to allow inexpensive battery production. Thus, in comparison, solid Li-ion batteries will be easily mass produced at less than a \$1 per Whr. The NiMH battery, after years of improvements, is being produced at approximately the same cost [4] [6].

A large number of characteristic of the Li-ion battery are favorable for electric and hybrid-electric vehicle applications. These include:

- High gravimetric and volumetric energy densities
- Ambient temperature operation
- Long life cycle
- Good pulse power density

Lithium-ion batteries is the most promising technology to be used in future hybrid-electric and full-electric vehicle applications, due to its many intrinsic advantages. These advantages make the lithium-ion batteries the most dominant candidate to fulfil the energy, power and efficiency requirements of the automotive field. Therefore, for the rest of this document, we will mainly talk about the Li-ion battery technology, when we refer to the battery or cells [4] [5].

2.5 Automotive Battery System Design

Automotive batteries are comprised of hundreds of individual elements, of which the electrochemical cells are the vital energy storage component. By performing detailed application analysis, it is possible to select the most appropriate cell chemistry and form factor to provide the most optimized technical solution for any given application. In order to build battery sub-modules and total pack solution, the selected cells will need to be connected in such a way to achieve the desired voltage and capacity for the application.

- **Series connections:** Voltages add, Capacity is Constant – Adding cells in a series increases the voltage by the value of the cell.
- **Parallel connections:** Voltage is constant, Capacities Add – Adding cells in a parallel connection increases the capacity by the value of the cell.
- **Series/parallel (XsYp) connections:** Combining the two methods above makes any combination of voltage and capacity possible, allowing a particular application's need to be met.

In addition to the energy storage cells there are a wide range of other vital components required within the battery system architecture. Some of the key battery elements are shown below [3].

- **Cells:** For automotive batteries, the most promising and attractive technological solutions utilizes Li-ion cells.
- **Busbars:** These are highly conductive metallic bars used to connect the cells and/or modules together electrically
- **Wiring harnesses:** Used to connect temperature and voltage sensors from the cells to the battery management system
- **Battery Management System (BMS):** These are the electronics that control the battery, and collectively are known as the Battery Management System (BMS).
- **Traction Cables:** A high voltage and current carrying cable that interconnects the cell module string together into a circuit able to deliver the main power to and from the battery.
- **Vehicle Interface:** A specific connection between the battery and the vehicle. Typically, communication from vehicle to battery is via information transferred by CAN-BUS, an

automotive standard communications protocol. Information may include parameters such as state of charge, battery voltages and temperature etc.

- **Current measuring device:** This allows the BMS to monitor the instantaneous current loads delivered and accepted by the battery during charge and discharge.
- **Isolation Monitoring Device:** A device to check the high voltage insulation of the battery system so that any insulation issue would be detected and allow the battery to be disconnected should there be a need to make it safe.
- **Main contactor relays:** The main high voltage switches on the battery, which turn off both positive and negative connections, thereby rendering the battery safe.

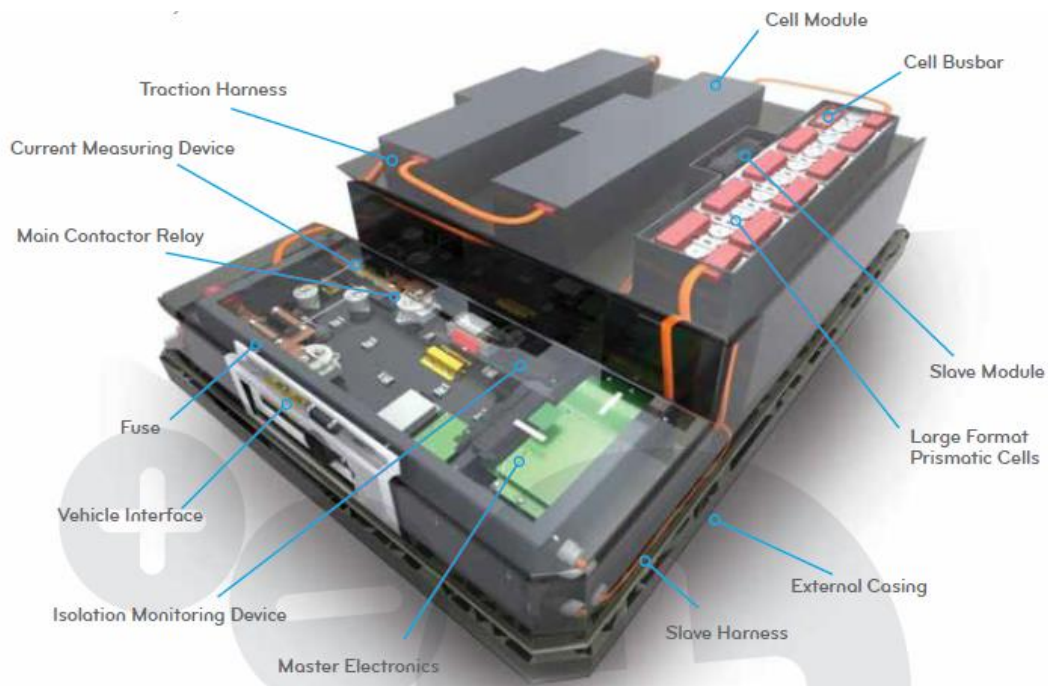


Figure 2.3 Automotive Battery System Example

2.6 Battery Safety

Battery safety is a main feature for the successful introduction of hybrid and electric vehicles to the market. The need for safety systems depends on the chosen technology, and the realization of safety systems can produce significant costs. This topic is particularly important when lithium-ion batteries are used as the management of lithium batteries is of higher complexity than that of lead-acid batteries, for example, and the chemistry is more reactive.

Safety precautions are divided into passive and active systems. Passive safety takes place at a cell level as well as at a system level. At a cell level, the choice of cell chemistry directly influences the safety. LiFePO₄ for instance is a relatively intrinsically safe material compared with lithium-metal-oxide cathode material using cobalt, nickel or manganese. The higher the passive safety of a cell, the lower is the cell voltage and the lower is the energy density. Moreover, safety components such as ceramic separators, positive-temperature coefficient (PTC) elements to limit the cell current, or flame-retardant additives can enhance cell safety. Additionally, the pack should be protected against crash impact by the housing and by fuses against being short circuited [4].

Active safety includes individual voltage control of each cell in a series connection, exact charge and discharge control management, as well as temperature control and cooling systems. The measured values have to be made plausible and a redundancy for faulty measurements should be given. Even though the technically safe state of the battery is to open the switches in the case of fault, this is only the ultimate option as the actual driving situation could be potentially more crucial than the fault itself. In general, the battery management system will not open the switches by itself unless there is at least one independent battery pack that ensures the operability of the vehicle. This again is an advantage of modular battery systems [4].

To evaluate the safety risks, batteries are tested on the basis of electrical impacts (e.g. overcharge or short circuit), thermal impacts (e.g. external heat source) and mechanical impacts (e.g. nail penetration or crash).

2.6.1 Voltage Levels

In vehicle applications, different main voltage levels are used. Micro-hybrid vehicles make use of the conventionally existing power system based on 12V batteries. The voltage of mild-hybrid vehicles is usually below 200V. As the threshold value of 60V is exceeded, these systems have to be treated as high-voltage systems. However, combined 12V-48V systems have been widely discussed in recent years. The 48V systems serve high-power loads up to 10kW using the electric machine to support the ICE and to optimize its operations, as well as to recover braking energy or for electronically assisted steering systems. The 12V system operates the low-power systems such as light, entertainment, control units, etc. Staying below 60V lowers the requirements on insulation, testing and system layout. Full-hybrid and electric vehicles mostly have a voltage level of around 400V but there are also systems with a lower voltage and a more modular system layout [6].

In general, the voltage level of large-scale automotive battery packs for electric vehicles or full-hybrid applications depends on the system architecture. A mostly parallel connection of cells leads to a relatively low voltage but serves higher current rates. On the other hand, having more cells and packs in parallel increases the reliability of the system as a single cell fault does not necessarily lead to a complete system failure as would be the case in a strictly serial connection. In contrast with the parallel structure, a serial connection of cells leads to a higher voltage and consequently to a lower current. On the other hand, a voltage measurement of each individual cell in a series connection is necessary as well as a charge-balancing system. Moreover, a strictly serial connection does not offer any redundancy in the case of a single cell fault [6].

2.6.2 Battery Management

Battery management systems secure safety aspects as well as long-lasting lifetime. Battery monitoring, diagnostics, electrical and thermal management as well as cell balancing are typical functions of such a system. Battery management systems monitor the battery pack's SOC and state-of-health and update its power capability. This information is used by the vehicle management, e.g. for the overall energy management. The battery management also provides the vehicle management with information on how to operate the battery to achieve the longest possible lifetime [3].

Cell management is most important for the lithium-ion technology as this technology does not imply any intrinsic overcharge mechanism. In addition, the SOC of each cell differs over time caused by the production and temperature variations between the cells. Charge equalization

systems are thus required to balance cells to a similar level. Different SOCs between the cells can also be avoided by a high production standard with equal qualities for all cells.

A detailed description of the different battery management system architectures, functionalities and applications will be given in the next chapter.

2.6.3 Thermal Management

Thermal management regulates the temperatures within a battery to be as constant as possible at a defined level. Deep temperatures are avoided because the cells usually have a reduced power capability at low temperatures. High temperatures, on the other hand, reduce the lifetime. In particular, for lithium-ion batteries, the maximum charge current must be limited at low temperatures to avoid risky states in the battery and accelerated ageing due to an effect called lithium plating. Moreover, safety issues of lithium-ion battery packs arise because of potential overheating. Under normal operating and ambient temperature conditions, battery systems can be easily controlled in the range of 20 – 55°C. Regarding stressful conditions, such as fast charge at a high cell temperature or a high ambient temperature, heat generation might increase tremendously and eventually lead to a so-called thermal runaway. An initial event triggers an exothermal reaction. The reaction causes heat, which further accelerates the exothermal reaction. This process can eventually lead to explosion or fire and therefore has to be prevented by all means [4].

The most important factors for efficient thermal management are the battery pack design and the cooling system. As a rule of thumb, a 10K temperature increase reduces the lifetime by a factor of 2. Today, various cooling systems are considered ranging from air-cooling via water cooling to phase-changing cooling liquids. For all cooling systems the number of temperature sensors needed, as well as their distribution within the pack, has to be considered. It is necessary to detect overheating of any cell within the pack with a high reliability. The thermal contacts of the cell to the cooling system depend on the chosen cell type (cylindrical, prismatic or pouch) and can be realized, for example, by cooling the bottom of the cell, the mantle or the contacts. On the one hand, the objective of temperature management is to operate the battery in an optimum temperature range (25 – 40°C during driving, and as low as possible during parking periods). On the other hand, the temperature gradient between the cells within a battery pack should be as low as possible. Because in a series connection of lithium-ion batteries the worst cell determines the total performance of the battery string, and because of the high impact of temperature on the lifetime, a minimized temperature gradient is a key factor to the desired performance of the whole battery system [4].

3 Battery Management Systems

3.1 Introduction

Battery management systems (BMSs) are real-time systems controlling many functions vital to the correct and safe operation of the electrical energy stored in the battery system. This includes monitoring of temperature, voltages and currents, maintenance scheduling, battery performance optimization, failure prediction and/or prevention as well as battery data collection and analysis.

Battery management systems are widely found in electric vehicles but are also commonly used in other battery applications as material handling, uninterruptible power supplies, off-grid power systems, marine and battery banks for alternative energy sources.

The requirements for the battery management system for these applications are often very similar to those in the automotive market, i.e. it is always important to control cell and pack in a robust, reliable and optimal way.

Electric vehicles always work in a complex operating environment with a variety of variables, such as temperature and humidity, load capacity, pressure, atmospheric corrosion, vibratory shock, input and output power, static placement, and so on. Therefore, the batteries also work in a complex environment and these factors pose great challenges to their security, cycle life and effective use. It is important to manage the battery to reduce its high cost and improve its anti-abuse ability. The abuse of the battery (including over-charging, over-discharging, over-heating, etc.) could cause a reduction in the battery cycle life, or even security accidents. These issues are more prominent in the battery pack because of the consistency differences of single cells. Ensuring the safety and cycle life of the battery pack in its use and management has become more and more urgent [7].

Besides the growth of the battery technology, the battery management system is a key element to make the utilization of battery systems in electric vehicles and other applications safe, reliable and efficient. The BMS comes to address some of the concerns regarding the integration of large battery systems in electric vehicles, that the progress of material in battery technology alone cannot overcome. Some of these concerns are the following [7].

- Cost – includes manufacturing, labor, maintenance, operation and replacement costs
- Lifetime – measured by the charge-discharge cycles and calendar life of the battery
- Power delivery – measured in terms of charge-discharge rate, energy storage level, ramp rate, and charge-discharge efficiency.
- Environmental impact and safety – measured in terms of the safety/risk factors due to the chemical composition of the battery, operating temperature, etc.

Technologies for scientific battery management include measures for monitoring battery parameters, which can estimate battery states, ensure safe use and avoid fast reduction in cycle life in practical application.

For the rest of this chapter, we will focus on the functionalities, topologies and architecture that are relevant to the automotive battery management systems, mainly referring to electric vehicle battery systems.

3.2 Functions of the Battery Management System

In electric vehicles, the battery management system has a great impact on safe operation, optimization of the strategy for vehicles, choice of the charging mode and reduction of operating costs. Either in the operation process or in the static charging process, the battery management system should provide real-time monitoring of battery states and fault diagnosis and inform the vehicle control unit or charger through communication. Then the vehicle control unit or charger can adopt the corresponding control strategy to achieve effective and safe use of the battery. The operation conditions of the battery pack vary according to vehicle type, and the relevant functions and parameters of the BMS will also be different [7].

In low-cost systems, there might be some differences in the requirements or functions for the BMS. Especially for a low number of cells in series (e.g. 12V systems with four cells in series), some battery system manufacturers propose a simple external undervoltage shutoff circuit and a charger with controlled end-of-charge voltage. For larger and more complex systems, the BMS guarantees the protection of highly expensive components and adds to the system functionality.

To begin with, it is important to mention again the difference between the terms “battery”, “module”, and “cell”. Basically, a battery is the completely assembled pack with electrical, mechanical and communication signal interfaces. The pack may consist of several modules that are wired in series and/or (less often) parallel. A module can be described as a part of the battery is normally contained in the battery housing, although with very large batteries that modules can also be connected separately through cables. In each module single cells are connected in series or parallel. If the modules are connected in parallel, then it is possible to obtain higher currents and a series connection leads to higher voltage [7].

In a module every cell has to be monitored to guarantee a proper function in the desired operating range (voltage, current, and temperature). In the battery pack level, all the measured values from all the modules are used to calculate historical values and incorporate any measures to protect the battery and maintain the performance of the pack.

The different architectures and topologies, regarding the design and implementation of a battery management system, based on the cell, module and battery terms that we introduced above, will be discussed separately in the following section.

To summarize, in order to achieve the efficient operation and extend the cycle life of the battery system, the battery management system should include the following functions:

- Cell voltage measurement
- Cell temperature measurement
- Battery pack current measurement
- Battery pack total voltage measurement
- Insulation resistance measurement
- Thermal management
- Battery pack state of health (SOH) estimation
- Battery pack state of charge (SOC) estimation
- Detection and analysis of battery failures and alarm functions
- Communication with vehicle main control unit
- Communication with battery charger

3.3 Architecture of the Battery Management System

The battery management system is constructed by using two basic architectures, the centralized architecture and the distributed architecture.

In a centralized architecture, there is a single control unit, we will refer as the battery management unit (BMU). The functions of the battery management unit are the measurement of voltage, temperature, current, insulation resistance, states estimation and communication, and so on. This is a low-cost option for a small number of cells and is usually assembled on a single printed circuit board. The major disadvantage of this approach is that each measurement signal has to be connected individually to the battery management system board, which increases the wiring complexity when the number of cells is large. Moreover, due to the large number of traction batteries and the limited space in vehicles, the batteries are usually distributed in large or even different areas in the electric vehicles, so the centralized architecture has gradually disappeared in EVs.

The distributed architecture term, includes many different topologies, but the most common and widely used, it the architecture of the battery management unit (BMU) and the module measurement unit (MMU). This topology is the standard topology for the distributed architecture, and there are many different alternative different terms for the two building blocks (battery control unit – BCU and battery measurement unit - BMU etc.). This topology can be regarded as a master – slave topology, with the MMU being the master module, and the MMUs being the slave modules.

The battery management unit is mainly used to process the battery parameters of each module management unit, and estimate the states of the battery pack, including SOC, SOE (state of energy) and SOH, which provide the basic data for the battery and charge control. Additional functions can be implemented based on the specific application requirements. These functions include: the total voltage measurement, current and energy measurement, insulation resistance measurement and high voltage relay control. The unit is usually installed in the battery container but it can also be installed in separate central control box.

The module management unit is mainly used to measure cell voltage and temperature, perform cell balancing and thermal management according to the control orders of the battery management unit. The MMU is almost always integrated in the cell module or is installed in a short distance from it.

This model increases the flexibility of design and arrangement and improves the reliability and safety of the system. Many variations of this topology can be implemented, regarding the functionalities and intelligence levels of the module management unit. For example, the battery states estimations can be carried out by the MMUs, and then communicated to the BMU, thus reducing the workload of the BMU. This is a preferred solution for very large battery systems like energy storage systems for grid connection. Overall, the final configuration depends heavily on the application as well as on the degree of safety and redundancy level required. Generally, the larger the battery, the more complex the configuration.

3.4 Design of the Battery Management System

The battery parameters measurement module, or the module management unit MMU, in the distributed architecture approach, is the key module of the battery management system for

obtaining battery states, and also is the core of the hardware design. Real-time measurements of electric vehicle battery parameters in a battery management system include battery cell voltage, temperature, current, the pack voltage and insulation and so on. Typically, only the voltage and temperature of each module are measured by the module management unit, while the other high voltage measurements are handled by the battery management unit [7].

3.4.1 Module Management Unit

3.4.1.1 Battery Cell Voltage Measurement

The cell voltage measurement is one of the most important parameters for battery external performance and the battery states largely depend on it. There are various voltage measurement methods for series-connected batteries. During the measurement, we should consider the problems of interference and high-low voltage isolation, and the cost and precision should be carefully considered. Along with the increase in series connections, common-mode voltage is applied to the battery cells. The common-mode voltage process should be considered during the hardware design [7].

At this stage, the battery pack consists of hundreds of cells connected in series and parallel, which is meant to meet the requirements of voltage and capacity. The normal performance of each cell will affect the performance of the battery pack, so it is necessary to monitor each cell. The cell voltage measurement is generally carried out by two schemes: discrete and integrated.

I.The Discrete Scheme

The discrete scheme consists of a sample and hold circuit, a strobe and an analog to digital conversion circuit, which are made from discrete components and an AD integrated chip. The main measurement methods are:

The Resistance Divider - The scheme is the common-mode measurement which turns the cell voltage of a series battery into the common ground voltage by the resistance divider. If the relative error λ of each voltage measurement, the actual value, the measurement value U'_n and the battery voltage U_{Bn} are given, we can get the measurement voltage:

$$U'_{Bn} = U'_n - U'_{n-1} = (U_n - U_{n-1}) + \lambda(U_n \pm U_{n-1}) = U_{Bn} + \lambda(U_n \pm U_{n-1})$$

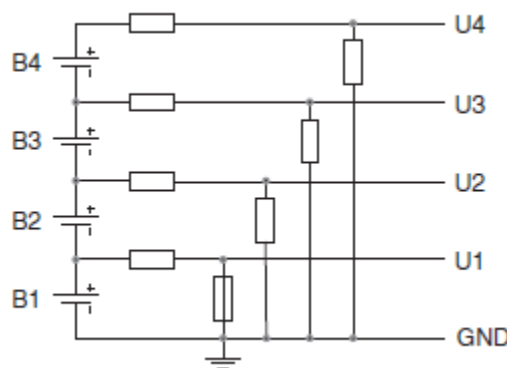


Figure 3.1 Resistance Divider Measurement Scheme

If there are a large number of batteries in series, the absolute value of U_n will be large and the relative error $\lambda(U_n \pm U_{n-1})$ will also be large, causing a major decline in measurement accuracy.

Relay Switching - By adopting this scheme, we could transfer the voltage of B_1 into U_1 , B_2 into U_2 and so on. Although U_1, U_2 , are non-ground signals in this way, we can regard the above voltage as the common ground signals because only one relay is connected at the same time. This measurement method is relatively simpler. Currently, with optically triggered solid state relays, the realization of the above circuit is easier. Moreover, the relay uses a contactless switch, which prolong the cycle life of the circuit [7].

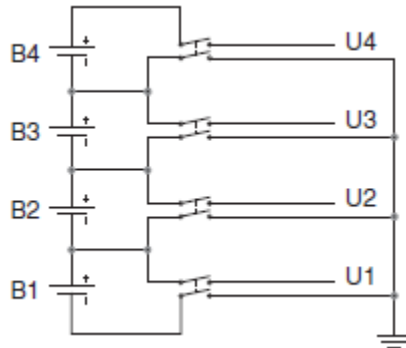


Figure 3.2 Relay Switching Measurement Scheme

II.The Integrated Scheme

The integrated scheme adopts the integrated voltage measurements chips of major market leaders for battery applications in electric vehicles. These chips generally integrate the sample, hold, strobe and analog to digital converter circuit, balance control and temperature circuit together. At present, mainstreams chips in the market are bq76PL536 of Texas Instruments, LTC6811 of Linear Technology and many others, but with Texas Instruments and Linear Technology having the edge in the current market [7].

The main features of these integrated battery monitoring solutions are:

- They can be used to measure the voltage of a fixed number of cells (a maximum of 6 or 12 are the main choices, with the total voltage not exceeding 60V)
- They can be built in a stackable structure in order to support battery system up to 1kV
- They offer very accurate measurement devices, with the maximum measurement error remaining below 0.25%
- Battery balance, on-chip passive battery balance switch which can also provide off chip balancing circuit
- Temperature sensor or general analog and digital inputs
- Built-in high-speed communication interface (SPI, UART etc.)
- High EMI immunity
- Integrated LDO voltage regulator
- Low power consumption

3.4.1.2 Temperature Measurement

Temperature measurement is the real-time monitoring of the operating temperature of the battery pack. Currently, the measurement methods include use of thermocouple, metal thermal resistance temperature detector, thermistor, analog integrated temperature sensor and digital temperature sensors [7].

Thermocouple - The thermocouple is widely used in temperature measurements. Its main features include wide measurement range, stable performance, simple structure, good dynamic response, small measurement error, remote transmission 4-20mA electrical signals, convenient automatic control and integrated control. The principles of a thermocouple are based on the thermoelectric effect. If two different conductors or semiconductors are connected into a loop and the two contact points have different temperature, then thermoelectric power is produced in the loop.

The output voltage of the thermocouple depends on the temperature difference between the hot and cool ends. In practice, it is necessary to add temperature compensation, use a special filter for enlarging the circuit and design a special temperature detection circuit at the cool end. When there are lots of temperature points to be measured, the connection wiring will be complex. The large amount of wiring will decrease the reliability of the system and cause inconvenience in placing the lines.

Thermal resistance - A thermal resistance detector is a common temperature detector in the middle-low temperature region. Its principles are based on the fact that the resistance of a conductor or semiconductor will change as the temperature changes. Most thermal resistance detectors are made of pure metals. Currently, the widely used metals are platinum and copper, and others, such as nickel, manganese and rhodium, and so on, are beginning to be used.

The main features of the thermal resistance detector include remote transmission signal, high sensitivity, good stability, good interchangeability and high accuracy. However, due to its large size and large thermal inertia, it cannot measure the speed of temperature changing with its low response speed. It needs external power stimulation. Its processing circuit and connection are as complex as those of the thermocouple.

Thermistor - The thermistor is a temperature measurement device comprising solid semiconductors with a high resistance temperature coefficient. According to the temperature coefficient, thermistors are classified into two types: positive temperature coefficient resistors (PTC) and negative temperature coefficient resistors (NTC).

The main features of the thermistor include high sensitivity, small size, good stability, strong overload ability, high response speed, and small delay. However, it has poor accuracy and pronounced nonlinearity. It is widely used in temperature control with less accuracy.

Analog integrated temperature sensor - An analog integrated temperature sensor is an integrated sensor made of silicon semiconductors, it is also called a silicon sensor or monolithic integrated temperature sensor. An analog integrated temperature sensor is a special IC which integrates temperature sensors into one chip. It can complete temperature measurement and output an analog signal.

The output signals of the analog integrated temperature sensor include current, voltage, frequency, and so on. The main features are low price, fast response speed, remote transmission

distance, small size and low power. It is suitable for measuring temperature at a remote distance. Nonlinear calibration is not necessary but it needs a complex processing unit.

Digital temperature sensor - The intelligent temperature sensor, also known as digital temperature sensor, integrates a temperature sensor, peripheral circuit, ADC, microcontroller and interface circuit into one chip, with the ability to measure temperature and communicate with a microprocessor.

The digital temperature sensor can output temperature data and relative temperature control data. It has good characteristics, such as high measurement accuracy, fast conversion time, programmability, multipoint measurement in parallel, convenient measurement and installation and easy positioning.

In most applications, the thermistor is the preferred temperature sensor choice, due to its high sensitivity and stability, the high response speed as well as the small size and low cost. The small size, and also the many packaging options are essential for battery applications where the temperature sensors need to be placed as close to the battery terminals as possible. Its low accuracy is not critical, since the temperature region is more significant than the actual temperature of the cells [7].

3.4.1.3 Battery Balancing/Equalization Management Circuit

Because of the different resistance of each cell, the different operating conditions, the inconsistency of the initial SOC and the inconsistency of self-charge, the inconsistency of each cell in a battery pack will increase after the battery pack has been used for a long time. In order to optimize the utilization of the battery capacity and energy, it is essential to equalize the battery. According to whether the equalization process consumes energy or not, the equalization control can be classified into the energy dissipative type and the energy non-dissipative type [7].

I.The Energy Non-Dissipative Type

The energy non-dissipative type adopts a capacitor and an electric inductance as the storage components, uses the power conversion circuit as the topology foundation and adopts the distributed or centralized structure, which achieves the scheme of unidirectional and bidirectional charging or discharging. Several energy non-dissipative types of battery equalizer are described in the following subsections [7].

Forward-Flyback Converter - The independent DC converter equalization method connects an independent DC converter to each cell in the battery pack. One side of the converter is connected to the two ends of each cell and the other side is connected to the two ends of the battery pack. When the voltage of a cell is too high, it will release energy by turning on the switch circuit. The energy coupling to the secondary side will be absorbed by the battery type to realize equalization. The DC transformation can be by either a forward converter or a fly-back converter. The bidirectional DC-DC module can be used to realize the energy bidirectional flow.

The distributed equalization method needs special DC-DC converters. Therefore, this method needs a number of power switches, with a large number of control signals and complex control logics. The cost of this system is high [7] [8].

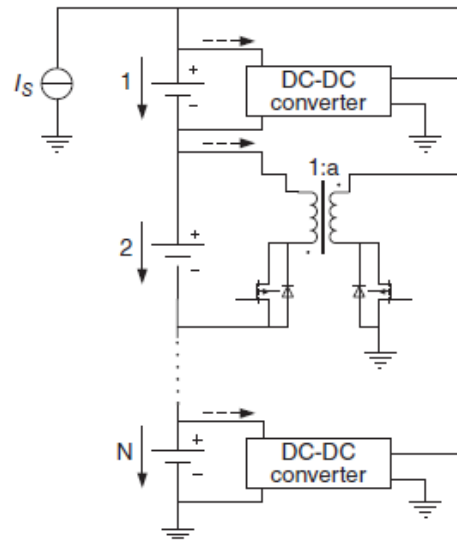


Figure 3.3 Forward - Flyback Converter Equalization Method

Shared Converter - The centralized equalization method could reduce hardware consumption with easy control. The use of unidirectional isolation fly-back converter and the multi-secondary side windings transformer could realize the centralized equalization control. The primary side of the transformer is connected to the battery pack ends and each secondary side is connected to each cell.

In this way, it could send the battery energy to the low energy cell. The charging voltage of the cell can be adjusted. When the system detects the low energy cell, the transformer secondary switch will be turned on and the primary side will form the loop circuit with energy stored in the transformer coils. When it is switched off, the storage energy will be released to the battery cell and the low energy cell will absorb the energy [7].

As shown in the scheme, the primary side of the transformer is connected to both ends of the battery pack. The energy comes from the battery itself. The loss of energy through the transformer coils, power components and other components will decrease the energy of the battery pack. Each secondary side of the coaxial multi-secondary side windings transformer is connected to each cell. As the number of series batteries increases, the transformer secondary side windings will increase and the design will become complex. Although the coaxial multi-secondary side windings transformer has the features of low leakage and controllable leakage magnetic flux, the secondary sides will bring more difficulty in transformer design and realization.

The centralized equalization structure is suitable for different kinds of batteries if the number of batteries is not large. Its main features are the small total volume, light weight and high maintenance. Once the high frequency transformer is broken, the entire equalization circuit will have to be replaced. The complex and application specific type of transformer, its high cost, the high maintenance costs, and its limited suitability for large number of batteries, makes this equalization solution non-viable for automotive applications [7] [8].

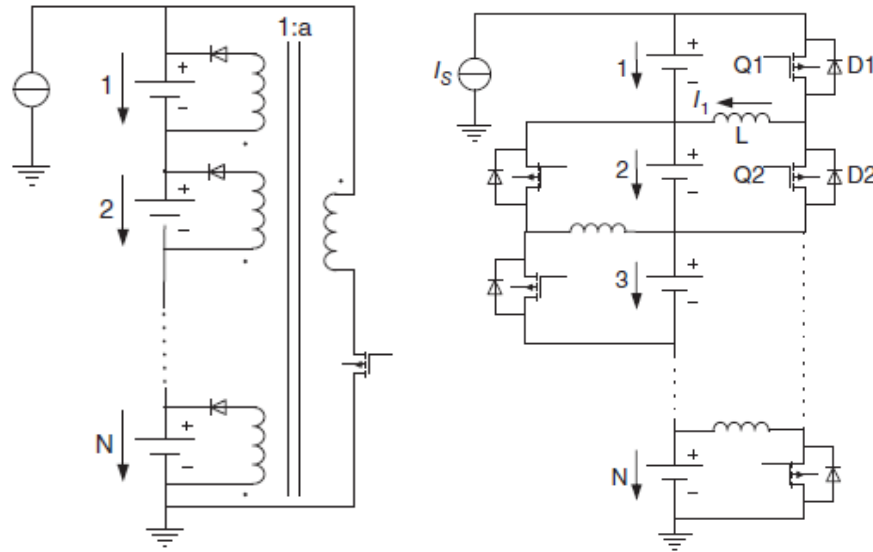


Figure 3.4 Shared Converter - Half Bridge Converter Equalization Method

The Half-Bridge Converter - The non-dissipative converter can transform the charging current of the fully charged energy cells to an adjacent cell to avoid excessive charging. Figure 3.4 shows the scheme of the non-dissipative converter, and this structure could also be used to realize bidirectional equalization [7] [8].

Each module consists of a pair of power switches, inductance, and a pair of diodes. Each end of the module is connected to one cell from the non-isolated half-bridge converter. When one cell voltage reaches equalization voltage, the relevant switch will be turned on and the energy will be stored in the inductance. When the switch is turned off, the stored energy will flow to adjacent cells and the current direction is the same as the charging current direction of the inductance. This method can directly release the energy of high voltage cells. However, it has small energy transferring capability, complex control strategy, lots of power switches and large switching losses.

Capacitive Equalization – Switching Capacitors - Using a capacitor as the storage component could realize cell equalization and energy transmission to reduce the inconsistency of cell energy. As shown in Figure 3.5, the cell will use the capacitor as the energy storage component. Through the control of a switch, adjacent cells can transfer energy from the higher voltage one to the lower voltage one to realize voltage equalization. For N batteries, N power switches and $N-1$ capacitors are required to make up the switch-capacitor network.

When using this method, if high voltage cells and low voltage cells are distributed at different ends of the battery pack, the energy will be transmitted from one side to the other side. This is time consuming and there is energy loss in each cell when transmitting the energy [7] [8].

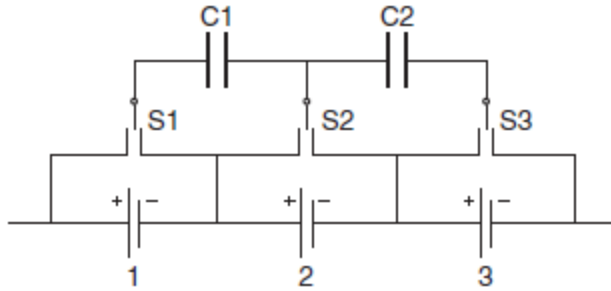


Figure 3.5 Switching Capacitors Equalization Method

Method	Pros	Cons
Switching Capacitors	Simple Control	Slow Balancing Rate
Shared Transformer	Rapid Balancing No Closed Loop Control Required	Complex Control – High Cost Transformer Must be Replaced if Cell Number Change
Flyback Converter	Suitable for Large Cell Stacks Easily Modularized Suitable for EV/HEV – Market Products	High Cost Complicated Control Scheme
Half-Bridge Converter	Rapid Balancing Suitable for EV/HEV	High Cost Complicated Control Scheme

Table 2 Energy Non-Dissipative Equalization Methods Comparison

II.The Energy Dissipative Type

The energy dissipative type equalization circuit realizes energy equalization using a bypass resistance, as shown in Figure 3.6.

Topology A uses a battery bypass resistance to realize the self-charging balance. The energy consumption of the resistance is proportional to the cell voltage. Therefore, the highest voltage cell consumes the most amount of energy. This uncontrolled and passive equalization method has large energy loss and low efficiency. Topology B is an improved version of A, which uses the cell equalization module to control the bypass current. If the cells that reach the equalization voltage are discharged, other bypass circuits should remain off [7].

This method is the simplest one and has the lowest cost by a large margin, but the equalization current is usually small so that it takes a long time to reach equalization.

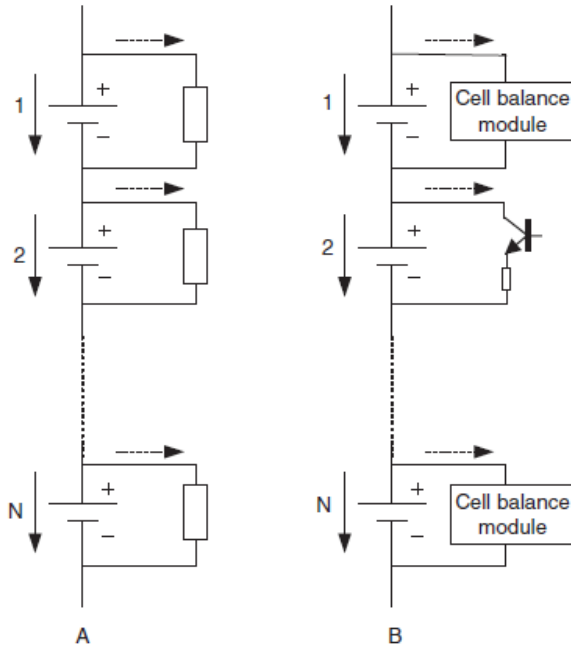


Figure 3.6 Energy Dissipative Equalization Method

Table 3 shows a comparison between the dissipative and non-dissipative techniques regarding cell charge equalization. In most application, including automotive, the energy dissipative type is the preferred solution, due to its simplicity and effectiveness, low cost and easy integration. Some of the reasons that make the dissipative technique dominant in battery management systems in EVs are the following:

- Balancing power in Li-Ion applications is usually small, typically less than 10W per cell, so “passive” vs “active” solutions effectively provide the same results.
- Generally, the higher cost of “active” balancing techniques makes this solution viable only when the energy saving is significant
- The real advantage of “active” equalization techniques is in its rapid balancing capabilities, transferring large amounts of energy in short periods of time
- SoC based equalization algorithms significantly increase the effectiveness of the equalization techniques, regardless of “passive” or active”

Taking into account the progress in Li-Ion battery technology, the main reason for any imbalance is the self-discharge of the cells, which is approximately 2-3% per month, but generally differs from cell to cell. Charge and discharge does have only a negligible effect on the cell imbalances. Therefore, it is evident that large balancing currents are not required in order to fix these small imbalances. Advanced estimation algorithms are widely developed, which can significantly increase the effectiveness and utilization of balancing. One more thing to consider, is that especially in automotive applications, the discharge currents are pretty large in proportion to the charge or balancing currents, therefore making the balancing procedure only viable during rest or charging periods. In these periods, passive balancing can satisfy the balance time requirements, even with small balancing currents.

Due to the high cost and complexity, active balancing techniques are rarely used in automotive battery management systems. Their high design complexity, component costs, increased circuit size and testing and reliability issues make the passive technique dominant in such applications. Nevertheless, active techniques are widely used in academic or research applications [7].

<i>Dissipative Type - "Passive"</i>	<i>Non-Dissipative Type - "Active"</i>
Simple Control – High Reliability	Complicated Control – Lower Reliability
Small Number of Components	Lot of Extra Components Sometimes Not Off-The Shelf Availability
Low Cost/per Cell	High Cost/per Cell
Small Balancing Currents	High Balancing Currents
Low Efficiency – Heat Dissipation	High Energy Efficiency
Integrated in Many Market IC Solutions	Few Market Solutions – Application ICs
Easily Integrated in Wide Range of Applications	Application Specific Designs – Hard to Integrate

Table 3 Energy Dissipative vs Non-Dissipative Equalization Methods Comparison

3.4.2 Battery Management Unit

The battery management unit is the main control element of the battery management system. The main data management and control actions are carried out by it. Moreover, it carries out the essential high voltage measurements that are needed for the functional requirements of the battery management system. These measurements include current, voltage and insulation. In this section we will only elaborate on the battery current measurement, since its essential for the SoC estimation algorithms, and overall is an integral part of the system. The voltage measurement is typically implemented using a resistance divider, with high resistor values in order to minimize the leakage current. The insulation measurement requires more complex techniques and is a key safety requirement in electric vehicles. It is many times considered a standalone system, and there are market products dedicated to this function. An in-depth analysis of the techniques is not part of this thesis.

3.4.2.1 Current Measurement

The current of charging or discharging is the external reflection of energy transfer and also the important base of the battery management system energy management. The current measurement provides data for estimating SoC, and for the charging and discharging control of the BMS. It is necessary to ensure its sampling accuracy, anti-interference ability, zero drift, temperature drift and linear error. The schemes of current measurement include the Hall effect current sensor, the shunt, and so on [7].

Hall Effect Current Sensor - The output signal of a current sensor is a secondary current, in proportion to the input signal (primary current). The secondary current generally only has a value of 10-400mA. If the output current goes through a measurement resistance, it will give a voltage output signal which is proportional to the primary current. Then through amplification and adjusting the circuit, the output signal is converted using an analog to digital converter. According to the form of current, the Hall effect current sensor is classified into two types: DC and AC, by the form of the feedback, it is classified into open loop and closed loop types [7].

Figure 3.7 is a diagram of the open loop current sensor. Its working principle is that if semiconductor Hall components are put into the space of the magnetic loop, the Hall current (secondary current) and the Hall voltage would change as the measured conductor current (primary current) changes. The change in voltage will be amplified through the amplifier that reflects the measured current.

In order to stably and accurately measure the primary current, compensation windings are placed around the magnet ring, as shown in figure 3.8. The compensation winding and output form the closed loop of the Hall negative feedback. The Hall equipment and the auxiliary circuit produce the secondary magnetic compensation current I_M , which reflects the measured current I_N . Through a sampling resistance R_L , the compensation current can produce a voltage drop which outputs in the form of voltage V .

The Hall effect current sensor has the characteristics of high accuracy, fast speed, wide band, better isolating function, strong overload ability and no loss of energy in the measured circuit. However, in the complex electromagnetic interference environment of electric vehicles, it is difficult to ensure the linearity of the measurement with some issues like the zero-drift, temperature-drift and so on [7].

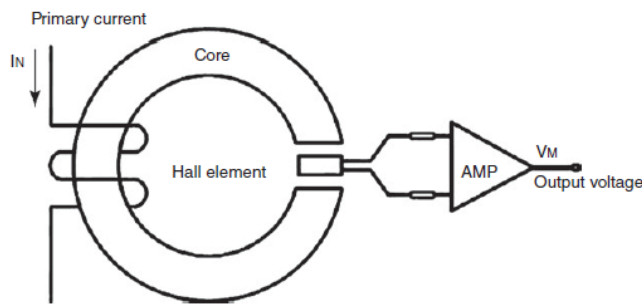


Figure 3.7 Open Loop Hall Current Sensor

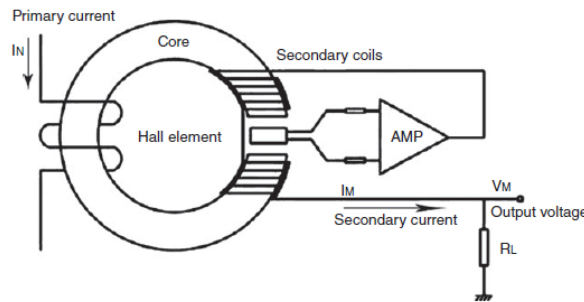


Figure 3.8 Closed Loop Hall Current Sensor

The Shunt - The shunt comprises a rod resistor of nickel, manganese copper alloy and copper strips with a nickel coating. When the DC current goes through the shunt, it produces a voltage at the two ends of the shunt. Its structure consists of the slot type and the non-slot type. The shunt connects directly with high voltage so an isolating circuit is required in the circuit design. The voltage signal, obtained by the shunt sampling, will be connected to an analog to digital converter after the filter and amplification.

In most cases, in order to utilize the shunt a dedicated analog to digital converter scheme needs to be designed. Due to its wide use, many dedicated integrated chip solutions are available in the market, which include all the needed circuitry for effectively utilizing the shunt. These features include an analog to digital converter, programmable digital filters, calibration circuitry and communication interface. The fact that the shunt is connected to high voltage and carries the battery current at all times introduces some energy losses and heat dissipation, and also requires a reliable isolation circuit. Though the hall sensors require less complex interface circuitry and are easier to integrate in any kind of system, the shunt is generally preferred due to its linearity and non-drift characteristics [7].

3.5 Data Communication

An important consideration for the battery pack management system is the communication interface. Data communication is the important link for data transmission inside the battery management system and data transmission between the itself and other devices. After sampling the voltage and temperature, the module management units should transmit these data to the battery management unit, which processes the information and makes control decisions regarding the system state. The amount of communication data is very large. The reliability, timely collection and transmission are the key premises for the performance of battery management systems in electric vehicles.

The choice of the communication bus is based on the type of application, the number of modules and the overall cost of the system. For communication between modules, common options include the Serial Peripheral Interface (SPI) bus and Inter-Integrated Circuit (I2C) bus. Each has low communications overhead, suitable for low interference environments. Another option is the Controller Area Network (CAN) bus, which has widespread use in vehicle applications. The CAN bus is very robust, with error detection and fault tolerance, but it carries significant communications overhead and high material costs. While an interface from the battery system to the main vehicle CAN bus may be desirable, SPI or I2C communications can be advantageous within the battery pack [7].

Despite the increased cost and complexity, in most battery management systems for electric vehicle, a separate CAN bus communication within the battery pack is preferred, mainly because of its noise immunity and robustness. This is significant advantage since the battery pack contains high voltages and currents which make it a high interference environment, which can really compromise the data integrity.

3.5.1 CAN Communication

CAN was developed by the German company Bosch and is one of the most widely used buses since the 1993 standardization (ISO 11898-1). It is the mainstream network in automobile electronics control. The network nodes of CAN are different electric control units (ECU). Currently,

many of the world leading car manufacturers have adopted CAN as the data communication bus between the automobile internal control system. Also, most of the market high power chargers which are used in electric vehicle applications, include a CAN interface in order to effectively communicate with the battery management system during the charging process [7].

CAN works in a multi-master way. Each node can send information to other nodes when necessary.

- The nodes of CAN have different levels of priority
- CAN adopts the non-destructive arbitration technology
- The nodes of CAN can realize the transmission either one-to-one, one-to-many or by universal broadcast
- The longest direct communication distance of CAN can reach 100 km in remote areas and the maximum communication speed is 1 Mbps
- The information in each frame of CAN has the CRC checking measurement
- The communication media of a CAN bus can be twisted pair, coaxial cable or optical fiber
- CAN has a high cost performance and a simple structure

The basic structure diagram of a CAN bus is shown in Figure 3.9. The communication data are transmitted into the CAN through special CAN controllers.

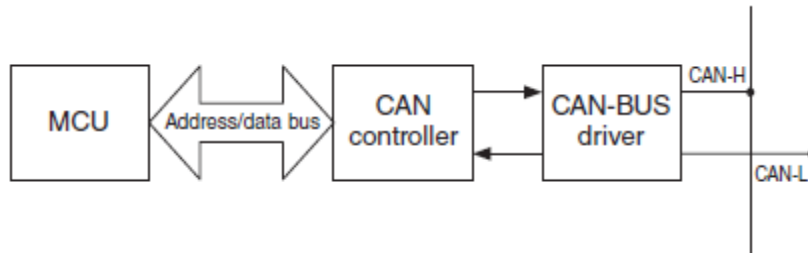


Figure 3.9 CAN-bus Structure

A large amount of data is required by the management system with good real-time communication. However, if all data are put on the same bus, the high load rate will lead to bus congestion, and poor real-time data communication. According to the function, structure and data type, these data could be sent to different buses.

One common method is to distribute the CAN data of BMS between three buses: the internal CAN bus, the charging CAN bus, and the vehicle CAN bus. Each bus undertakes the relevant output tasks for reliable and real-time transmission of the data.

The internal CAN bus is mainly used for collecting the battery management system internal battery information and transmitting control commands. The voltage of each cell, temperature, total voltage and current are all transmitted on the internal CAN bus.

The charging CAN bus is mainly used for communication between the battery management system and the charger. Its main information includes charger state, start or stop charging, maximum permissible charge current and so on. In consideration of the generality of electric vehicle charging stations, it is necessary to have the same regulations for the charge interface and protocol. In accordance with the national standard, the communication protocol of the charger

and the battery management system should produce a message at the handshake stage, parameter configuration stage, charging state, end charging state and wrong stage [7].

The vehicle CAN bus is mainly used for communication between the battery management system and the vehicle control unit. Besides the battery management system and vehicle control unit, there are the motor controller and other devices as nodes in this bus, which is the most important data bus. The BMS should transmit information on the SOC, total voltage, and maximum permissible power/current to the bus.

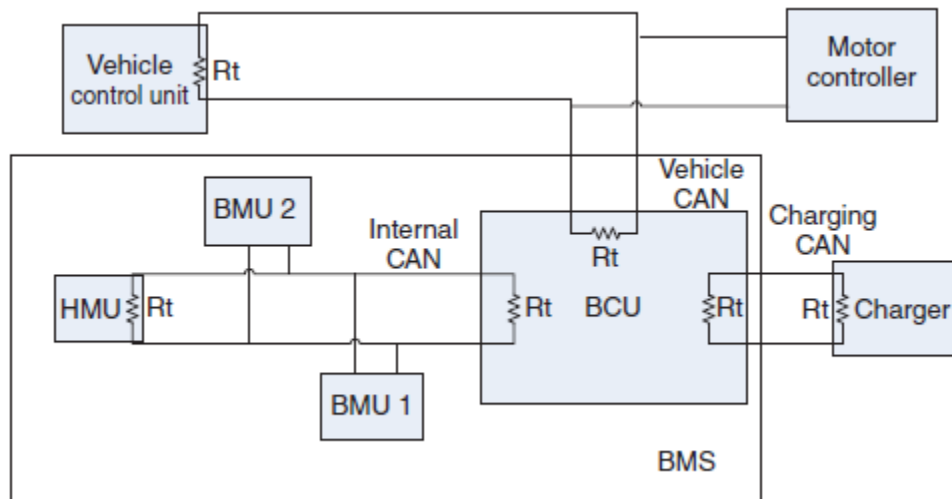


Figure 3.10 Electric Vehicle CAN network [7]

3.5.2 Data Communication Topologies

Besides the general CAN bus architecture, with the separate buses for the different functionalities of the battery management system, there is a variety of different architecture approaches, that make use of other communication protocols, and may be useful depending on the requirements of the system. CAN bus is still used for the communication between the battery management system and the vehicle control unit, but other solutions are utilized such as SPI, for the internal communication between the modules of the system.

Three architectures for the structure of the battery management system itself based on its communication interface are depicted below. In every case, it is assumed that each module management unit is monitoring a fixed number of cells, and the different topologies and communication configurations are explored. Each case provides a CAN bus interface to the battery management unit and is galvanically isolated from the rest of the electronic equipment of the system [9].

Parallel independent CAN modules - Each module management unit is equipped with a microcontroller, a CAN interface and a galvanic isolation transformer. The large amount of battery monitoring data required for the system would overwhelm the vehicle's main CAN bus, so the CAN modules need to be on a local CAN sub-net. The CAN sub-net is coordinated by the battery management unit, which also provides the gateway to the vehicle's main CAN bus [9].

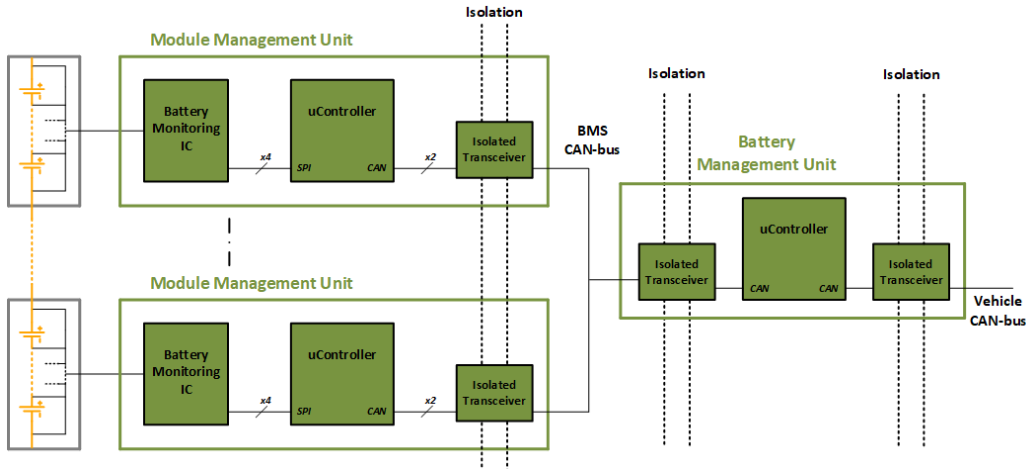


Figure 3.11 Parallel Independent CAN modules

Parallel modules with CAN gateway - Each module management unit contains a digital isolator. The modules have independent interface connection to the battery management unit, which contains a CAN interface and a galvanic isolation transformer. The battery management unit coordinates the modules and provides the gateway to the vehicle's main CAN bus. The third architecture is a simplified approach with minimal limitations, but is less reliable, since it is susceptible to communication loss, even if only one communication line is problematic [9].

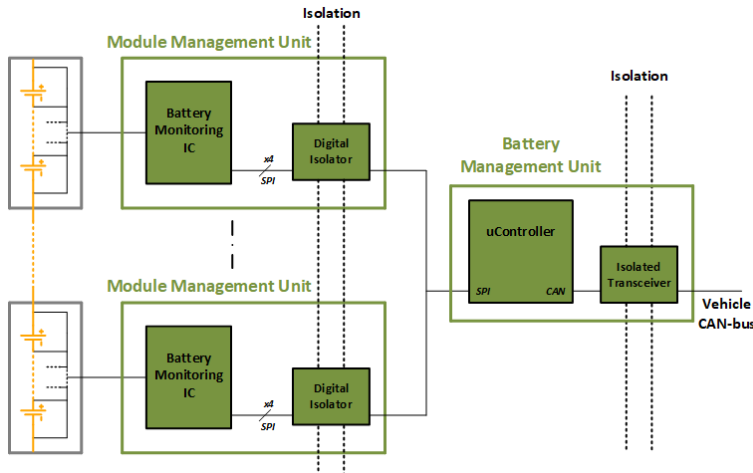


Figure 3.12 Parallel Modules with CAN gateway

Series modules with CAN gateway - The module management units are in a daisy chain configuration, which is coordinated by the battery management unit, which also acts as the gateway to the vehicle main CAN bus. Once again, a galvanic isolation transformer is needed to complete the architecture [9].

The first and second architectures are generally problematic due to the significant number of connections and the external isolation required for the parallel interface. For this added complexity, the design has independent communication to each module management unit, which greatly increases the system's flexibility and reliability [9].

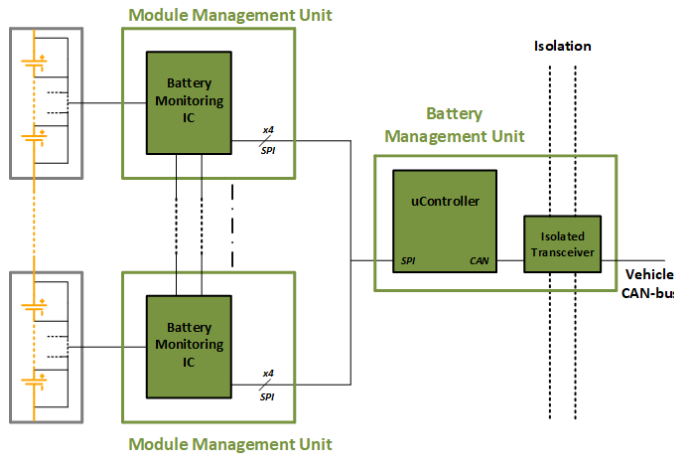


Figure 3.13 Series Modules with CAN gateway

3.6 Battery Management Requirements

There are at least five major requirements that need to be balanced when deciding between battery management system architectures. Their relative importance depends on the application unique features [3].

Accuracy – To take advantage of the maximum possible battery capacity, the battery monitor need to be accurate. A vehicle, however is a noisy system, with electromagnetic interference over a wide range of frequencies. Any loss of accuracy will adversely affect battery pack longevity and performance.

Reliability – Automobile manufacturers must meet extremely high reliability standards, irrespective of the power source. Furthermore, the high-energy capacity and potentially volatile nature of some battery technologies is a major safety concern. A failsafe system that shuts down under conservative conditions is preferable to catastrophic battery failure. To minimize both false and real failure, a well-designed battery pack system must have robust communications, minimized failure modes and fault detection.

Manufacturability – Adding sophisticated electronics and wiring to support an EV/HEV battery system is an additional complication for automotive manufacturing. The total number of components and connections must be minimized to meet stringent size and weight constraints and ensure that high volume production is practical.

Cost – Minimizing the number of relatively costly components, like microcontrollers, interface controllers, galvanic isolators and crystals can significantly reduce the total system cost.

Power – The battery monitor itself is a load on the batteries. Lower active current improves system efficiency and lower standby current prevents excessive battery discharge when the system is off.

4 Battery Management System Concept

In this section, we are going to describe the proposed battery management system that was designed and implemented during the course of this thesis. The general architecture will be presented as well as all the parts of the system that were implemented and tested. At this point we should mention that the system is designed for automotive applications using lithium-ion batteries, regarding hybrid or electric vehicle technologies that were described earlier. This statement does not exclude the use of the proposed system in other kinds of applications, such as energy storage, battery powered systems etc.

4.1 General Description

The proposed system is a distributed battery management system architecture with an isolated CAN-bus. The architecture can be perceived as a master-slave topology, in which each module management unit is responsible for the monitoring and balancing of a battery module, and therefore can be regarded as the slave units. The battery management unit, which is the master unit, controls the function of the battery pack, performs insulation monitoring and current measurement, detects battery failures, handles emergency actions, and is responsible for the data communication to the main vehicle control unit.

Each slave unit is considered as a standalone system, implemented in a separate circuit board. Thus, it can be placed near or inside the battery module. The master unit, is also considered a standalone system, and its only dependency to the slave units is the communication wiring. This greatly increases the flexibility of the system, but also increases the overall cost. It is evident that each design decision comes with trade-offs between complexity, cost and flexibility.

A simplified schematic of the system's architecture is shown below, highlighting the key components of the system as well as their interconnection:

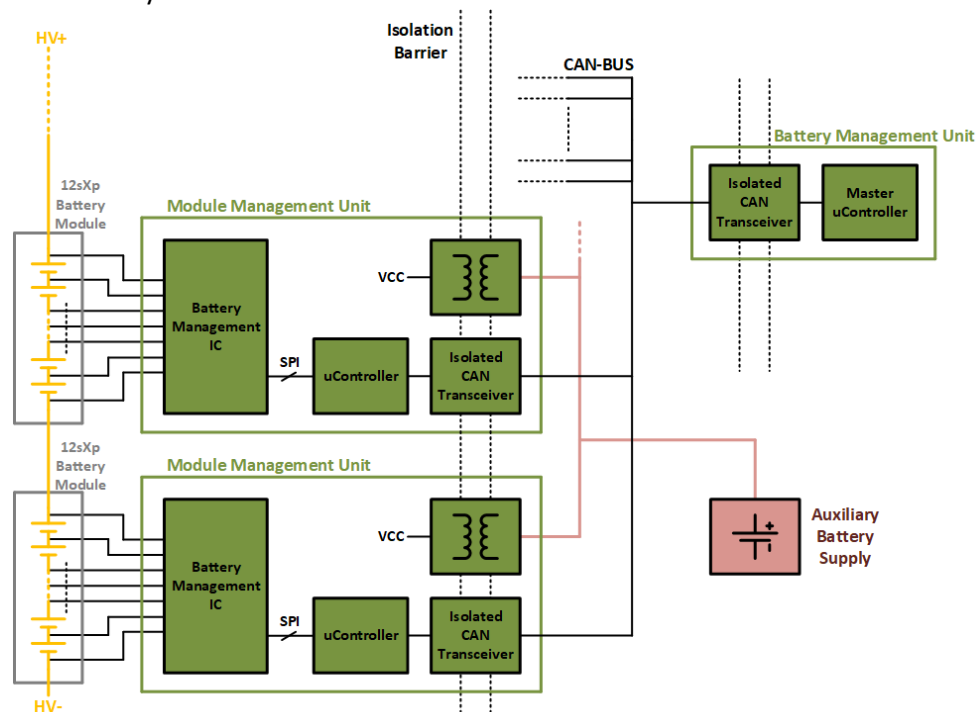


Figure 4.1 Battery Management System Proposed Architecture

The module management unit features a battery monitoring IC, which is responsible for the measurement of up to 12 cell voltages and temperatures. The selected IC is LTC6811 by Linear Technology. The chosen data communication bus is the isolated CAN-bus. This is the widespread standard for automotive applications, and also provides reinforced EMI immunity, which is valuable in the high-voltage and current environment of a battery pack. A uController is also embedded in the system. This is mandatory for the operation of the CAN-bus and monitoring IC, but it also increases the design flexibility and function capabilities of the system.

The system will be supplied by the auxiliary battery supply, which is always present in automotive systems, for the power supply of the electronic equipment. Nevertheless, there are use cases where the system should be able to function when the auxiliary supply is off, for example, balancing during the vehicle idle states or balancing during the charging process. Therefore, the module management unit shall be able to remain functional during such use case scenarios. A dual power supply scheme is implemented, enabling the system to select its power supply, either from the external power source or from the battery module that it monitors.

One of the main goals of the design process was design and functional flexibility. The presented architecture is suitable for this kind of design approach due to its following characteristics:

1. Independent of the total number of cells in the battery pack

Since each module management unit is capable of monitoring 12 battery cells connected in series, these units can be stacked in order to monitor an arbitrary large number of cells, without any system modifications.

2. Independent of the battery pack architecture – topology

The distributed approach makes the system suitable for all kinds of battery pack topologies, since its approach is module-wise. This means that the system can be effectively used regardless of a series or parallel connection of the various battery modules.

3. It can be easily integrated in a battery module

The modular approach of this architecture, with every component implemented in a separate circuit board, makes it suitable for various kinds of battery container mechanical designs, and enables its easy and fast integration in a battery system.

4. Easier to manufacture/prototype/test

The core functionalities of the system are performed by the module management unit. Thus, the core functional principles of the architecture can be tested and validated using a manufactured prototype of this unit only, replacing the battery management unit by an abstract controller. This is a great advantage for rapid manufacturing and experimental results.

Since we have presented the basis of the architecture, we should discuss the different advantages and disadvantages that it provides. The trade-offs between these characteristics played a major role during the design phase, in order to conclude to the desired architecture that provides the best compromise between its features and problems.

The main advantages of the proposed architecture are:

- Increases the functional capabilities of each module management unit

- Improves the overall system flexibility and performance, by distributing the total computational and data transfer duties to several uControllers
- Makes effective use of each uController, concentrating its functionalities on each module individually
- Allows the usage of additional functional components which can achieve more functionalities (extending cell temperature inputs etc.)
- Reduces wiring inside the battery pack compared to a centralized approach
- Provides robust data communication and integrity through the isolated CAN-bus

The main disadvantages of the proposed architecture are:

- Increased cost
- Increased power consumption, which is generally negligible compared to the high-capacity cells that are usually used
- Increased complexity, due to the controller network
- In terms of monitoring, the same results can be achieved using a single central uController

In summary, the proposed architecture is a semi-distributed modular approach. The monitoring and balancing workload is evenly distributed to each module management unit, while the functionality is monitored and controlled by the battery management unit. The addition of the uController in each slave unit increases its functional capabilities, allowing a more modular solution, where the module management units can perform tasks as state estimations and failure detections. Thus, the master unit is restricted to a more supervisory and redundant role. This concept renders the proposed system suitable for a variety of distributed architecture applications, providing a high level of design flexibility on regard to the distribution of different tasks between the module and battery management units.

4.2 System Requirements

Since the module management unit is the fundamental component of the system, carrying out the basic functions of the system, it was selected to be implemented in order to validate the overall system functionality. A computer interface was used to represent the battery management unit, in order to develop the validation software and obtain experimental results of the system. The detailed description of the design solutions as well as the hardware design will be presented in the following paragraph.

The system requirements for the module management unit are presented below, organized by their functional aspects. At first, we provide a simple reference so that the overall functional goals can be easily perceived.

Battery Monitoring - Balancing

1. The system shall monitor a module of 12 series connected Li-Ion Cells.
2. The system shall be able to detect undervoltage or overvoltage on any cells, with adjustable thresholds.
3. The system shall feature passive cell balancing, with nominal balancing current up to 60mA, and maximum of 250mA.
4. The system shall be able to monitor up to four NTC temperature sensors mounted inside the battery pack.

Data Communication

5. The system shall feature a uController.
6. The system shall support an isolated CAN-bus interface for communication with external components.

Power Supply

7. The system shall feature a dual power supply option.
8. The primary power supply shall be an isolated external source of 5-36VDC, providing up to 200mA of output current.
9. The secondary power supply shall be the monitored cells, (Top (V+) and Bottom (V-) Cell of the Battery Module: ~50VDC).
10. The power supply shall be uninterruptible, such as the secondary supply must be able to automatically switch on in case of primary supply failure.
11. The uController shall monitor the primary power supply rail, and be able to switch to the secondary, only in case that there is an ongoing cell balancing procedure.
12. A step-down regulator supplied either by the isolated external source or the Battery pack shall provide a 5VDC supply for the uController and peripherals with a maximum current consumption of 250mA.
13. The power supply of the CAN transceiver (connector side) shall be provided by a linear voltage regulator supplied from the external power supply

Isolation

14. The isolation barrier shall be able to continuously withstand at least 1500VDC minimum.
15. The isolation barrier separates the external primary power supply and the CAN-bus connection from the balancing circuit and the uController.

Board Temperature Monitoring

16. The system shall be able to monitor the board temperature during balancing using NTC temperature sensors.
17. The temperature sensors shall be located near the balancing resistors in the layout of the module management PCB.

Now that the system requirements are laid out, we can start to elaborate on them and discuss their importance and reason behind their selection. The first set of requirements are associated with the monitoring and balancing features of the slave unit. Following, we have the data communication and power supply requirements. Another key feature that was not mentioned before is the system's isolation, which is a vital component in order to protect the rest of the electronic equipment from the high-voltage battery pack. Finally, board temperature sensing is included in the module management unit due to the "passive" balancing method, which can cause heating problems on the balancing resistors.

As it was mentioned in the general description, the module management unit is able to monitor the voltages of up to 12 series connected lithium-ion cells. Moreover, monitoring is considered complete only when undervoltage and overvoltage conditions can be detected. In our case, these conditions are detectable while the threshold values are adjustable, thus extending the range of applications of the system. Moreover, the cell temperatures are measured through 4 NTC thermistor inputs. The number of temperature sensors can be increased using a

multiplexer. Nevertheless, this was not used in our design, in order to decrease the overall complexity since the number of sensors can provide adequate information about the module's temperature state.

A nominal balancing current of 60mA was selected for the equalization circuit. Although the balancing value seems low, it is sufficient since the main reason for imbalance in the modern cells is the self-discharge of the cells, thus the charge that needs to be balanced is significantly low. Furthermore, the balancing process mainly takes place during idle or charging periods, hence the available balancing time is sufficient to achieve equalization even with small balancing currents. Nevertheless, the balancing circuit was sized to a maximum current of 250mA so that it can satisfy even some more demanding rapid balancing applications.

As we mentioned earlier, the module management unit will be supplied by the auxiliary battery supply. However, in order to maintain isolation between the electronic equipment and the high-voltage battery system, power that directly supplies the battery monitoring equipment shall be isolated. For this reason, an isolated DC-DC converter stage is used, supplied directly by the electronics power source, which provides a stable isolated power supply rail for the components of the module management unit that are connected to the battery module. Moreover, since there are cases when the system shall be able to function although the auxiliary battery would be powered off, the monitored battery cells are used to provide a secondary power source. A power supply switch, controlled directly by the uController, is used in order to achieve the uninterruptible power supply requirement. Finally, it is crucial to maintain stable operating power supply voltage levels for the uController and the rest of the components of the system regardless of the power supply option. Thus, a step-down regulator is introduced in series to the power supply switch, which is able to provide a stable output rail in any case of input power supply voltage level.

The isolated DC-DC converter provides isolation between the vehicle electronics power supply and the system's supply. In order to achieve complete isolation, an isolated CAN transceiver is used, isolating the data communication between the module and battery management units. The isolation barrier is set to 1.5kV. Appropriate circuit spacing and properly rated components are used to ensure that this requirement is satisfied.

Since the balancing method used is energy-dissipative, the energy dissipation appears as heat dissipation in the balancing resistors. Excessive and repeated overheating of the resistors can cause minor changes in their value as well as result to unexpected failure. Moreover, since the resistors are placed tight together, overheating problems can also affect the circuit board, resulting in desoldering failures, as well as the adjacent components. Therefore, NTC temperature sensors are placed near to the balancing circuit so that the temperature can be effectively monitored. The board temperature monitoring allows the prevention of such failures and can be useful for the definition of the balancing cycles.

4.3 Block Diagram

The block diagram of the module management unit is illustrated in the figure below. The main components of the system are shown, as well as, the connections with the battery module and the battery management unit.

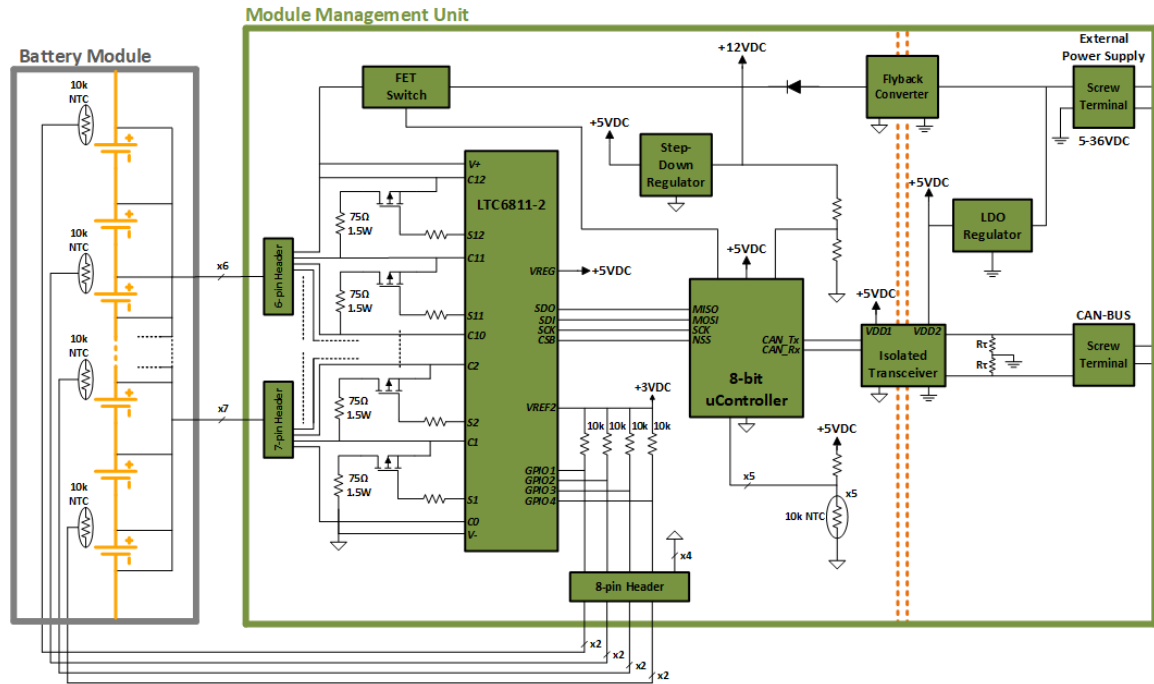


Figure 4.2 Module Management Unit Block Diagram

The battery voltage sense lines, one line for each cell voltage and an additional line for the negative terminal, which is the system's respective ground potential, are connected to the system through header-plug connectors. The connectors have different number of pins so that the bottom and top part of the stack are easily distinguished. The temperature probes are connected in the same way, using a signal and a ground line for each sensor. A screw terminal connector is used for the system's power supply as well as for the CAN-bus interface.

Apart from the battery voltage and temperature lines, the battery management IC is connected to the uController. The monitoring and balancing actions are communicated by the uController to the IC via the SPI interface. The analog inputs of the uController are utilized for monitoring the board temperature sensors and the power supply rail. The power supply switch, which connects the battery module voltage to the input of the step-down regulator, is controlled by one of the uController's digital output lines.

An isolated transceiver is used for the control of the CAN-bus. Since the chosen uController includes a CAN controller, the data messages are constructed by the uController and then sent to the transceiver via the Tx line. The transceiver then handles the message conversion and overall bus function. When receiving data messages from the bus, the transceiver translates the received data and sends it to the uController through the Rx line.

As we already mentioned, the monitoring circuitry is directly connected to the battery module and should be isolated from the rest of the electronic equipment. For the monitoring circuitry, the negative terminal of the battery module is used as the respective ground potential. So, in case of a battery pack with many series connected modules, each module management unit is grounded to the negative terminal of its respective module. This way, even if a unit is connected

to a module which carries high-voltage in respect to the battery pack, the unit is always connected to the module voltage regardless of its connection to the pack.

4.4 Component Description

4.4.1 Battery Monitoring IC

The battery monitoring IC selected for our application is Linear Technology's LTC6811. Linear Technology LTC6811 high voltage battery stack monitor is a complete battery measuring IC for hybrid/electric vehicles that incorporates a deep buried Zener voltage reference, high voltage multiplexers, 16-bit delta-sigma ADCs and a 1Mbps isolated serial interface. An LTC6811 can measure up to 12 series connected battery cells with a total measurement error of less than 1.2mV. The cell measurement range of 0V to 5V makes the LTC6811 suitable for most battery chemistries. Multiple LTC6811 devices can be connected in series, permitting simultaneous cell monitoring of long, high voltage battery strings. Using the LTC6811-2, multiple devices are connected in parallel to the host processor, with each device individually addressed. The LTC6811 can be powered directly from the battery stack or from an isolated supply and includes passive balancing for each cell, with individual PWM duty cycle control for each cell. Other features include an onboard 5V regulator, five general purpose I/O lines and a sleep mode, where current consumption is reduced to 4 μ A. The LTC6811 is fully specified for operation from 40°C to 125°C. It has been engineered for ISO - 26262 (ASIL) compliant systems with extensive fault coverage via its redundant voltage reference, logic test circuitry, cross-channel testing, open wire detection capability, a watchdog timer and packet error checking on the serial interface [10].

4.4.1.1 Pin Description

In this section, the function of the key pins of the IC are described, in order to provide a more comprehensive understanding of its basic functionalities.

C0 to C12: Battery Cell Inputs

S1 to S12: Balance inputs/outputs. 12 internal N-MOSFETs are connected between S(n) and C(n-1) for discharging.

V⁺: Positive supply pin.

V⁻: Negative supply pin. The V- pins must be shorted together, external to the IC.

V_{REF1}: ADC Reference Voltage. No DC loads allowed.

V_{REF2}: Buffered 2nd Reference Voltage for driving multiple 10k Thermistors.

GPIO [1:5]: General Purpose input/output. Can be used as digital inputs or digital outputs, or as analog inputs with a measurement range from V- to 5V.

DTEN: Discharge Timer Enable. Connect

VREG: 5V regulator input.

WDT: Watchdog timer output pin. This is an open drain NMOS digital output. If the LTC6811 does not receive a valid command within 2 seconds, the watchdog timer circuit will reset the LTC6811 and the WDT pin will go high impedance.

CSB, SCK, SDI, SDO: 4-wire serial peripheral interface (SPI). Active low chip select (CSB), serial clock (SCK) and serial data in (SDI) are digital inputs. Serial data out (SDO) is an open drain NMOS output pin.

A0 to A3: Address Pins. These digital inputs are connected to V_{REG} or V⁻ to set the chip address for addressable serial commands.

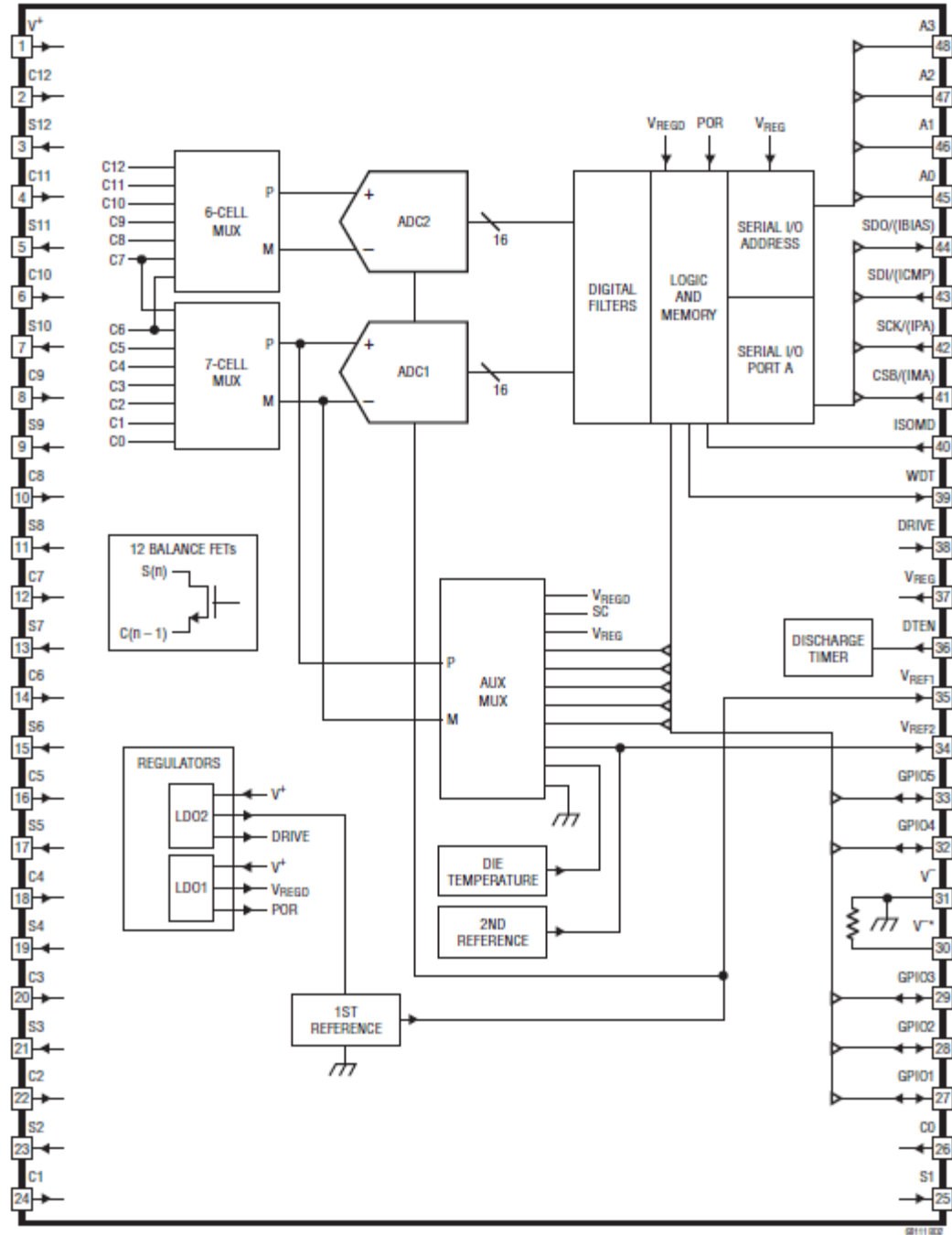


Figure 4.3 Linear Technology LTC6811-2 Block Diagram [10]

4.4.1.2 Operation States

The operation of the LTC6811 is divided in a set of separate operating states:

SLEEP State: The reference and ADCs are powered down. The watchdog timer has timed out. The discharge timer is either disabled or timed out. The supply currents are reduced to minimum levels. If a WAKEUP signal is received, the LTC6811 will enter the STANDBY state.

STANDBY State: The reference and the ADCs are off. The watchdog timer and/or the discharge timer is running. When a valid ADC command is received or the REFON bit is set to 1 in the Configuration Register Group, the IC pauses for a certain time interval to allow for the reference to power up and then enters either the REFUP or MEASURE state. Otherwise, if no valid commands are received for that time (when both the watchdog and discharge timer have expired), the LTC6811 returns to the SLEEP state. If the discharge timer is disabled, only the watchdog timer is relevant.

REFUP State: To reach this state the REFON bit in the Configuration Register Group must be set to 1. The ADCs are off, while the reference is powered up so that the LTC6811 can initiate ADC conversions more quickly than from the STANDBY state. When a valid command is received, the IC goes to the MEASURE state to begin the conversion. Otherwise, the LTC6811 will return to the STANDBY state when the REFON bit is set to 0, either manually or automatically when the watchdog timer expires.

MEASURE State: The LTC6811 performs ADC conversions in this state. The reference and ADCs are powered up. After the ADC conversions are complete, the LTC6811 will transition to either the REFUP or STANDBY state, depending on the REFON bit. Additional ADC conversions can be initiated more quickly by setting REFON bit to 1, to take advantage of the REFUP state.

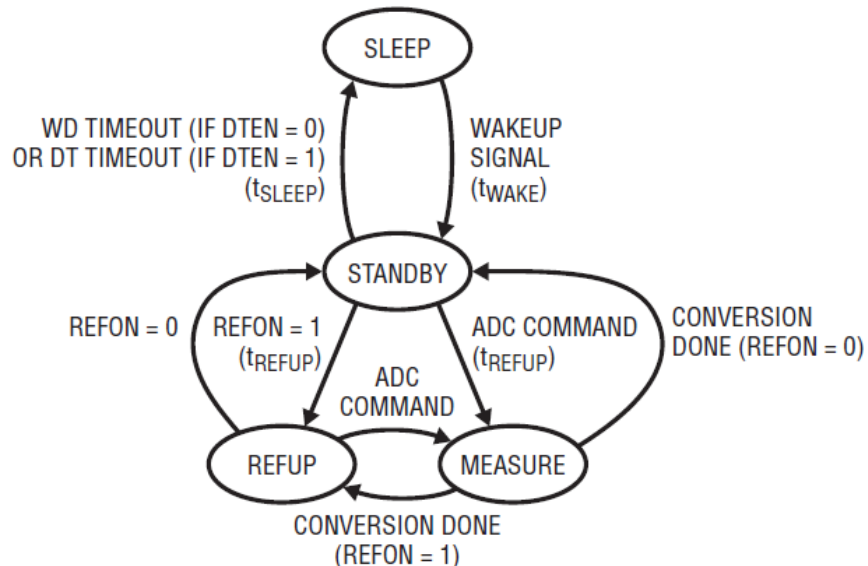


Figure 4.4 LTC6811-2 Operation State Diagram [10]

When there is no valid command for more than 2 seconds, the watchdog timer expires. This resets the contents of the IC's memory, regarding its Configuration Register Group. The watchdog timer is always enabled and it resets after every valid command with matching command packet error code. The discharge timer is used to keep the discharge switches turned on for a programmable time duration. If the discharge timer is being used, the discharge switches are not turned off when the watchdog timer is activated. This enables the IC to enter sleep mode, while the discharge circuitry is still on, reducing its power consumption.

4.4.1.3 ADC Converter

There are two ADCs inside the LTC6811. The two ADCs operate simultaneously when measuring twelve cells. Only one ADC is used to measure the general-purpose inputs. The following discussion uses the term ADC to refer to one or both ADCs, depending on the operation being performed.

The ADCOPT bit in the Configuration Register Group and the mode selection bits MD [1:0] in the conversion command together provide eight modes of operation for the ADC, which correspond to different oversampling ratios. The accuracy and timing of these modes are summarised in the following table. In each mode, the ADC first measures the inputs and then performs a calibration of each channel. The names of the modes are based on the -3dB bandwidth of the ADC measurement.

MODE	-3dB FILTER BW	-40dB FILTER BW	TME SPEC AT 3.3V, 25°C	TME SPEC AT 3.3V, -40°C, 125°C
27kHz (Fast Mode)	27kHz	84kHz	±4.7mV	±4.7mV
14kHz	13.5kHz	42kHz	±4.7mV	±4.7mV
7kHz (Normal Mode)	6.8kHz	21kHz	±1.2mV	±2.2mV
3kHz	3.4kHz	10.5kHz	±1.2mV	±2.2mV
2kHz	1.7kHz	5.3kHz	±1.2mV	±2.2mV
1kHz	845Hz	2.6kHz	±1.2mV	±2.2mV
422Hz	422Hz	1.3kHz	±1.2mV	±2.2mV
26Hz (Filtered Mode)	26Hz	82Hz	±1.2mV	±2.2mV

Table 4 LTC6811-2 ADC Mode Options Comparison

Mode 7kHz (Normal): In this mode, the ADC has high resolution and low total measurement error. This is considered the normal operating mode because of the optimum combination of speed and accuracy.

Mode 27kHz (Fast): In this mode, the ADC has maximum throughput but has some increase in the total measurement error. So, this mode is also referred as the fast mode.

Mode 26Hz (Filtered): In this mode, the ADC digital filter -3dB frequency is lowered to 26Hz by increasing the oversampling ratio. This mode is also referred to as the filtered mode due to its low -3dB frequency.

The other operating modes provide additional options for the ADC digital filter -3dB frequency. The accuracy of these modes is similar to the accuracy of the normal mode.

The measurement of cell voltages is controlled by a single command, which has options to select the number of cells to measure as well as the desired ADC mode. The measurement of the sum of the cell voltages is also possible, using a similar command. The measurements are stored in memory, in the Cell Voltage Register Groups.

Whenever the cell voltage inputs are measured, the results are compared to undervoltage and overvoltage thresholds that are stored in the IC's memory. If the reading of a cell is above the overvoltage limit, a bit in memory is set as flag. Similarly, measurement results lower than the undervoltage limit cause a flag to be set. The overvoltage and undervoltage thresholds are stored in the Configuration Register Group while the flags are stored in the Status Register Group.

A similar command is used for the measurement of the GPIO ports of the IC. Again, there are options regarding the number of GPIO to be measured as well as the desired ADC mode. The measurement of the reference voltage is also possible with the same command. The GPIOs are commonly used for the measurement of battery temperature sensors. The readings are stored in memory, in the Auxiliary Register Groups. The synchronous measurement of the cell voltages and GPIO ports is also possible with a single command, allowing consistent and time-stamped data collection.

4.4.1.4 Cell Balancing

With passive balancing, if one cell in a series stack becomes overcharged, an S output can slowly discharge this cell by connecting it to a resistor. Each S output is connected to an internal N-channel MOSFET with a maximum on resistance of 25Ω . The internal switches (MOSFETs) S1 through S12 can be used to passively balance cells with balancing current of 60mA or less. For applications that require balancing currents above 60mA, the S outputs can be used to control external transistors. The LTC6811 includes an internal pull-up PMOS transistor with a 1k series resistor. The S pins can act as digital outputs suitable for driving the gate of an external MOSFET.

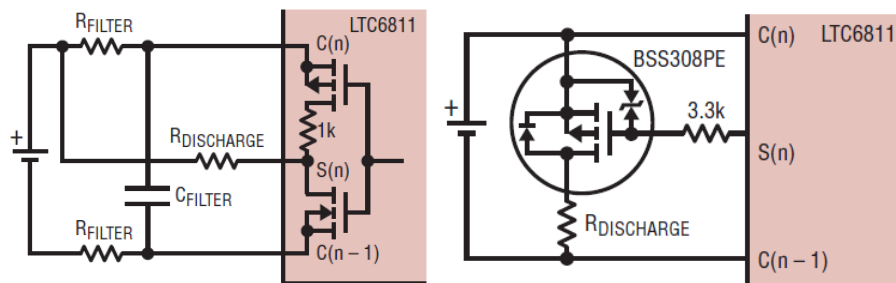


Figure 4.5 LTC6811-2 Cell Balancing Circuit

If the discharge permitted (DCP) bit is high at the time of a cell measurement command, the S pin discharge states do not change during cell measurements. If the DCP bit is low, S pin discharge states will be disabled while the corresponding cell or adjacent cells are being measured. If using an external discharge transistor, the relatively low $1k\Omega$ impedance of the internal LTC6811 PMOS transistors should allow the discharge currents to fully turn off before the cell measurement.

4.4.1.5 External Temperature Sensors

Figure 4.6 shows the typical biasing circuit for a negative temperature coefficient (NTC) thermistor. The 10k at 25°C is the most popular sensor values and the $V_{\text{REF}2}$ output stage is designed to provide the current required to bias several of these probes. The biasing resistor is selected to correspond to the NTC value so the circuit will provide 1.5V at 25°C ($V_{\text{REF}2}$ is 3V nominal). The overall circuit response is approximately $-1\%/\text{C}$ in the range of typical cell temperatures, as shown in figure 4.6.

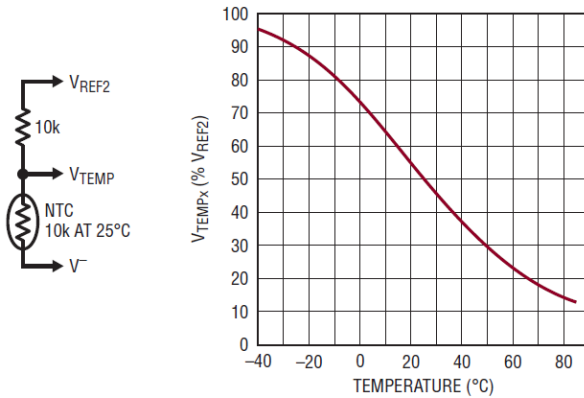


Figure 4.6 LTC6811-2 External Temperature Probe Reading

4.4.2 Microcontroller

The STM8AF5288 is the selected microcontroller for our application. The STM8AF528x is an automotive 8-bit microcontroller family. They offer 32kByte up to 128kByte of non-volatile memory and integrated data EEPROM. The devices provide the following benefits: reduced system cost, performance and robustness, short development cycles and product longevity. The STM8AF52 series also features a CAN interface.

The key features of the selected microcontroller are summarized in the table below:

Type:	STM8AF5288
Temperature Range:	-25 °C to +85 °C
Package Type:	LQFP-48
CPU Core:	Advanced STM8A core with Harvard architecture and 3-stage pipeline
Clock Frequency:	Max. 24MHz
Flash Memory:	64 KByte
RAM:	6 KByte
Core Voltage:	1.8V
Digital I/O Voltage:	5V
AD Reference:	5V
AD Channels:	16
CAN Interface:	High speed 1 Mbit/s CAN 2.0B interface
SPI Interface:	SPI interface up to 10 Mbit/s

Table 5 ST Microelectronics STM8AF5288 General Characteristics

The low cost and high performance, combined with the integrated CAN interface were the key factors that led to the choice of the specific microcontroller for our applications. Furthermore, the lack of need of a complex peripheral circuit for its proper functionality, makes it especially effective in our design, where circuit board space saving plays a significant cost factor. A variety of free software development and programming tools are also available, reducing the software development and debugging time.

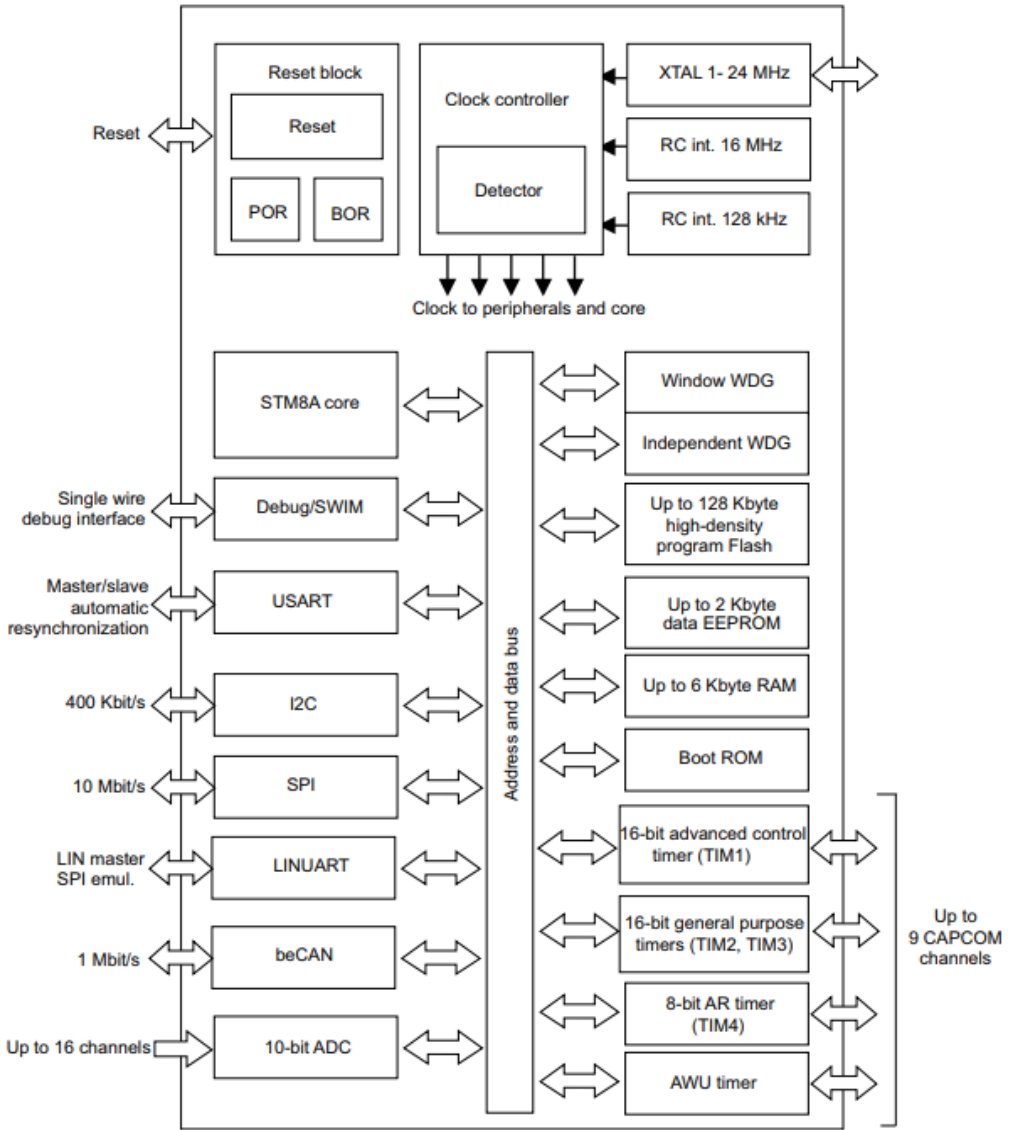


Figure 4.7 ST Microelectronics STM8AF5288 Block Diagram [11]

4.4.2.1 Programming and Debugging

The programming and debugging of the microcontroller is implemented through the single wire interface module (SWIM). The single wire interface module, together with an integrated debug module, permits non-intrusive, real time in-circuit debugging and fast memory programming. The device can be activated in all device operation modes and can be connected to a running device (hot plugging). The maximum data transmission speed is 145bytes/ms.

The non-intrusive debugging module features a performance close to a full-scale emulator. Besides memory and peripheral operation, CPU operation can also be monitored in real-time by means of shadow registers. Read and write operations of RAM and peripheral registers is available in real-time, while read/write operations of all resources are possible when the application is stopped.

4.4.3 Isolated Flyback Converter

The isolated flyback converter topology is based on the Linear Technology LT8302 monolithic isolated flyback converter control IC. The LT8302 is a current mode switching regulator IC designed especially for the isolated flyback topology. By sampling the isolated output voltage directly from the primary-side flyback waveform, the part requires no third winding or optoisolator for regulation. The output voltage is programmed with two external resistors and a third optional temperature compensation resistor. A 3.6A, 65V MOS power switch is integrated along with all the high voltage circuitry and control logic into a single package. The LT8302 operates from an input voltage range of 2.8V to 42V and delivers up to 18W of isolated output power [12].

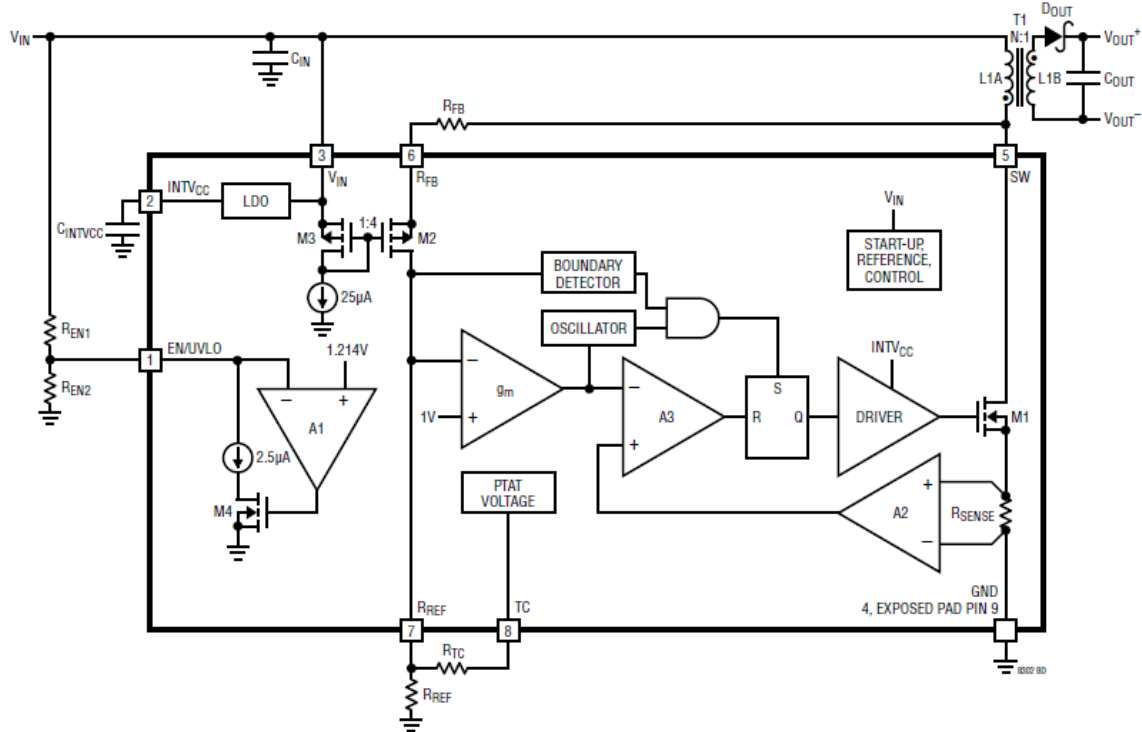


Figure 4.8 Linear Technology LT8302 Block Diagram [12]

4.4.3.1 Design Methodology

The design considerations and steps for implementing a flyback converter topology using the LT8302 are presented in the following [12]:

- **Output Voltage**

The R_{FB} and R_{REF} resistors as depicted in the block diagram are external resistors used to program the output voltage. The LT8302 operates similar to traditional current mode switchers, except in the use of a unique flyback pulse sense circuit and a sample-and-hold error amplifier, which sample and therefore regulate the isolated output voltage from the flyback pulse.

The equation for the output voltage V_{OUT} , is given in terms of the R_{FB} and R_{REF} resistors, transformer turns ratio N_{PS} , and diode forward voltage V_F :

$$V_{OUT} = V_{REF} \left(\frac{R_{FB}}{R_{REF}} \right) \left(\frac{1}{N_{PS}} \right) - V_F \quad (1)$$

- **Output Temperature Compensation**

The first term in the V_{OUT} equation does not have temperature dependence, but the output diode forward voltage, V_F , has a significant temperature coefficient, which produces approximately 200mV to 300mV voltage variation on the output across temperature. To compensate the negative temperature coefficient of the output diode, a resistor R_{TC} , connected between the TC and R_{REF} pins generates a current proportional to temperature.

With the R_{TC} resistor in place, the output voltage equation is revised as follows:

$$V_{OUT} = V_{REF} \left(\frac{R_{FB}}{R_{REF}} \right) \left(\frac{1}{N_{PS}} \right) - V_F(TO) - \left(\frac{\delta V_{TC}}{\delta T} \right) (T - TO) \left(\frac{R_{FB}}{R_{TC}} \right) \left(\frac{1}{N_{PS}} \right) - \left(\frac{\delta V_F}{\delta T} \right) (T - TO) \quad (2)$$

Where,

- TO = Room Temperature 25°C
- $\left(\frac{\delta V_F}{\delta T} \right)$ = Output diode forward voltage temperature coefficient
- $\left(\frac{\delta V_{TC}}{\delta T} \right) = 3.35mV/\text{°C}$

To cancel the output diode temperature coefficient, the following two equations should be satisfied:

$$V_{OUT} = V_{REF} \left(\frac{R_{FB}}{R_{REF}} \right) \left(\frac{1}{N_{PS}} \right) - V_F(TO) \quad (3)$$

$$\left(\frac{\delta V_{TC}}{\delta T} \right) \left(\frac{R_{FB}}{R_{TC}} \right) \left(\frac{1}{N_{PS}} \right) = - \left(\frac{\delta V_F}{\delta T} \right) \quad (4)$$

- **R_{REF}, R_{FB}, R_{TC} Resistor Selection**

The LT8302 uses a unique sampling scheme to regulate the isolated output voltage which contains repeatable delays and error sources. Therefore, a simple re-evaluation process is recommended for selecting resistor values.

A rearrangement of the expression for V_{OUT} in the previous section yields the starting value for R_{FB} :

$$R_{FB} = \frac{R_{REF} N_{PS} (V_{OUT} + V_F(TO))}{V_{REF}} \quad (5)$$

The equation shows that the R_{FB} resistor value is independent of the R_{TC} resistor value. The R_{REF} resistor value should be approximately 10k because the LT8302 is trimmed and specified using this value.

First, build and power up the application with the starting R_{REF} and R_{FB} values without the R_{TC} resistor yet, and measure the regulated output voltage, $V_{OUT(MEAS)}$. The new R_{FB} value can be adjusted to:

$$R_{FB(NEW)} = \frac{V_{OUT}}{V_{OUT(MEAS)}} R_{FB} \quad (6)$$

Secondly, with a new R_{FB} resistor value selected, the output diode temperature coefficient in the application must be taken into consideration to determine the R_{TC} value. Extrapolating data from a diode data sheet and with at least two data points spreading across the operating temperature range, the output diode temperature coefficient can be determined by:

$$-\left(\frac{\delta V_F}{\delta T}\right) = \frac{V_{OUT}(T1) - V_{OUT}(T2)}{T1 - T2} \quad (7)$$

An exact R_{TC} value can be selected, using the output diode temperature coefficient, using the following equation:

$$R_{TC} = \frac{\left(\frac{\delta V_{TC}}{\delta T}\right)}{-\left(\frac{\delta V_F}{\delta T}\right)} \left(\frac{R_{FB}}{N_{PS}}\right) \quad (8)$$

- **Transformer Primary Inductance Requirement**

The LT8302 obtains output voltage information from the reflected output voltage on the SW pin. The conduction of secondary current reflects the output voltage on the primary SW pin. In order to ensure proper sampling, the secondary winding needs to conduct current for a minimum of 350ns. The following equation gives the minimum value for primary-side magnetizing inductance:

$$L_{PRI} \geq \frac{t_{OFF(MIN)} N_{PS} (V_{OUT} + V_F)}{I_{SW(MIN)}} \quad (9)$$

Where,

- $t_{OFF(MIN)}$ = Minimum Switch-off Time = 350ns (Typical)
- $I_{SW(MIN)}$ = Minimum switch current limit = 0.87A (Typical)

In addition to the primary inductance requirement for the minimum switch-off time, the LT8302 has minimum switch-on time that prevents the chop from turning on the power switch shorter than approximately 160ns. Therefore, the following equation relating to maximum input voltage must also be followed in selecting primary-side magnetizing inductance:

$$L_{PRI} \geq \frac{t_{ON(MIN)} V_{IN(MAX)}}{I_{SW(MIN)}} \quad (10)$$

Where,

- $t_{ON(MIN)}$ = Minimum Switch-on Time = 160ns (Typical)

In general, it is advised to choose a transformer with its primary magnetizing inductance about 40% to 60% larger than the minimum values calculated above.

Transformer specification and design is perhaps the most critical part of successfully applying the LT8302. It should be considered that Linear Technology has worked with several leading magnetic component manufacturers to produce pre-designed flyback transformers to use with the LT8302.

- **Transformer Turns Ratio**

The choice of an R_{FB}/R_{REF} resistor ratio to set the output voltage, gives relative freedom in selecting a transformer turns ratio to suit a certain application. Typically, the transformer turns ratio shall be chosen to maximize the available output power. However, it should be noted that the SW pin sees a voltage that is equal to the maximum input supply voltage plus the output voltage multiplied by the turns ratio. In addition, leakage inductance will cause voltage spikes ($V_{LEAKAGE}$) on top of the reflected voltage. This total quantity needs to remain below the 65V absolute maximum rating of the SW pin to prevent internal breakdown.

These conditions place an upper limit on the turns ratio, N_{PS} , for a given application:

$$N_{PS} < \frac{65V - V_{IN(MAX)} - V_{LEAKAGE}}{V_{OUT} + V_F} \quad (11)$$

- **Snubber Circuit**

Transformer leakage inductance on either the primary or secondary causes a voltage spike to appear on the primary after the power switch turns off. To clamp and damp the leakage voltage spikes, an RC+DZ snubber circuit is recommended. The RC (resistor-capacitor) snubber quickly damps the voltage spike ringing and provides great load regulation and EMI performance. The DZ (diode-Zener) ensures well defined and consistent clamping voltage to protect the SW pin from exceeding its 65V absolute maximum rating.

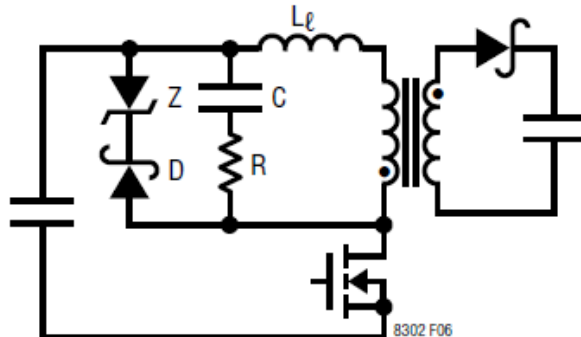


Figure 4.9 Flyback Converter Snubber Circuit

A 470pF capacitor in series with a 39Ω resistor provides a good starting point for the RC snubber circuit. For the DZ snubber, care should be taken when choosing both the diode and the Zener diode. Schottky diodes are typically the best choice. The reverse voltage rating of the diode should be higher than the maximum SW pin voltage. For the Zener diode breakdown voltage, the following equation can be used to make a suitable choice:

$$V_{ZENER(MAX)} \leq 60V - V_{IN(MAX)} \quad (12)$$

4.4.3.2 Design Calculations

This section contains the design calculation for the isolated flyback converter of our system. As we stated earlier in the requirements, the isolated flyback converter should operate from a 5V to 36V input voltage range and deliver a 12V output voltage, providing 200mA output current.

Therefore, the design parameters are the following:

$$V_{IN(MIN)} = 5V, V_{IN(NOM)} = 24V, V_{IN(MAX)} = 36V$$

$$V_{OUT} = 12V, I_{OUT} = 200mA$$

Step 1: Selection of transformer turns ratio.

$$N_{PS} < \frac{65V - V_{IN(MAX)} - V_{LEAKAGE}}{V_{OUT} + V_F}$$

Where,

$V_{LEAKAGE}$ = Margin for transformer leakage spike = 15V

V_F = Output diode forward voltage = ~0.3V

Therefore, for our application:

$$(11) \Rightarrow N_{PS} < \frac{65V - 36V - 15V}{12V + 0.3V} = 1.46 \quad (13)$$

Clearly, $N_{PS}=1$ is chosen as the turns ratio for our application.

Step 2: Primary inductance determination.

$$(9) \Rightarrow L_{PRI} \geq \frac{t_{OFF(MIN)} N_{PS} (V_{OUT} + V_F)}{I_{SW(MIN)}} = \frac{350ns \times 1 \times (12V + 0.3V)}{0.87A} = 4.9\mu H \quad (14)$$

$$(10) \Rightarrow L_{PRI} \geq \frac{t_{ON(MIN)} V_{IN(MAX)}}{I_{SW(MIN)}} = \frac{160ns \times 36V}{0.87A} = 6.62\mu H \quad (15)$$

Taking into consideration that most transformers specify primary inductance with a tolerance of $\pm 20\%$ as well as the design rule to choose a transformer with primary inductance 40% to 60% larger than the minimum values, we can conclude based on the suggested transformer list provided by Linear Technology, that the suitable transformer for our application is the 750313443 by Wurth Electronik, with primary inductance value of $L_{PRI} = 9\mu H$.

Since the primary inductance has been selected, the maximum switch current limit can be calculated as:

$$D = \text{Duty Cycle} = \frac{N_{PS}(V_{OUT} + V_F)}{N_{PS}(V_{OUT} + V_F) + V_{IN}} = \frac{1 \times (12V + 0.3V)}{1 \times (12V + 0.3V) + 24V} = 0.33 \quad (15)$$

$$I_{SW(MAX)} = \frac{2V_{OUT}I_{OUT}}{\eta V_{IN}D} = \frac{2 \times 12V \times 0.2A}{0.8 \times 24V \times 0.33} = 0.75A \quad (16)$$

Where, η = efficiency = ~0.8

Step 3: Selection of output diode.

Two main criteria for choosing the output diode include forward current rating and reverse-voltage rating. The maximum load requirement is a good first-order estimate at the average current requirement for the output diode. A conservative metric, considering also output short circuit conditions, is 6%- of the maximum switch current limit multiplied by turns ratio:

$$I_{DIODE(MAX)} = 0.6I_{SW(MAX)}N_{PS} = 0.6 \times 0.75A \times 1 = 0.45A \quad (17)$$

Next, we can calculate the reverse voltage requirement using maximum V_{IN} :

$$V_{REVERSE} = V_{OUT} + \frac{V_{IN(MAX)}}{N_{PS}} = 12V + \frac{36V}{1} = 48V \quad (18)$$

Therefore, a 3A - 60V diode is chosen as the output diode.

Step 4: Selection of output capacitor.

The output capacitor should be chosen to minimize the output voltage ripple. The capacitance value can be calculated using the following equation:

$$C_{OUT} = \frac{L_{PRI}I_{SW}^2}{2V_{OUT}\Delta V_{OUT}} = \frac{9\mu H \times (0.75A)^2}{2 \times 12V \times 0.1V} = 2.2\mu F \quad (19)$$

This capacitance value corresponds to a desired voltage ripple less than $\pm 1\%$ of V_{OUT} (100mV). Considering that ceramic capacitors can lose up to 40% of quoted capacitance with applied voltage, a 10uF, with at least 50V rating, ceramic capacitor is chosen as output capacitor.

Step 5: Design of the snubber circuit.

A 470pF capacitor in series with a 39Ω resistor is chosen as the RC snubber. For the DZ snubber, the maximum Zener breakdown voltage is set according to the maximum V_{IN} :

$$(12) \Rightarrow V_{ZENER(MAX)} \leq 60V - V_{IN(MAX)} = 60V - 36V = 24V \quad (20)$$

A 24V, 1.5W Zener from Central Semiconductor (CMZ5394B) is chosen for optimal protection and minimized power loss. A fast diode with sufficient reverse voltage breakdown shall be chosen to complete the snubber circuit:

$$V_{REVERSE} > V_{SW(MAX)} = V_{IN(MAX)} + V_{ZENER(MAX)} = 36V + 24V = 60V \quad (21)$$

A 100V, 1A diode from Diodes Inc. (DFLS1100) is chosen.

Step 6: R_{REF} and R_{FB} resistor selection.

Using the following equation, we can calculate the starting value for R_{FB} :

$$R_{REF} = 10k \quad (22)$$

$$(5) \Rightarrow R_{FB} = \frac{R_{REF}N_{PS}(V_{OUT} + V_F(TO))}{V_{REF}} = \frac{10k \times 1 \times (12V + 0.3V)}{1V} = 123k \quad (23)$$

For 1% standard resistor values, a 124k resistor is chosen.

Step 7: Adjustment of R_{FB} resistor.

Since we have not implemented the circuit yet, we are not able to actively measure the regulated output voltage. The adjustment is based on the simulation results that we are going to present in the following section. The adjusted R_{FB} resistor value is calculated by the following equation:

$$(6) \Rightarrow R_{FB(NEW)} = \frac{V_{OUT}}{V_{OUT(MEAS)}} R_{FB} = \frac{12V}{12.3V} 124k = 121k \quad (24)$$

Step 8: R_{TC} resistor selection.

Using the output diode forward voltage characteristics, we can calculate its forward voltage temperature coefficient, $\left(\frac{\delta V_F}{\delta T}\right)$, using values from different points on the temperature range:

$$(7) \Rightarrow -\left(\frac{\delta V_F}{\delta T}\right) = \frac{V_{OUT}(T1) - V_{OUT}(T2)}{T1 - T2} \cong \frac{12.2V - 12.4V}{85^{\circ}C - 25^{\circ}C} = -\frac{3.3mV}{^{\circ}C} \quad (25)$$

The value of the R_{TC} resistor is given by the following equation:

$$(8) \Rightarrow R_{TC} = \frac{\left(\frac{\delta V_{TC}}{\delta T}\right)}{-\left(\frac{\delta V_F}{\delta T}\right)} \left(\frac{R_{FB}}{N_{PS}}\right) = \frac{\frac{3.35mV}{^{\circ}C}}{\frac{3.3mV}{^{\circ}C}} \left(\frac{121k}{1}\right) = 113k \quad (26)$$

4.4.3.3 Circuit Presentation

The desired converter topology, derived by the calculations above is presented in the following figure:

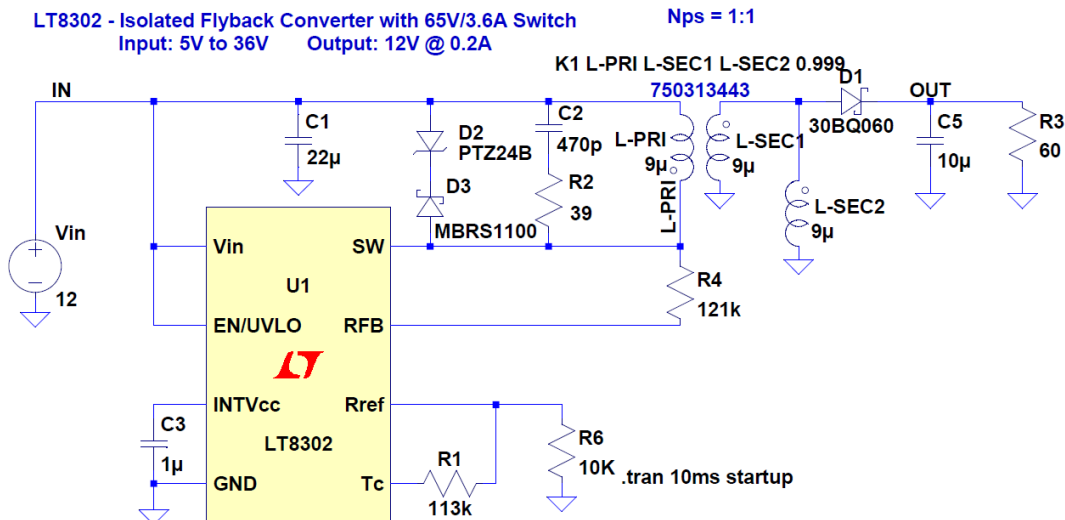


Figure 4.10 Isolated Flyback Converter Topology

The circuit was simulated using Linear Technology's LTspice simulator, schematic capture and waveform viewer. The LT8302 circuit model library is provided by Linear Technology. The diodes

used in the simulation were selected by the component library that is supported by LTspice. Nevertheless, they have equivalent characteristics to those that were derived by the design calculations. The simulation circuit is shown in the following diagram:

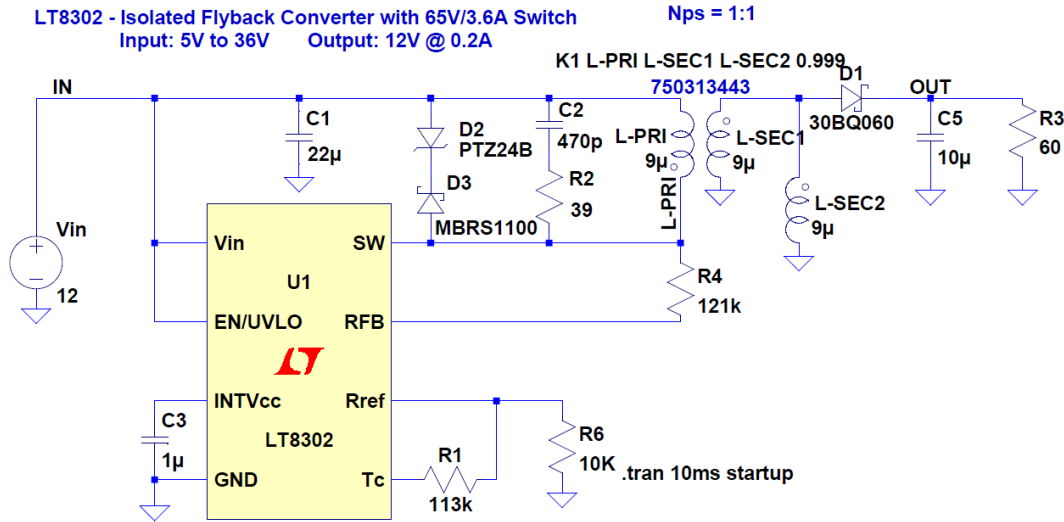


Figure 4.11 Isolated Flyback Converter LTspice Simulation Model

The output voltage and current waveforms, with 12V input voltage and 200mA resistive load, are presented in the following figure:

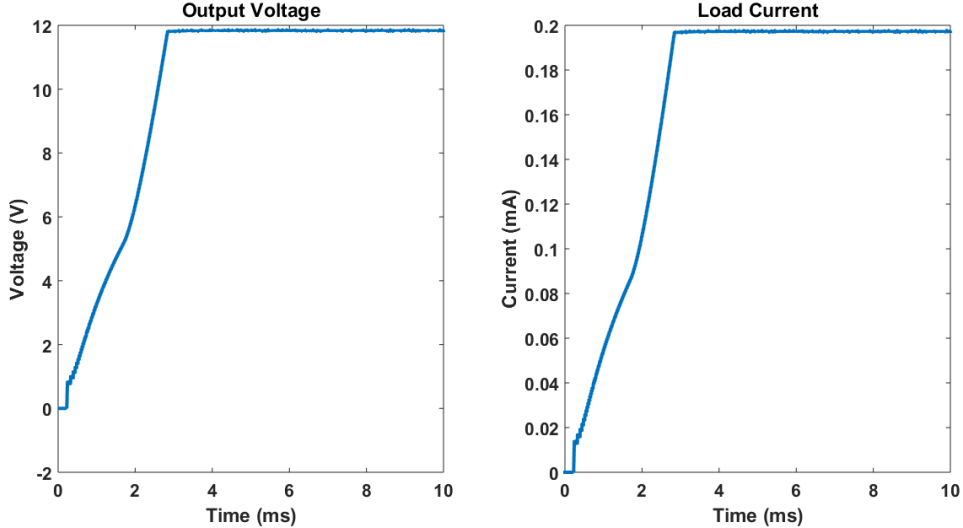


Figure 4.12 Isolated Flyback Converter Simulation Results

As we can observe, the circuit is functioning properly, and meets its design requirements. Therefore, we can safely conclude that the design calculations performed in the previous section, provided the desired isolated flyback converter topology.

4.4.4 Step-Down Regulator

The step-down regulator topology is based on Linear Technology's LT3990 monolithic buck switching regulator control IC. The LT3990 is a constant frequency, current mode step-down regulator that accepts a wide input voltage range up to 62V. A high efficiency switch is included on the IC along with the catch diode, boost diode, and the necessary oscillator, control and logic circuitry. The part is able to provide up to 350mA output current and consumes only 2uA at a nominal input voltage of 12V [13].

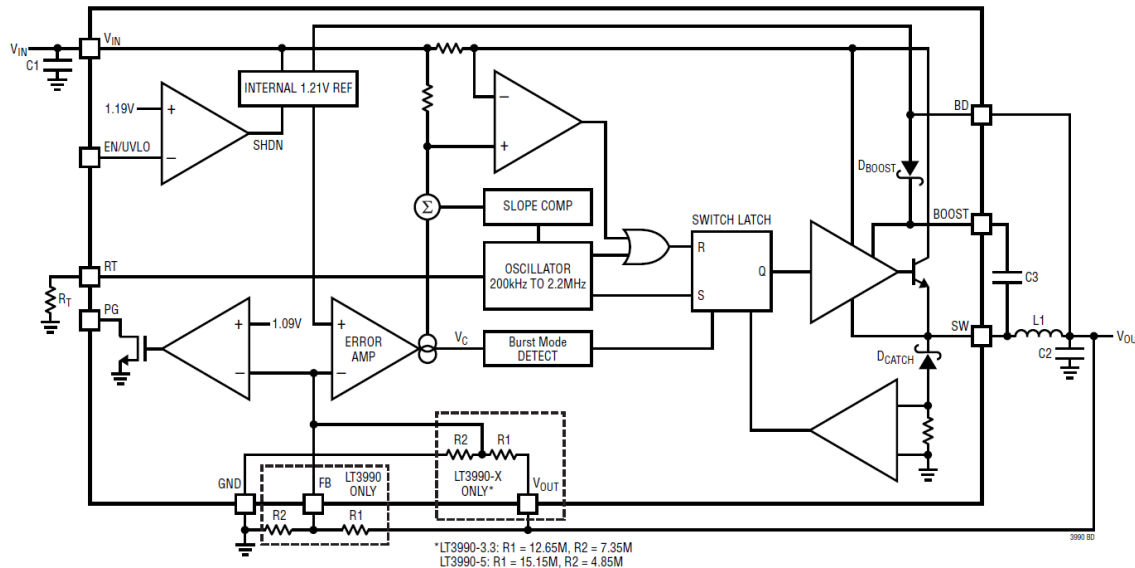


Figure 4.13 Linear Technology LT3990 Block Diagram [13]

4.4.4.1 Design Methodology

The design considerations and steps for implementing a buck regulator topology using the LT3990 are presented in the following [13]:

- **FB Resistor Network**

The output voltage is programmed with a resistor divider between the output and the FB pin. The resistors should be chosen according to:

$$R1 = R2 \left(\frac{V_{OUT}}{1.21} - 1 \right) \quad (27)$$

- **Setting the Switching Frequency**

The LT3990 uses a constant frequency PWM architecture that can be programmed to switch from 200kHz to 2.2MHz by using a resistor tied from the RT pin to ground. A reference table providing the necessary RT resistor values for different switching frequencies is provided by Linear Technology.

The selection of the operating frequency is a trade-off between efficiency, component size, minimum dropout voltage and maximum input voltage. The advantage of high frequency operation is that smaller inductor and capacitor values may be used while the disadvantages are lower efficiency, lower maximum input voltage and higher dropout voltage. Lower switching

frequencies are necessary to achieve high V_{IN}/V_{OUT} ratios. It is evident that a good selection of switching frequency should allow adequate input voltage range and keep the inductor and capacitor values relatively small.

The highest acceptable switching frequency for a given application can be calculated as follows:

$$f_{SW(MAX)} = \frac{V_{OUT} + V_D}{t_{ON(MIN)}(V_{IN} - V_{SW} + V_D)} \quad (28)$$

Where,

- V_{IN} = Typical input voltage
- V_{OUT} = Typical output voltage
- V_D = Integrated catch diode voltage drop ($\sim 0.7V$)
- V_{SW} = Internal switch voltage drop ($\sim 0.5V$ at maximum load)
- $t_{ON(MIN)}$ = Minimum switch on-time ($\sim 160\text{ns}$)

- **Input Voltage Range**

The minimum input voltage is determined by either the LT3990's minimum operating voltage of 4.2V or by its maximum duty cycle. The minimum input voltage due to duty cycle is:

$$V_{IN(MIN)} = \frac{V_{OUT} + V_D}{1 - f_{SW}t_{OFF(MIN)}} - V_D + V_{SW} \quad (29)$$

Where,

- f_{SW} = the selected switching frequency
- $t_{OFF(MIN)}$ = Minimum switch off-time ($\sim 160\text{ns}$)

The highest allowed input voltage during normal operation is limited by minimum duty cycle and can be calculated by the following equation:

$$V_{IN(MAX)} = \frac{V_{OUT} + V_D}{f_{SW}t_{ON(MIN)}} - V_D + V_{SW} \quad (30)$$

- **Inductor Selection**

For a given input and output voltage, the inductor value and switching frequency will determine the ripple current. The ripple current increases with higher V_{IN} or V_{OUT} and decreases with higher inductance and faster switching frequency. A good starting point for the inductance value is given by the following equation, where L is in μH and f_{SW} is in MHz:

$$L = 3 \frac{V_{OUT} + V_D}{f_{SW}} \quad (31)$$

This simple design guideline may not always result in the optimum inductor selection. As a general rule, lower output voltages and higher switching frequency will require smaller inductor

values. If the application requires less than 350mA load current, then a lesser inductor value than the one calculated may be acceptable. However, low inductance may result in discontinuous mode operation, which is acceptable but reduces maximum load current.

- **Output Capacitor**

The output capacitor has two essential functions. The first function is that it stores energy in order to satisfy transient loads and stabilize the LT3990's control loop. Ceramic capacitors are the preferred choice, since they have very low equivalent series resistance (ESR) and provide the best ripple performance. A good starting capacitance value is given by the following equation, where f_{SW} is in MHz and C_{OUT} is in μF :

$$C_{OUT} = \frac{50}{V_{OUT}f_{SW}} \quad (32)$$

A lower value of output capacitor can be used to save space and cost but transient performance will degrade.

The second function is that the output capacitor, along with the inductor, filters the square wave generated by the LT3990 to produce the DC output. In this role, it determines the output ripple, so low impedance at the switching frequency is important. When choosing a capacitor, care must be taken when looking at the data sheets to find out the actual capacitance under operating conditions (applied voltage, temperature). A physically larger capacitor or one with a higher voltage rating may be required.

4.4.4.2 Design Calculations

This section contains the design calculation for the step-down regulator of our system. As we stated earlier in the requirements, the regulator should operate from a 9V to 52V input voltage range and deliver a 5V output voltage, providing 250mA output current.

Therefore, the design parameters are the following:

$$V_{IN(MIN)} = 9V, V_{IN(NOM)} = 12V, V_{IN(MAX)} = 52V$$

$$V_{OUT} = 5V, I_{OUT} = 250mA$$

Step 1: Setting output voltage and switching frequency.

Since the desired output voltage is 5V, the LT3990-5 model will be used, which features the output voltage resistor divider integrated in the package and is specifically designed for 5V application. The switching frequency is set at 400kHz. Therefore, there is no need for additional calculations regarding these design parameters.

$$f_{SW} = 400kHz \quad (33)$$

Step 2: Input voltage range.

Under normal operating conditions the step-down regulator will be supplied by the 12V output of the isolated flyback converter. However, when the auxiliary supply is turned off, the

regulator will be directly supplied by the battery module (~50V). So, it is necessary to verify if this V_{IN}/V_{OUT} is available by the selected switching frequency:

$$(30) \Rightarrow V_{IN(MAX)} = \frac{V_{OUT} + V_D}{f_{SW} t_{ON(MIN)}} - V_D + V_{SW} = \frac{5V + 0.7V}{400kHz \times 160ns} - 0.7V + 0.5V = 88.85V \quad (34)$$

Therefore, the upper voltage limit is satisfied. Since the lower voltage limit is higher than the minimum operating voltage of the LT3990, we can safely conclude that the lower voltage limit of our application is satisfied as well. So, the selected topology covers the input voltage requirements of our system.

Step 3: Inductor Selection

As we mentioned in the previous section, a good reference starting point for the inductor value is:

$$(31) \Rightarrow L = 3 \frac{V_{OUT} + V_D}{f_{SW}} = 3 \frac{5V + 0.7V}{0.4MHz} = 42.75\mu H \quad (35)$$

Since the maximum load current requirement for our application is 250mA, we may be able to use a smaller inductance value. Examining a reference design by Linear Technology for a similar 5V application, a $33\mu H$ inductor is selected, so that we can minimize the physical size of the inductor. After we obtain simulation results for this topology, we will be able to decide if this is an acceptable inductor value for our system.

Step 4: Output Capacitor

As we mentioned in the previous section, a good reference starting point for the capacitor value is:

$$(32) \Rightarrow C_{OUT} = \frac{50}{V_{OUT} f_{SW}} = \frac{50V}{5V \times 0.4MHz} = 25\mu F \quad (36)$$

For 1% standard capacitor values, a $22\mu F$ capacitor is chosen.

4.4.4.3 Circuit Presentation

The desired buck regulator topology, derived by the calculations above is presented in the following figure:

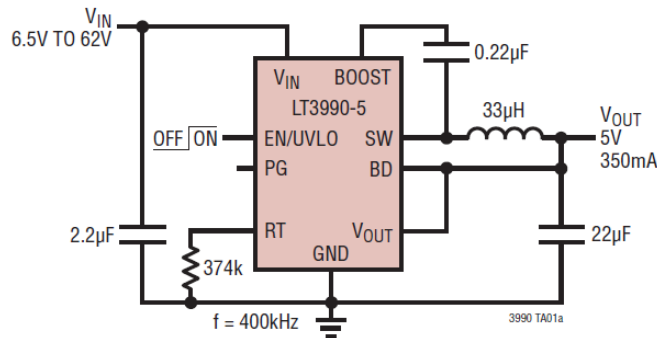


Figure 4.14 Step-Down Regulator Topology

As with the isolated flyback converter, the circuit was simulated using Linear Technology's LTspice. The LT3990-5 circuit model library is not provided by Linear Technology. However, the adjustable output voltage model of the same family, LT3990 is available. Therefore, the R1 and R2 resistor divider sets the output voltage level of 5V. The simulation circuit is shown in the following diagram:

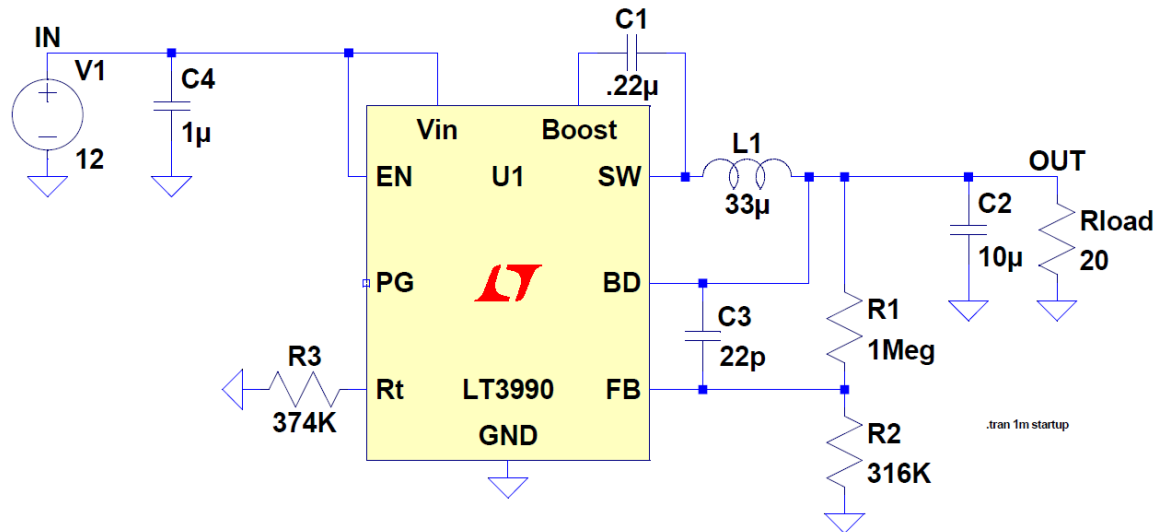


Figure 4.15 Step-Down Regulator LTspice Simulation Model

The output voltage and current waveforms, with 12V input voltage and 250mA resistive load, are presented in the following figures:

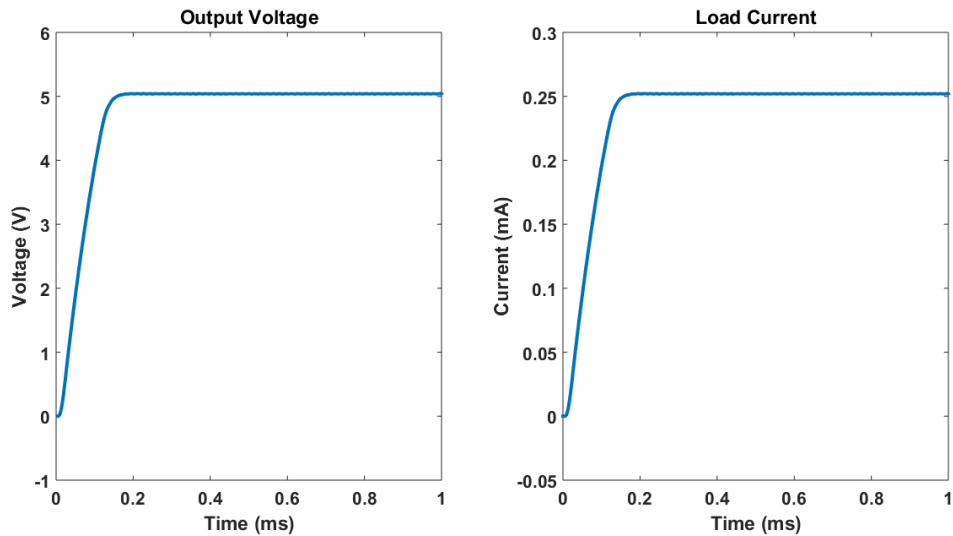


Figure 4.16 Step-Down Regulator Simulation Results - 1

It is evident by the simulation results, that the circuit functioning within its specifications. The next figures, illustrate the circuit behavior, when the input voltage is 52V, representing the battery module:

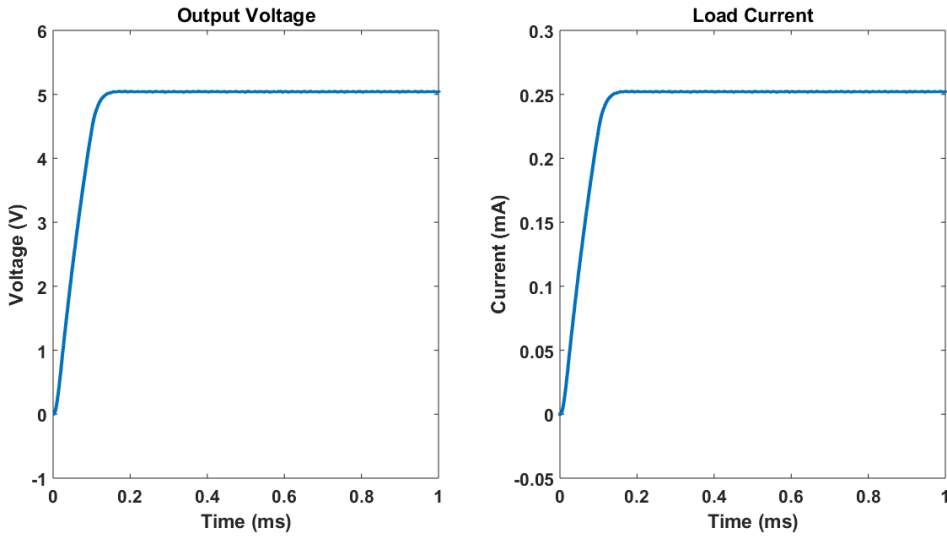


Figure 4.17 Step-Down Regulator Simulation Results - 2

As we can observe, the circuit has equivalent behaviour within its specified input voltage operating range. Therefore, we can safely conclude that the design calculations performed in the previous sections, provided the desired step-down regulator topology.

4.4.5 CAN Transceiver

The ADM3054 by Analog Devices was chosen as the CAN transceiver for our system. The ADM3054 is a 5KV rms signal isolated controller area network (CAN) physical layer transceiver. The device combines a 3-channel isolator and a CAN transceiver into a single package. It is compliant with the ISO 11898 standard and is also qualified for automotive applications [14].

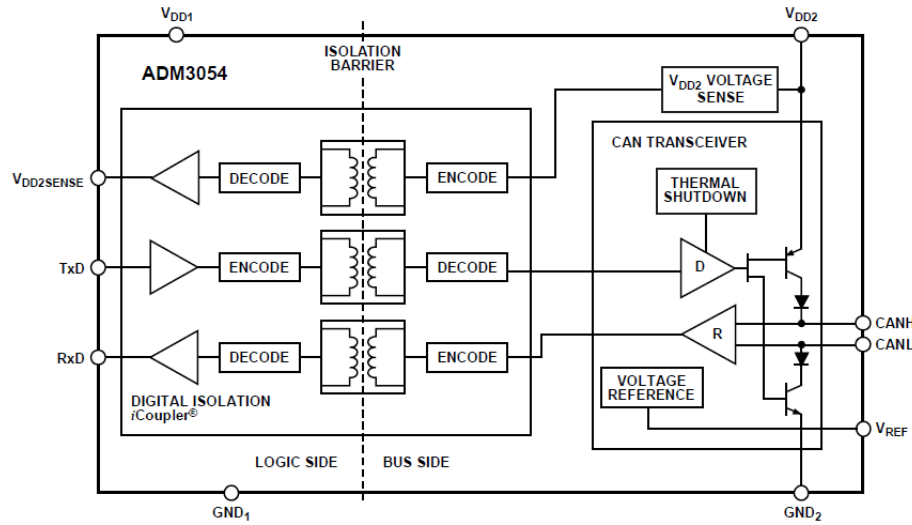


Figure 4.18 Analog Devices AD3054 Block Diagram [14]

The logic side of the device can be powered by a 3.3V or 5V supply while the bus side can be powered only by a 5V supply. Another feature is that loss of power on the bus side can be detected, and also signalled by an integrated sense signal output. The ADM3054 creates an isolated interface between the CAN protocol controller and the physical layer bus and it is capable

of running at data rates up to 1Mbps. The device has integrated protection against shorts to power/ground in the bus pins as well as current-limiting and thermal shutdown features.

4.4.6 Power Supply Switch

For the power supply switch, a standard load switch topology was used to effectively control the transition of the system from the primary to the secondary power supply. The load switch can be controlled by a microcontroller digital output and connects or disconnects a voltage rail to a specific load. It is comprised by two main elements, the pass transistor and the on/off control block, as shown in the following figure.

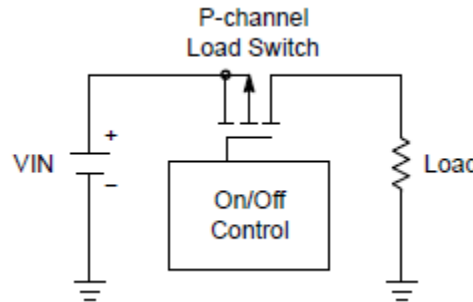


Figure 4.19 Load Switch Simplified Topology

The pass transistor is most commonly a MOSFET that passes the voltage supply to a specified load when the transistor is on. The selection of a P-channel or N-channel load switch depends on the specific needs of the application. The P-channel MOSFET has a distinct advantage over the N-channel MOSFET, and that is in the simplicity of the on/off control block. The N-channel load switch requires an additional voltage rail for the gate, while the P-channel load switch does not. When using a P-channel MOSFET in a load switch circuit, the source is directly connected to the input voltage rail and the drain is connected to the load. In order for the load switch to turn on the source to gate voltage must be greater than the threshold voltage. Therefore:

$$V_{IN} \geq V_G + V_{TH} \quad (37)$$

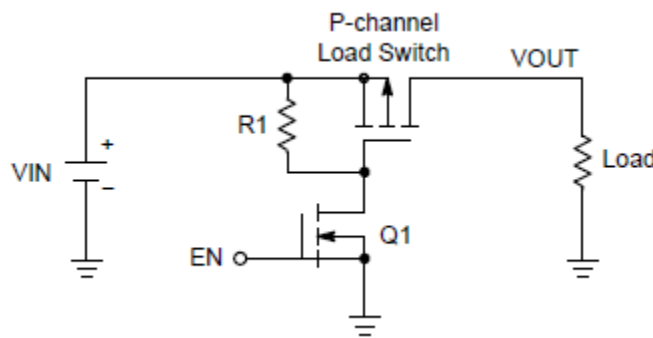


Figure 4.20 P-channel MOSFET Load Switch Circuit

The figure above shows an example load switch control circuit for a P-channel pass transistor. A logic signal (EN) from the system's control circuit (e.g. microcontroller) turns the load switch on and off via a small signal NMOS transistor Q_1 . When EN is in logic low, Q_1 is off and the gate of

the P-channel MOSFET is pulled up to VIN. When EN is in logic high, Q1 turns on, the pass transistor gate is pulled to ground, and the load switch turns on. As long as the input voltage rail is higher than the threshold voltage of the PMOS transistor, it will turn on when EN is high without the need of additional voltage source. The resistor R1 is selected so that millamps of current or less flow through R1 when Q1 is on. A standard range is $1\text{k}\Omega - 10\text{k}\Omega$.

4.4.6.1 Circuit Presentation

The power supply switch topology is illustrated in the following figure. The battery voltage power supply line is considered the input voltage source (VIN), as described in the previous section, while the rest of the system is considered as the switch's load.

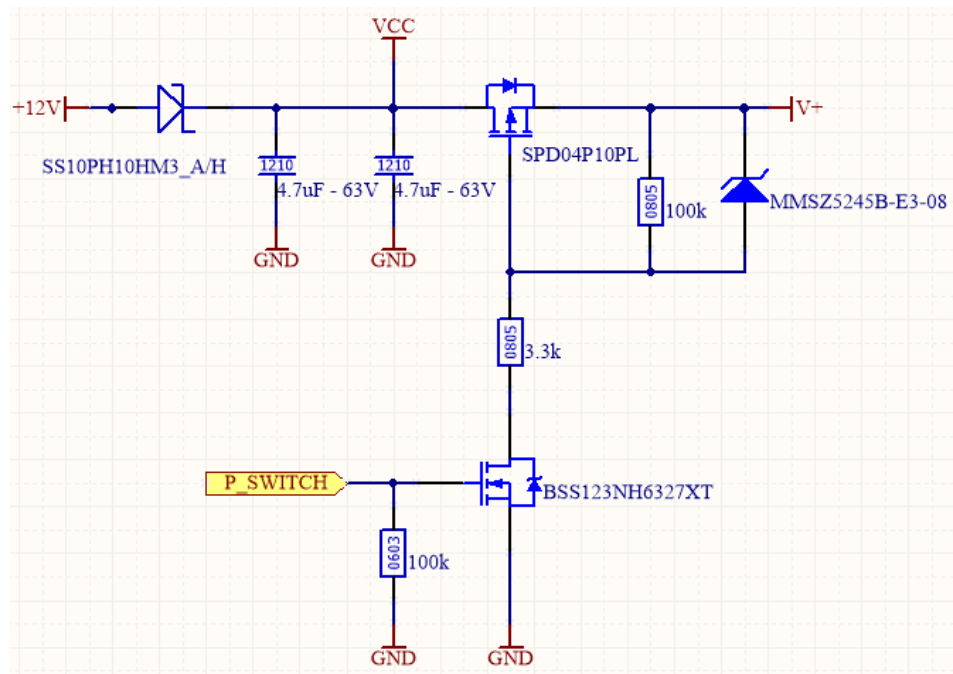


Figure 4.21 Power Supply Switch Circuit

The $3.3\text{k}\Omega$ resistor is used to control the turn-on speed of the switch. The R1 and R2 resistors form a voltage divider that determines the voltage seen at the gate of the pass transistor. An additional Zener diode, rated at the calculated gate voltage is also applied, in order to protect the circuit from voltage spikes during the transition stages of the switch. R2 is the pull-up resistor mentioned at the previous section, and its selected value is $100\text{k}\Omega$ due to the relatively high battery voltage applied to the switch.

A simulation model was created in Orcad Pspice, in order to verify the proper functionality of the switch. The simulation circuit is presented in the figure below, and was created using prototype resistor, capacitor and transistor models that were available in the Pspice libraries. Nevertheless, the MOSFETs used in the model, have equivalent voltage and current characteristics to the components that are needed for our application.

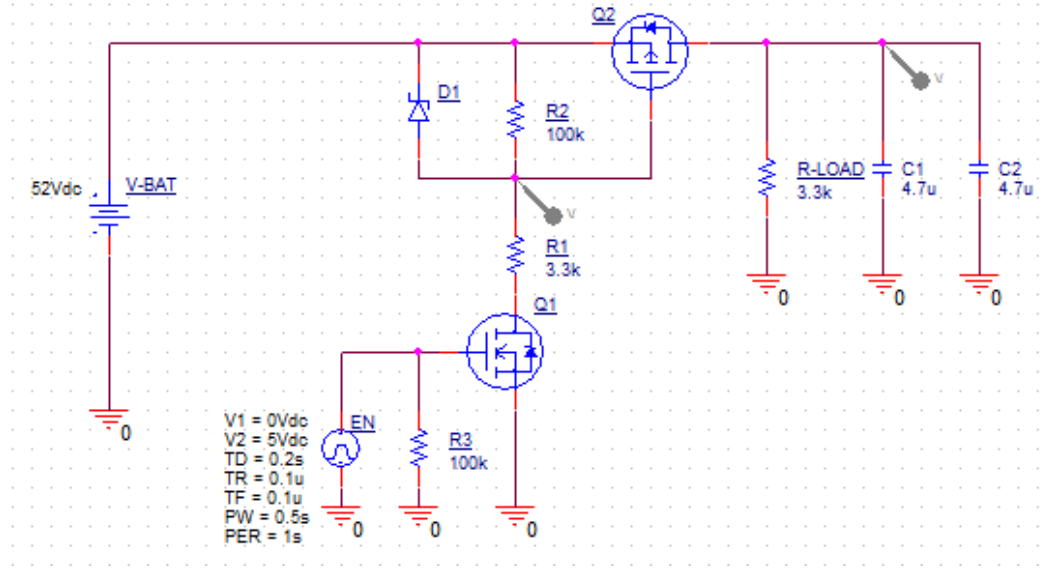


Figure 4.22 Power Supply Switch Pspice Simulation Model

The results of a transient analysis, using a $3.3\text{k}\Omega$ resistive-capacitive load are presented in the following figure.

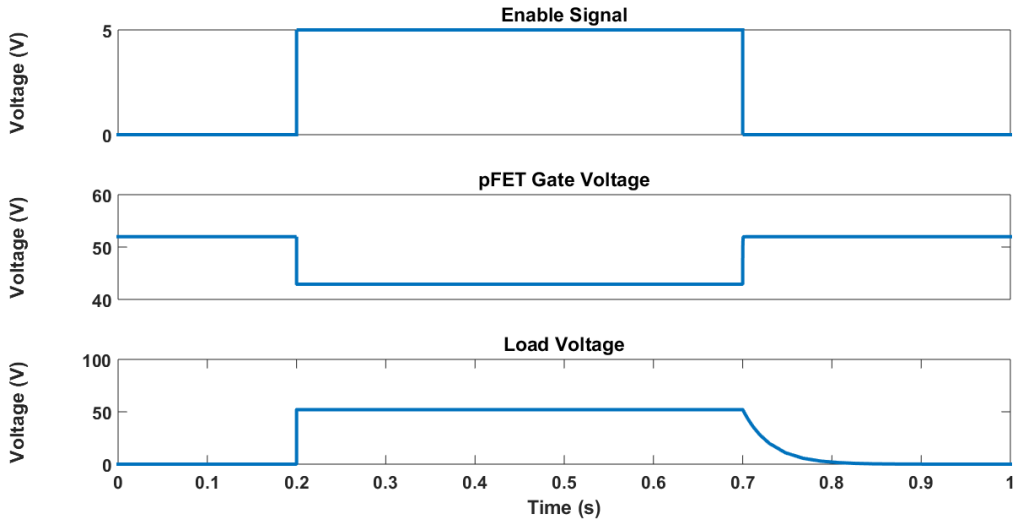


Figure 4.23 Power Supply Switch Simulation Results

5 Hardware Description

In the following sections, we are presenting the detailed schematic diagrams of the final circuit implementation, the PCB layout design guidelines that were used as well as the final 3D view of the designed board, highlighting the main points of interest. For the schematic layouts as well as the PCB layout, the Altium Designer software suite was used.

5.1 Schematic Layout

5.1.1 Monitoring & Balancing Circuit

The battery module cell voltage sense cables are connected to the board via the connector headers H100 and H101, as shown in the figure above. The header H102 is used for the cells temperature sensors. A decoupling RC filter is connected to each voltage sense line along with a series inductance. A LED indicator is placed in parallel with the balancing resistors R136-R147, which provides a visible verification of the activation of the balancing circuit.

Regarding the LTC6811, the address pins of the device (A0, A1, A2, A3) are tied to ground, and zero-ohm bypass resistors are placed in the A2 and A3 lines, to provide an easy modification of the device's address. The recommended bypass capacitors are placed on the outputs of the internal voltage regulator of the IC, and pull-up resistors are used in the watchdog and SPI data-out pin, since they are recommended by the manufacturer. Moreover, a LED indicator is connected to the DRIVE pin, which allows an easy verification of the device's state.

5.1.2 Microcontroller Circuitry

The selected microcontroller, as mentioned in the previous section, requires a few number of external components for its functionality. Namely, besides the bypass capacitors in the power supply pins, a 16MHz ceramic resonator was used as an external clock source. A resistor divider topology was implemented for the ADC readings of the board temperature sensors and of the primary power supply rail. Four LEDs were placed for debugging purposes as well as for a visible indication for various system functionalities.

The H200 header is used as the debugger/programmer connector, which provides access to the microcontroller memory and allows the on-line monitoring of its contents.

5.1.3 Power Management Circuitry

The power supply circuitry is identical to the one presented on the previous chapter. The single addition is the diode D404, which is placed between the isolated flyback converter output and the power supply switch (V-M and V+ net), in order to protect the secondary side of the transformer when the switch is activated and the battery module voltage is applied to this net. The input for the step-down regulator is the V+ net.

The H400 header is the connector for the auxiliary battery supply. A reverse polarity protection diode D400 is placed in series to the power supply input to protect the system from false connections.

5.1.4 CAN-bus Circuitry

A CAN-bus protection circuit is placed on the bus side of the CAN transceiver along with the termination resistors (R300, R301). The protection circuit consists of a common mode choke,

varistors, transient voltage suppression (TVS) diodes and bypass capacitors. The H300 header is the CAN-bus connector, carrying the CAN_H and CAN_L lines.

5.2 PCB Layout

5.2.1 PCB Technical Description

The system was implemented in a 120mm x 72mm circuit board. The board physical size was a major design goal, in order to meet the manufacturing cost requirements and also provide a versatile product solution, which can be integrated in a variety of battery container mechanical designs.

The PCB was decided to be a multilayer board and to have four layers made out of the standard FR-4 glass epoxy panel. The four layers made it possible to have a ground plane, a power plane and two signal layers. This layer structure was a very cost-effective approach in order to reduce current loops and achieve an efficient layout for the microcontroller and power converter circuits. Through-air cuts were also included in the PCB, in order to reinforce the isolation in critical parts, like the flyback transformer and CAN transceiver.

5.2.2 PCB Design Methodology

Circuit noise and disturbances are a common problem when realizing a schematic circuit layout into a PCB layout. This is mainly due to the fact that the components are not ideal and that the signal traces cannot be made infinitely short and thereby give rise to phenomena's such electromagnetic interference (EMI) because of unwanted coupling to other circuits caused by capacitive, inductive or conductive coupling. A first approach in order to minimize these unwanted effects when designing a PCB is to follow certain PCB design guidelines. These guidelines speed up the design process significantly but is necessary to investigate whether a guideline is applicable to each design case [15].

Firstly, different circuits were placed relatively far from each other in order to reduce the risk of coupling, while elements of the same circuit were placed close together to save circuit board space. The battery monitoring IC and the cell voltage filtering circuitry were placed tightly together. The power converters were placed far from the measurement circuit and the microcontroller in order to ensure that chances of noise coupling in the analog measurements and SPI communication are minimized.

A large ground plane, for the respective ground of the measuring circuit, helped to reduce the signal current loop areas since they provided the signals with a close and low-impedance path. The different power planes were placed on a single layer, while the power supply plane was placed alone in a separate layer, in order to prevent coupling between two different power buses. To furtherly minimize EMI, decoupling capacitors were placed as close to the power supply pins as possible with direct via holes to the ground plane. Furthermore, certain ground plain cut-outs were used in the proximity of high-frequency components, such as the ceramic resonator and the inductor of the step-down regulator, in order to minimize high-frequency disturbances in the ground plane.

All of the connectors onto the PCB were placed at the edges of the board in order to minimize the length of the connector cables. The SPI lines were routed on the intermediate layer, buried between power and ground planes, to minimize interaction with the rest of the circuit. The distance of the microcontroller from the battery monitoring IC and the CAN transceiver was kept as close as possible, to achieve the shortest trace length for their communication lines. For

balancing lines, 1mm trace width was used, while 0.3mm traces were used for all the other signal lines.

5.3 Circuit Board Presentation

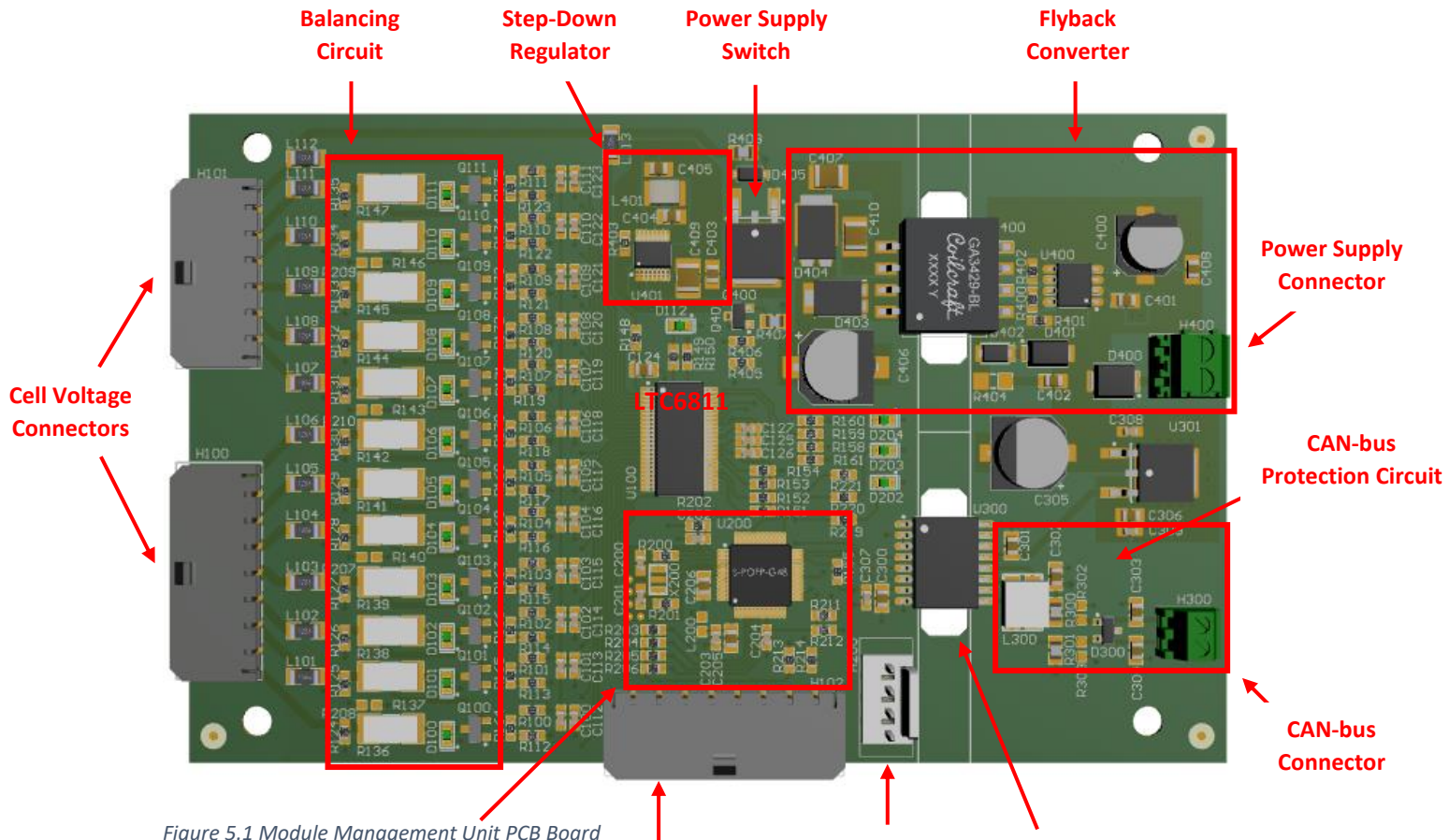


Figure 5.1 Module Management Unit PCB Board

Microcontroller Circuit	Temperature Sensor Connector	Debug Connector	CAN Transceiver
-------------------------	------------------------------	-----------------	-----------------

As we already discussed, the monitoring and balancing circuit was placed tight together in the left side of the PCB. The balancing resistors are located near the board's edge, in order to provide more space for heat dissipation without affecting the filtering and the measurement circuit. The LTC6811 was placed in the center of the board, in order to efficiently route all the voltage measurement lines. The microcontroller lies in the bottom part of the board, in a short distance apart from the CAN transceiver and battery management IC. The power converters are situated in the top part of the board, in order to minimize their impact on the rest of the circuits.

The through-air board cut-outs are placed directly underneath the isolation components to further reinforce the system's isolation. A 6mm component clearance is implemented between the measuring circuit side and the electronics side.

6 Software Description

6.1 Function Summary

The software is designed for the management of a 12-cell lithium-ion battery cell module. The system continuously monitors the voltages of up to 12 lithium-ion battery cells. The board and battery temperature are also measured, with 4 available battery temperature sensor inputs, and 4 integrated board temperature sensors. The cell temperature measurements are performed by the battery management IC while the board temperature is monitored directly by the uController. The system also controls the connection of a parallel resistor to each of the cell terminals, allowing the implementation of passive cell balancing. The primary power supply rail is continuously monitored by the uController, and the system is capable of switching to the secondary power supply automatically, without brown-out problems, when a failure is detected. A CAN-bus interface is also available but is not yet implemented in the current software version.

The software design is based on STMicroelectronics's STM8 Standard Peripheral Library. The STM8 uController peripherals that are used to achieve the system functionalities are the AD converter, the SPI interface and an integrated programmable timer. The system implements a simple clock-driven scheduling, using time triggered tasks, in order to meet the different functionality requirements.

The SPI interface is used exclusively to communicate with the LTC6811 battery management IC. The IC is unable to take any action on its own, and it requires certain valid commands received on the SPI bus, in order to perform its different functionalities. These commands are transmitted by the uController, which is responsible for the proper operation of LTC6811. The cell voltage and temperature measurements are performed by the balancer IC, and the measurement data is then transferred to the uController through the SPI bus. The balancing switches are activated through dedicated drive pins of the LTC6811. The activation sequence as well as the switch selection is decided by the uController and then commanded to the balancer IC.

The uController features a 12-bit ADC converter, which is used for the board temperature sensor measurements as well as the power supply monitoring. The uController power supply voltage is also used as reference voltage for the AD converter. The power supply rail channel is measured continuously, while the temperature sensors are sampled every 500ms.

The data handling is implemented using static variables, global for each source(.c) file. This approach was also used for visualization purposes. The global static variables can be monitored in real time, using the debugger interface, while any local data, defined in functions, is not accessible. Data can be also written on the fly, using the same interface allowing dynamic access to the program data, which is very useful for development/debugging purposes.

6.2 Software Architecture

6.2.1 Operation Modes

The module management unit features three different modes of operation:

- Normal Mode
- Autonomous Mode
- Sleep Mode

A functional description of these operation modes is given in the following:

Normal Mode: This mode is entered when the module management unit is supplied by the auxiliary battery supply and is communicating with the battery management unit. The cell voltage and temperature readings are sent to the battery management unit in fixed time intervals. The balancing actions, if required, are controlled by the battery management unit, and carried out by the module management unit accordingly. This balancing mode, will be referred as commanded balancing mode. In this operating mode, the module management unit is functioning strictly as a slave unit, awaiting commands from the master unit regarding the cell management.

Autonomous Mode: This mode is entered when the module management unit is not supplied by the auxiliary battery supply, and power is drawn from the battery module to supply the system. In the autonomous mode, the module management unit keeps monitoring the cell voltages and temperatures and carries out any pending balancing command that has been received from the battery management unit earlier. There is no communication with the battery management unit as long as the system is in this operation mode since there is no power supply in the bus side of the CAN transceiver. After the pending balancing action are completed, the system can either transition to Sleep Mode, or remain on Autonomous Mode and perform further balancing cycles. This balancing mode is referred as autonomous balancing.

Sleep Mode: The sleep mode is directly entered when the module management unit is not supplied by the auxiliary battery supply and there is no pending commanded balancing request or the autonomous balancing mode is not furtherly required. In this mode, the current consumption of the system shall be minimized and all the components must enter a low-power mode. The system in this mode continues to be supplied by the monitored battery module but remains in the low-power state until further action is requested by the battery management unit.

6.2.2 Scheduling

The integrated uController timer TIM2 is used to provide a time base, for the clock driven time triggered scheduling scheme that is used in the system. The internal oscillator is used as the system clock, without prescaling, resulting in a CPU clock of 16MHz. The timer clock is prescaled by a factor of 2048, and the reload value is set at 15000, which will provide a time base of 2 seconds, as dictated in the formula below:

$$\text{Timer Reload(sec)} = \frac{\text{Prescaler} \times \text{Reload Count}}{F_{CPU}} \quad (38)$$

so, in our case,

$$\text{Timer Reload(sec)} = \frac{2048 \times 15625}{16000000} = 2 \text{ sec} \quad \#(39)$$

The main function, after initialization of the uController and the balancer chip, configures the timer, and enters an endless loop. In each execution, the counter value is stored in a variable, and then compared to certain count values, which correspond to time intervals. When the timer value matches a time interval compare value, the routine inside that conditional branch is executed.

The next figure illustrates the scheduling scheme of the system. The power supply monitoring routine is executed continuously, while there are four major sub-routines, which are executed every 10ms, 100ms, 500ms and 1s respectively.

Time Triggered Scheduling					
	Continuous	10ms	100ms	500ms	1s
Function	Power Supply Monitor	Cell Voltage Measurement	UV/OV Detection Cell Imbalance Detection	Temperature Measurement	Balancing Switches Control

Figure 6.1 Software Scheduling

The cell voltages are sampled every 10ms and averaged over a 100ms period. Along with the cell voltages, the balancer UV/OV flags are read, in order to detect cell failure conditions. Every 100ms, a routine checks the UV/OV flags of each cell and starts an incremental counter in case of a set flag. The most recent voltage samples are averaged, and the cell voltages are compared for imbalances. In case an imbalance is detected, an incremental counter is set.

The cell and board temperatures are measured every 500ms. The battery temperature is provided by the LTC6811, while the board temperature is monitored using the uController AD converter. Moreover, the balancing parameters are checked and the cell balancing flags are set or reset, regardless of the balancing mode. The control of the activation or deactivation of the balancing switches is performed every 1 second, based on the most recent value of the cell balancing flags.

6.2.3 LTC6811 Firmware

The LTC6811 balancer IC can be interfaced via SPI communication. The main functionality of the chip, is dictated by the contents of its configuration register group. The main configuration options are made from the values of these registers. The chip is unable to operate or perform any action without receiving proper commands from the SPI bus. These commands include read and write register actions, as well as ADC triggering. A complete description of the registers and the relevant commands can be found on the LTC6811 datasheet.

6.2.3.1 Serial Peripheral Interface (SPI)

Each LTC6811 command has a unique 10-bit command code, which defines the command functionality. There are 6 more extra bits, which are used for the IC addressing. Every data exchange between the IC and the uController is verified through a CRC check over the transmitted data, named packet error code (PEC). The correct PEC must be calculated and sent by the uController along with the command code, in order for the command to be acknowledged and accepted by the balancer IC. The IC calculates on his own the PEC of the data that it is transmitted, so that a transmission data corruption check can be implemented.

The 4-wire serial port is configured to operate in a SPI system using CPHA=1 and CPOL=1. Consequently, data on SDI (input port) must be stable during the rising edge of SCK (system clock). The timing is depicted in the following figure. The maximum data rate is 1Mbps.

6 | Software Description

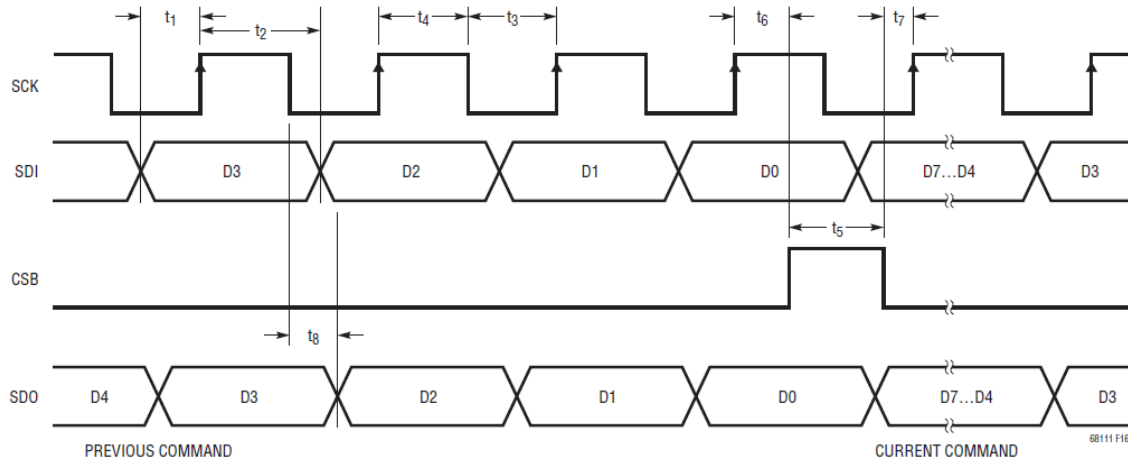


Figure 6.2 Serial Peripheral Interface (SPI) Configuration [10]

All data transfers on LTC6811 occur in byte groups. Every byte consists of 8 bits. Bytes are transferred with the most significant bit (MSB) first. CSB must remain low for the entire duration of a command sequence, including between a command byte and subsequent data. On a write command, data is latched on the rising edge of CSB.

The Packet Error Code (PEC) is a 15-bit cyclic redundancy check (CRC) value calculated for all of the bits in a register group in the order they are passed, using the initial PEC value of 0x10, and the following characteristic polynomial: $x^{15} + x^{14} + x^{10} + x^8 + x^7 + x^4 + x^3 + 1$. The next figure illustrates the simple procedure that can be established for the calculation of the 15-bit PEC value. For longer data streams, the PEC is valid at the end of the last bit of data sent to the PEC register [10].

NAME	RD/WR	BIT 7	BIT 6	BIT 5	BIT 4	BIT 3	BIT 2	BIT 1	BIT 0
CMD0	WR	1	a3*	a2*	a1*	a0*	CC[10]	CC[9]	CC[8]
CMD1	WR	CC[7]	CC[6]	CC[5]	CC[4]	CC[3]	CC[2]	CC[1]	CC[0]

Figure 6.3 Address Command Format [10]

8	8	8	8	8		8	8	8
CMD0	CMD1	PEC0	PEC1	Data Byte Low	...	Data Byte High	PEC0	PEC1

Figure 6.4 Write Command Format [10]

8	8	8	8	8		8	8	8
CMD0	CMD1	PEC0	PEC1	Data Byte Low	...	Data Byte High	PEC0	PEC1

Figure 6.5 Read Command Format [10]

The command formats are shown in the previous figures. Each command has a unique 11-bit command code. Since the LTC6811-2 is used in our system, which is an addressable device, it will respond to a command only if the physical address of the device on pins A3 to A0 match the

address specified in the address command. An address command has a value 1 for CMD0[7] followed by the 4-bit address (a3,a2,a1,a0) of the device in bits CMD0[6:3].

6.2.3.2 Registers

There are two types of registers on the LTC6811 IC. The ones that store the data of the ADC conversions and the internal diagnostics, and the control registers, that their content changes the configuration and functionality of the IC. The registers are divided in register groups, depending on their content. For a complete description of the registers and their contents, refer to the LTC6811 datasheet.

The core registers of the IC, are found on the configuration register group (CFRG). The CFGR consists of 6 registers, which store important values, and contain configuration bits for different IC functionalities.

REGISTER	RD/WR	BIT 7	BIT 6	BIT 5	BIT 4	BIT 3	BIT 2	BIT 1	BIT 0
CFGRO	RD/WR	GPIO5	GPIO4	GPIO3	GPIO2	GPIO1	REFON	DTEN	ADCOPT
CFGR1	RD/WR	VUV[7]	VUV[6]	VUV[5]	VUV[4]	VUV[3]	VUV[2]	VUV[1]	VUV[0]
CFGR2	RD/WR	VOV[3]	VOV[2]	VOV[1]	VOV[0]	VOV[11]	VOV[10]	VOV[9]	VOV[8]
CFGR3	RD/WR	VOV[11]	VOV[10]	VOV[9]	VOV[8]	VOV[7]	VOV[6]	VOV[5]	VOV[4]
CFGR4	RD/WR	DCC8	DCC7	DCC6	DCC5	DCC4	DCC3	DCC2	DCC1
CFGR5	RD/WR	DCTO[3]	DCTO[2]	DCTO[1]	DCTO[0]	DCC12	DCC11	DCC10	DCC9

Table 6 LTC6811-2 Configuration Register Group [10]

The key configuration bits are the following:

- **ADCOPT**: ADC mode selection, provides different ADC sampling values selection.
- **GPIOx** : Configures the GPIO pins of the IC (input/output – pull down on/off).
- **VUV** : Undervoltage Comparison Value = (VUV+1)*16*100uV (Default 0x000).
- **VOV** : Overvoltage Comparison Value = VOV*16*100uV (Default 0x000).
- **DCCx** : Discharge Cell x (1-> Activates Discharge Switch).

The cell voltage measurements are stored in four cell voltage register groups, (CVAR, CVBR, CVCR, CVDR). The 16-bit measurements are stored in 8-bit registers, so every registers group consists of 6 registers which contain the voltages of 3 cells. The auxiliary register groups (AVAR, AVBR), contain the GPIO measurement data, as well as the internal reference voltage value. The cell temperature values are stored in this register group. The status register groups (STAT, STBR), contain the sum of cells measurement, the under-voltage and over-voltage flags, as well as the internal LDO supply voltages.

LTC6811 Configuration - For the needs and requirements of our system the LTC6811 IC is configured in the following manner:

- **ADCOPT**: 0 -> Default ADC Configuration
- **GPIOx** : 1 -> Pull-Down off (Input mode)
- **REFON** : 1 -> Reference remains powered up until Watchdog Timeout
- **DTEN** : 0 -> Disabled (Configured by Hardware)
- **DCTO** : 0 -> Disabled

The VUV and VOV are defined as constants in the source files and can be altered depending on the application requirements. The DCCx values are initialized 0x00 (balancing switches deactivated), but they are updated by software depending on the balancing modes.

Balance Switches Control - The cell balancing switches are controlled directly by the DCC bit values of the configuration register group. In order to activate a balancing switch, the DCCx bit must be set, and then the LTC6811 will activate the respective S(x) drive pins, which activates the external pFET switch.

6.2.3.3 ADC Measurements

The process of triggering an AD conversion and reading the measurement data is identical for the cell voltages, GPIO and status registers. First of all, a valid ADC command must be received by the battery management IC, in order to initiate the conversion. Once the command is received, the IC will start the conversion procedure. The uController needs to send an ADC poll command to verify the end of conversion, or simply wait the necessary conversion time. The polling method is preferred, because the ADC conversion time is different depending on the ADC configuration. During the polling command, the balancer will pull the SDO SPI line low, while the conversion is still in progress, and then release the SDO line when the conversion is finished.

Once the conversion is finished, the uController needs to send a read command, in order to read the measurement results. Once the command is received, the balancer IC starts to transmit the requested register data on the SPI bus. The next figure illustrates the ADC measurement procedure.

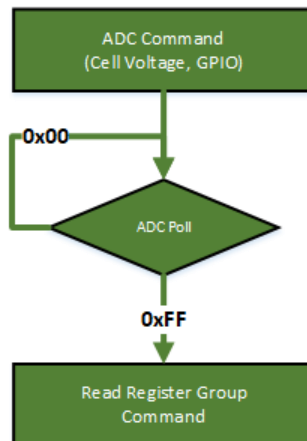


Figure 6.6 LTC6811-2 ADC Measurement Method

The LTC6811 offers some configuration options for the ADC conversions. The ADC is configured by the ADC command code, which contains the following configuration bits:

- **MD[1:0]** : ADC Mode, offers different filtering option for the ADC measurement
- **DCP** : Discharge Permitted, when set, enables the ADC measurement when a cell balancing switch is activated
- **CH[2:0]** : Channel Selection for the Cell Voltage ADC, selects the cell voltages to be measured

- **CHG[2:0]** : Channel Selection for the GPIO voltage ADC, selects the GPIO pins to be measured
- **CHST[2:0]**: Channel Selection for the Status voltage ADC, selects the status voltages to be measured

6.2.4 uController Functionalities

This section describes the main system routines, and the way they interact with the uController peripherals and balancer IC.

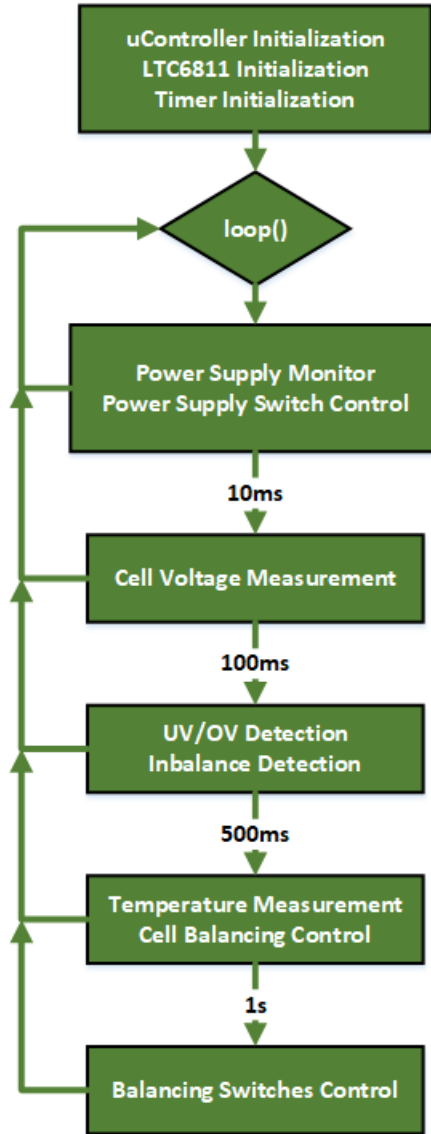


Figure 6.7 uController Software Flowchart

power_supply_monitor (): This routine continuously measures the primary power supply rail. The rail voltage level is measured through a voltage divider. The system compares the measured value to a critical threshold value. When the measured value is lower than this threshold value, an incremental counter is set, representing a failure detection. If the failure is persistent for four

consecutive ADC readings, a power supply failure is considered present. In that case, the power supply switch control signal is activated and the system transitions to the secondary (battery) power supply.

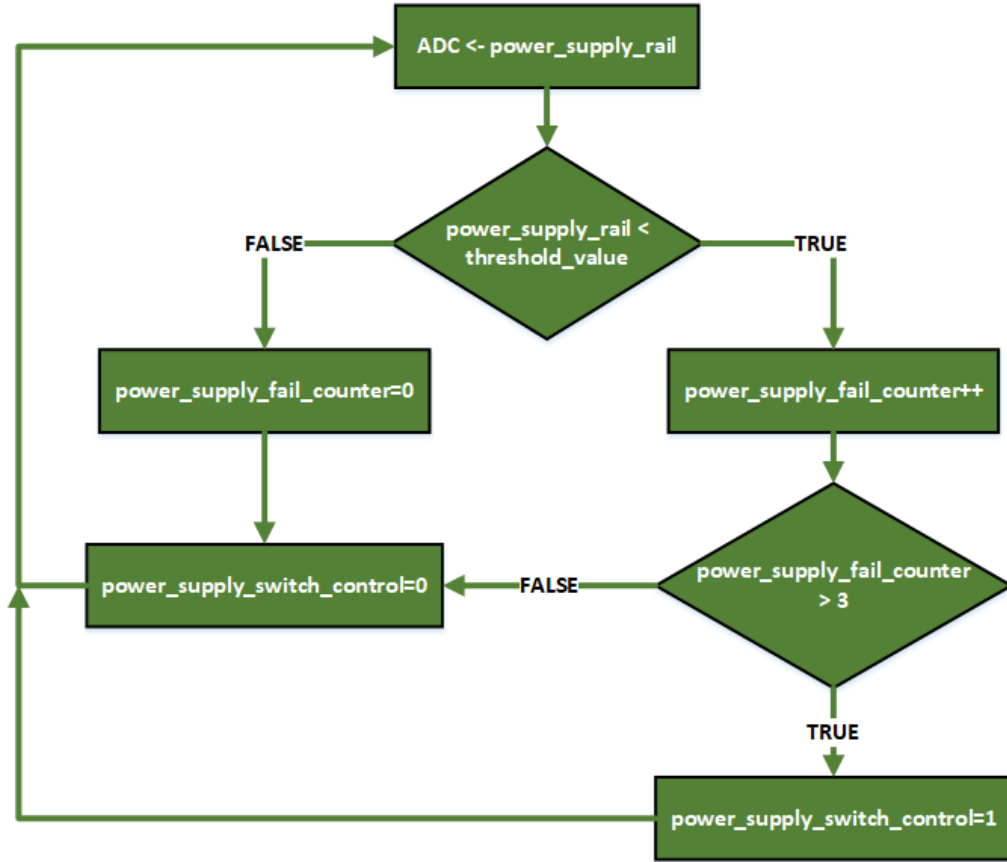


Figure 6.8 power_supply_monitor() Routine Flowchart

ltc_monitor_cells(): This is the basic routine for the cell voltage measurements. After initiating a cell voltage ADC command, the routine reads all the cell voltage registers of the balancer IC. Then, the status registers are read, and the UV/OV bit-flags of the cells, are stored in 16-bit variables. After the communication with the LTC6811 is completed, a moving average calculation function is executed. This function sums up and averages the measured cell voltages, with a sample period of 10 measurements.

cell_monitoring(): This routine extracts some basic data out of the cell voltage measurements. The value of the 16-bit UV/OV flag variable is checked, and in case a bit flag is set, an incremental counter is set, in order to determine if there is a real failure in the respective cell (*UV/OV_counter[cell]*). The threshold values of these counters and the action regarding a failure detection are handled by the cell_management() routine. If cell balancing is not activated, meaning that the voltage measurements indicate the real state of the cells, the routine implements a cell imbalance check. The cell with the minimum voltage is located, and the remaining cell voltages are compared to a threshold deviation value. When a voltage deviation value exceeds the threshold value, an incremental counter is set (*inbalance_counter[cell]*), in order to determine if the deviation is persistent for a certain number of samples.

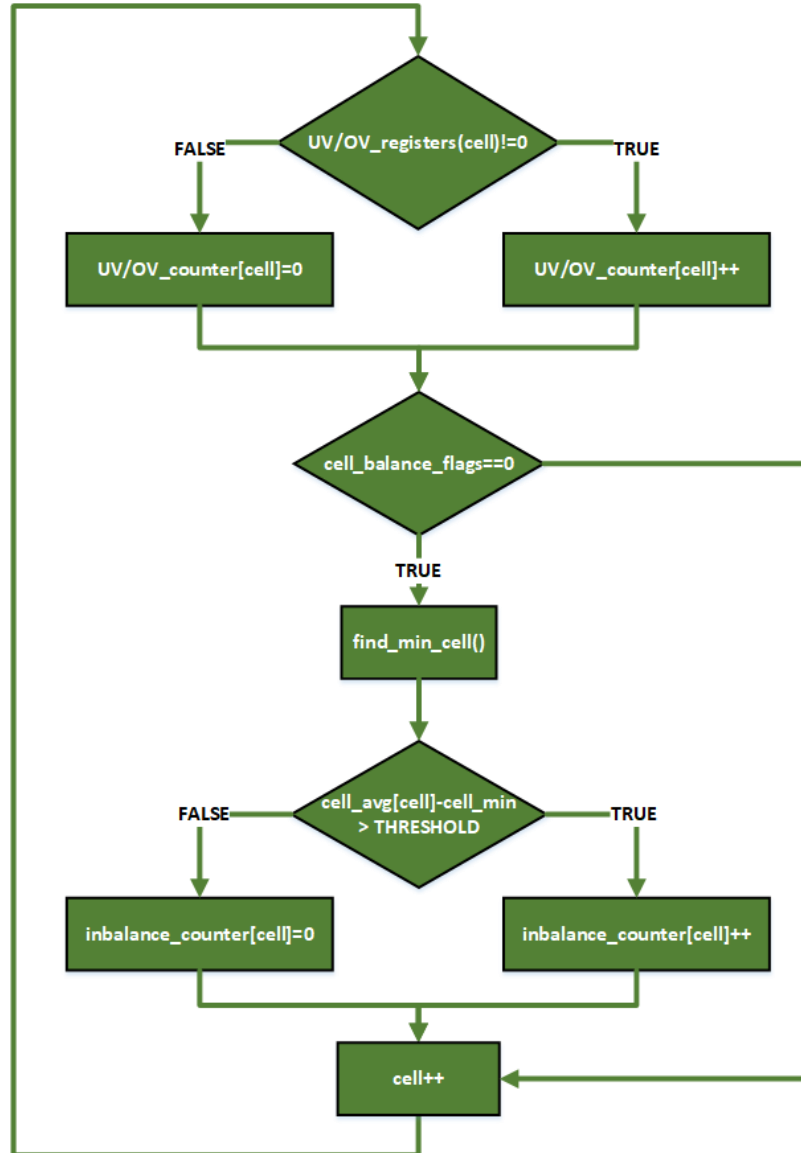


Figure 6.9 cell_monitoring() Routine Flowchart

cell_management(): The control of the balancing procedure as well as the cell failure detection are implemented in this routine. The UV and OV counter values set by the cell_monitoring() routine are compared to certain threshold values, which represent time intervals. When a timer value exceeds the time interval threshold, the corresponding cell is considered problematic, and a respective failure bit-flag is set. The failure detection threshold values are adjustable and can be set according to the battery technology specifications and needs.

Depending on the balancing state, the routine then sets the value of the *cell_balance_flags* 16-bit variable, which determines the state of the cell balancing switch. In the commanded balancing mode, the value of the *ubal_time[cell]* parameter is checked for each cell. This value is sent to the module management unit by the battery management unit and indicates the balancing time for the corresponding cell, in minutes. If this value is positive, and is not exceeding the maximum allowed balancing time, *ubal_time_par*, the system compares it to the last saved

ubal_time[cell] parameter value (*ubal_history[cell]*). In case the values are not equal, which indicates that the value is updated, the respective bit-flag in *cell_balance_flags* is set.

The value of an incremental counter (*balance_counter[cell]*), which represents the elapsed balancing time for each cell is compared to the latest *ubal_time[cell]*, in order to determine whether the balancing interval is over, and the cell balancing needs to be de-activated.

When the system is in the autonomous balancing mode, the cell imbalance counters set by the cell_monitoring() routine are compared to a certain threshold values, representing a number of consecutive deviation samples. When a counter value exceeds this threshold, the corresponding bit in the *cell_balance_flags* is set, and a balancing time of 1min is assigned for this cell, through the *ubal_time[cell]* parameter. The same procedure as in the commanded balancing mode is followed, in order to reset the triggered *cell_balance_flags* bit-values, omitting the balancing history check, which in this case is irrelevant.

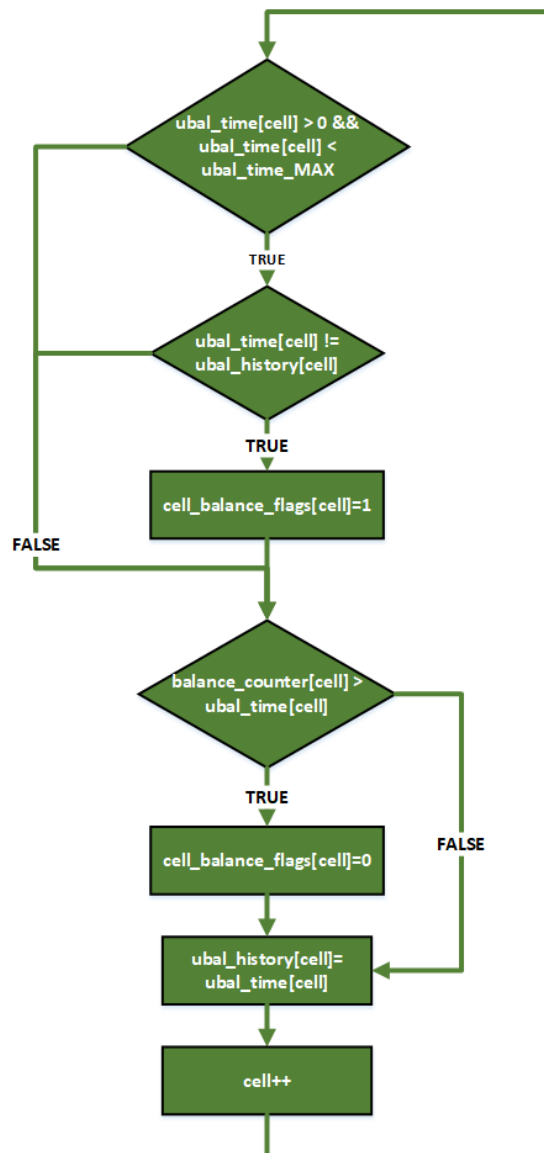


Figure 6.10 *cell_management()* Routine Flowchart

measure_temperature(): This routine implements the monitoring regarding to the battery and board temperature. The routine triggers an ADC conversion of the auxiliary registers on the balancer IC, and the values of the relevant registers are then read back. After the battery temperature measurement is completed, the board temperature sensors are measured. The ADC measurements are converted to voltage values. The sensor resistance is found using voltage divider equations, and then it is translated to temperature, through linear interpolation and a look-up table of the resistance vs temperature curve of the NTC sensor.

cell_balance(): This routine controls the activation of the cell balancing switches. The value of the *cell_balance_flags* determines which of the switches is activated. In case of a set bit-flag in *cell_balance_flags*, an incremental counter is set (*balance_counter[cell]*), measuring the elapsed time since the switch activation. The value of *cell_balance_flags* is then written on the DCC bits of the configuration register group of LTC6811, activating each of the switches that its corresponding bit-flag is set.

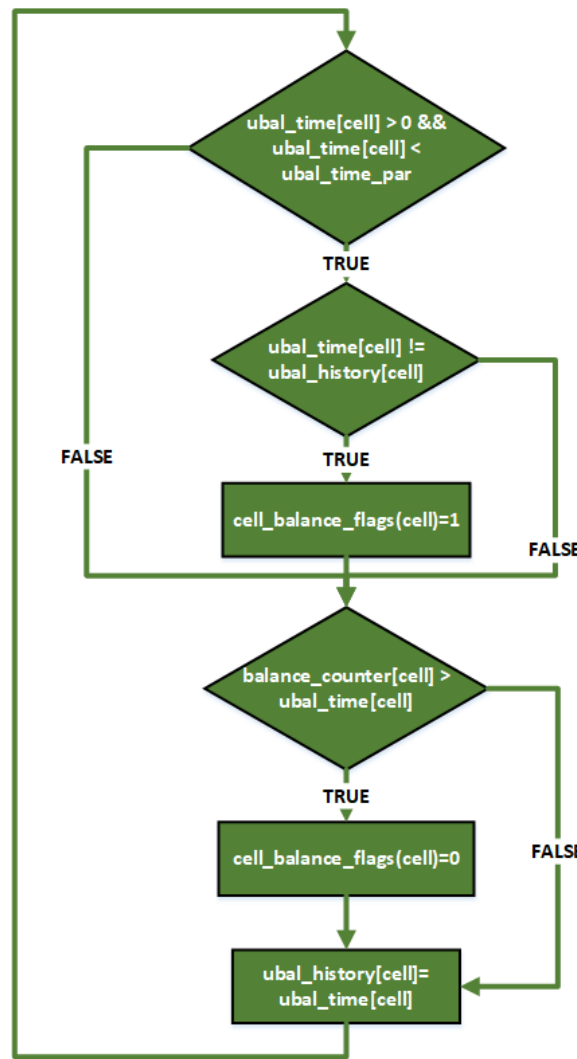


Figure 6.11 Commanded Balancing Algorithm Flowchart

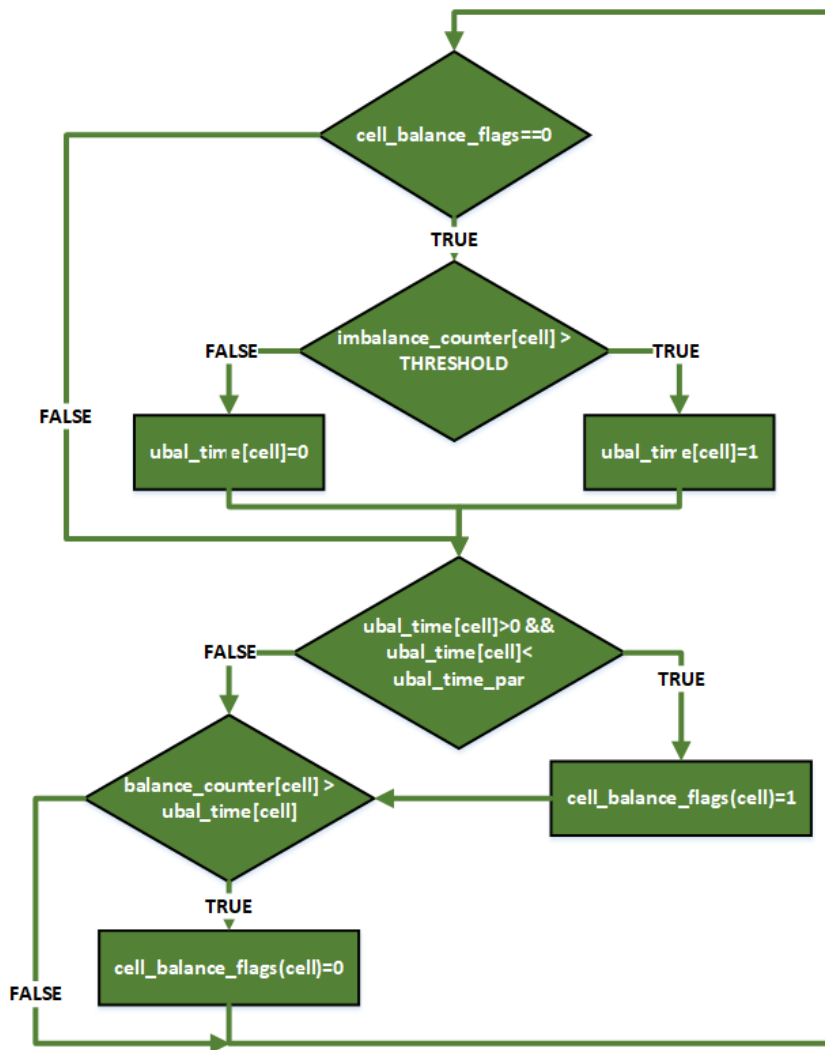


Figure 6.12 Autonomous Balancing Algorithm Flowchart

7 Experimental Results

In this chapter, we present the hardware testing and experimental results of the system. The testing procedure was divided in two separate parts. First of all, the power converters were isolated from the rest of the circuit so that we could verify that the previously specified functional requirements are satisfied. Afterwards, some basic balancing experiments were laid out, in order to prove the firmware functionality. The commanded and autonomous balancing algorithms were used in these experiments, and their results are presented in the following sections.

7.1 Hardware Testing

In this section we will describe the testing of the overall power supply scheme, including the power converters as well as the power supply switch. Each component test cases will be described separately, while oscilloscope captures will be used as results. It should also be pointed out that during the testing procedure the circuits under test were completely isolated from the rest of the circuit and that we will present only representative results for each component for the sake of simplicity.

7.1.1 Isolated Flyback Converter

Regarding the flyback converter, the testing procedure was divided in three parts in order to prove that the power converter is able to provide the desired output voltage and current under different load conditions within the specified input voltage range. Namely, the first examines the minimum load behaviour, the second part examines the behaviour of the converter under different resistive loads and the third part examines the load step-response of the circuit.

The input-output waveforms of the converter with a 200mA resistive load, and the start-up transient response are presented in the following figures:

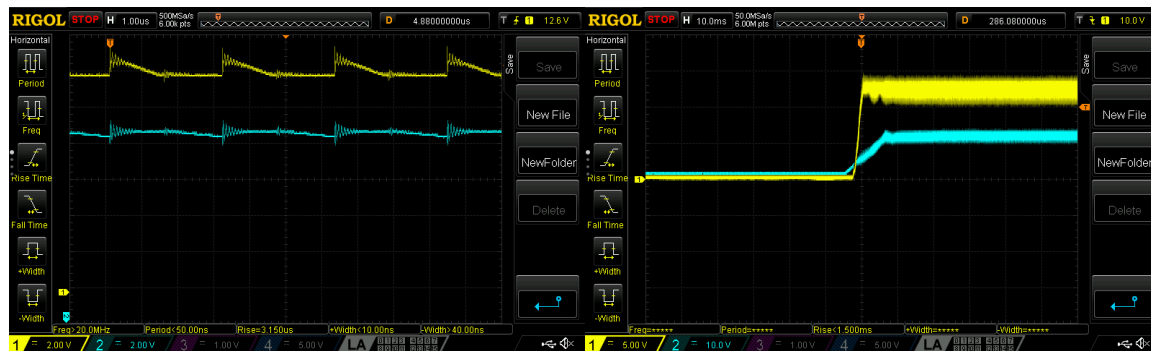


Figure 7.1 Isolated Flyback Converter Experimental Results

Input Voltage 12VDC - Load 200mA

Ch. 1.	Output Voltage	2 V/div
Ch. 2.	Input Voltage	2 V/div

Input Voltage 12VDC – Start Up

5	V/div
10	V/div

Observing the waveforms, we can conclude that the voltage output waveform of the converter is compliant with the one described in the components datasheet. The output voltage is approximately 12V with a ripple of 1V, which is sufficiently suppressed. The ripple value may be

considered value, but it is not unacceptable for our system, since the flyback output is fed to the step-down regulator input capacitance, which can effectively smooth these voltage transients.

7.1.2 Step-Down Regulator

For the step-down regulator, a different approach was taken regarding the structure of the testing procedure. The experiments were performed twice. At first, a power supply was connected directly to the converter input so that we could verify the functionality of the circuit alone. Subsequently, the testing procedure was repeated connecting the flyback converter to the converter input.

As for the flyback converter, the testing procedure was divided in three parts in order to prove that the power converter is able to provide the desired output voltage and current under different load conditions within the specified input voltage range. The first part examines the minimum load behaviour, the second examines the behaviour of the converter under different resistive loads and the third examines the load step-response of the circuit.

The input-output voltage waveforms of the converter are presented in the following figures. Figure 7.2 illustrates the circuit's behaviour with an external power supply as input, while figure 7.3 illustrates the combined behaviour of the two power converters connected in series.



Figure 7.2 Step-Down Regulator Experimental Results - 1

Input Voltage 12VDC - Load 250mA		Load Variation – Min. to Max. Load	
Ch. 1.	Output Voltage	2 V/div	500 mV/div
Ch. 2.	Input Voltage	5 V/div	1 V/div

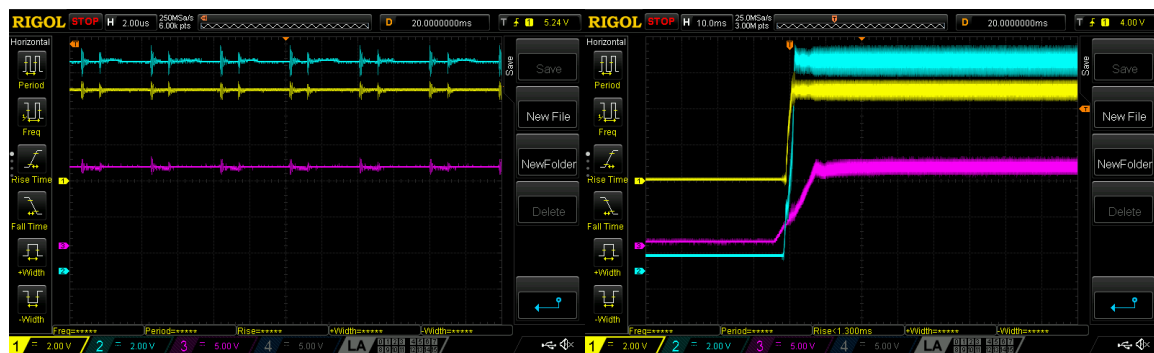


Figure 7.3 Step-Down Regulator Experimental Results - 2

Input Voltage 12VDC - Load 250mA			Input Voltage 12VDC – Start Up		
Ch. 1.	Regulator Output	2V/div		2V/div	
Ch. 2.	Flyback Output	2V/div		2V/div	
Ch. 3.	Input Voltage	5V/div		5V/div	

It is evident by the oscilloscope captures that the flyback converter transients are reflected on the output of the step-down regulator. Comparing the output voltages of the regulator in each test case, we can observe that although its output is stable at 5V, when it is connected to the flyback converter its voltage ripple is significantly larger. Nevertheless, the ripple is acceptable since the transients are sufficiently suppressed and each component connected to the regulator output is equipped with adequately sized input capacitors, which can effectively reject these transients.

7.1.3 Power Supply Switch

The purpose of the test cases of the power supply switch is to prove that the switch is able to turn on and off at different loads and voltage levels. Furthermore, the turn-on time of the switch is also measured in order to ensure that the transient response of the system is fast enough so that the output of the step-down regulator remains active and stable.

The testing procedure was divided in four parts. First of all, the switch was tested with voltage connected to its source side, acting like a simple turn-on voltage switch. Then, voltage was applied both to its source and drain sides, using two external power supplies, in order to verify that the circuit can effectively switch between voltage levels. In the third part, resistive loads were applied to the drain side, examining the effect of load conditions on the switching performance. In the final part, the output of the flyback converter was connected to the source side, which is the real use case of the circuit.

Throughout the testing procedure the output of the step-down regulator was disconnected from the rest of the system making sure that unexpected responses will not cause any damage to the other components. The uController was also not interfaced in these tests, and the control signal was produced by an external signal source.

The switching performance of the circuit is presented in the following figures. The voltage levels are chosen as 52VDC for the high-side, representing the battery module nominal voltage, and 12VDC for the low-side, which is the nominal output of the flyback regulator.



Figure 7.4 Power Supply Switch Experimental Results - 1

7 | Experimental Results

Switching 12VDC - 52VDC - Load 200mA

Ch. 1.	pFET Drain	10 V/div
Ch. 2.	pFET Gate	10 V/div
Ch. 3.	Control Signal	5 V/div

Switching 12VDC – 52VDC - Load 200mA

Regulator Output	2 V/div
Regulator Input	10 V/div
Control Signal	5 V/div

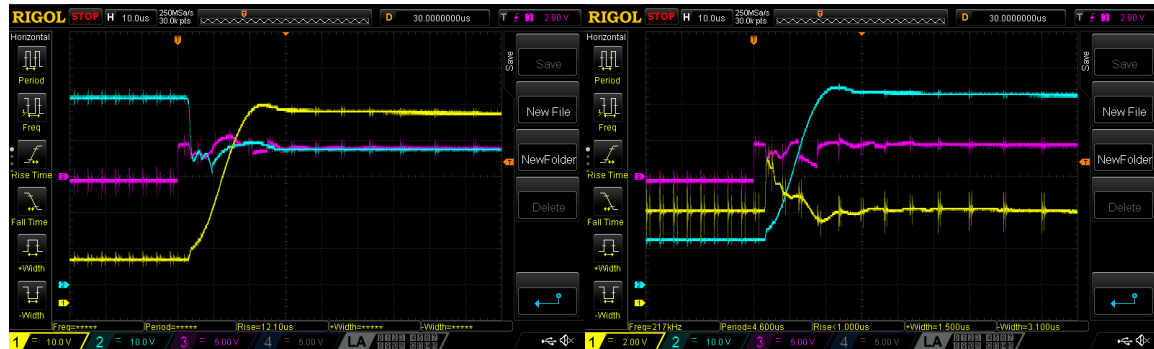


Figure 7.5 Power Supply Switch Experimental Results - 2

Switching 12VDC - 52VDC - Load 200mA

Ch. 1.	pFET Drain	10 V/div
Ch. 2.	pFET Gate	10 V/div
Ch. 3.	Control Signal	5 V/div

Switching 12VDC – 52VDC - Load 200mA

Regulator Output	2 V/div
Regulator Input	10 V/div
Control Signal	5 V/div

As we can observe from the waveforms in figure 7.4, a voltage spike is introduced in the pFET gate voltage. The drain switching is smooth without any transients. The gate voltage transient is then propagated to the regulator output waveform. Its amplitude was increasing with the drain switching voltage level, with its peak reaching two times the nominal regulator output voltage. The regulator output transient is sufficiently suppressed in 5us, but this duration is capable of causing overvoltage problems to the system. From the resistive loads tests, we can safely conclude that the load conditions do not affect the switching performance. The switching response times and waveforms are equivalent to the minimum load conditions. Nevertheless, the regulator output transient is still present, but it is not dependent on the load values.

The flyback converter does not affect the performance of the switch, as it is clearly illustrated in Figure 7.5. The waveforms and the switching response time are equivalent to the previous test case. The regulator voltage transients are still present and are not affected by the presence of the flyback converter.



Figure 7.6 Power Supply Switch Experimental Results - 3

Switching 12VDC - 52VDC - Load 200mA			Switching 12VDC – 52VDC - Load 200mA		
Ch. 1.	pFET Drain	10 V/div	Regulator Output	2 V/div	
Ch. 2.	pFET Gate	10 V/div	Regulator Input	10 V/div	
Ch. 3.	Control Signal	5 V/div	Control Signal	5 V/div	

The voltage transients in the regulator output are not desired. A low pass filter was used in the load switch control signal, in order to decrease the slew rate of the control pulse. In addition, a capacitor was placed between the pFET gate and source terminals, in order to furtherly smoothen the gate voltage switching waveform. Since, as we mentioned, the load conditions did not affect the switching performance, the following test was conducted in maximum load.

As illustrated in Figure 7.6, the additional components significantly reduce the regulator output voltage transients. The capacitor also affects the switching time, increasing the switching response but not outside of the accepted range. The selected value of 22nF was considered optimal since a large value of capacitance would increase the response time even more.

The updated topology of the power supply switch is presented in the following figure. The components that were added to the original design are necessary to achieve the desired performance of the circuit.

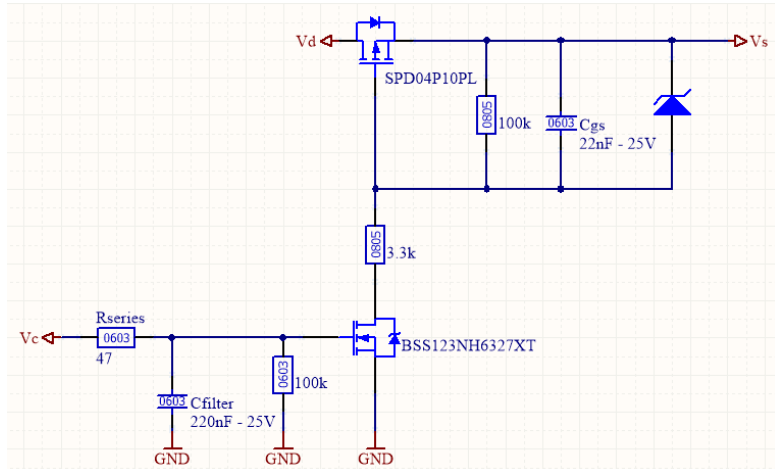


Figure 7.7 Power Supply Switch Updated Topology

7.2 Balancing Experiments

In this section we will describe the balancing experiments that were conducted in order to test the functional requirements of the system. The experiments were designed primarily to provide a proof of concept and were mainly focused on the validation of the developed software. Therefore, it shall be noted that the presented results focus on the functionality of the balancing circuitry and not on the actual cell balancing performance.

7.2.1 Experimental Setup

A battery module of twelve lithium-ion cells connected in series was used throughout the experiments. The module featured integrated voltage measurement probes for each cell as well as four NTC temperature sensor probes. The module management unit was connected directly to

7 | Experimental Results

the measurement lines and a PC interface was used for monitoring and data logging purposes. The experimental setup is shown in the following figure:

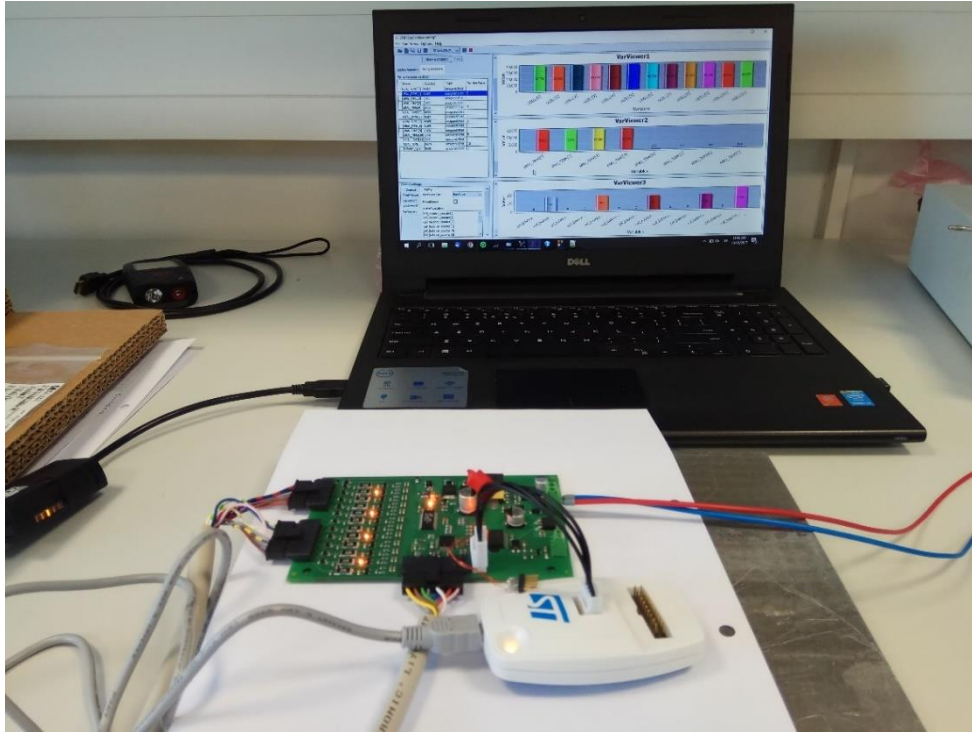


Figure 7.8 Module Management Unit Experimental Setup - 1



Figure 7.9 Module Management Unit Experimental Setup - 2

The microcontroller debugging module provides a full-scale emulator, as we mentioned in previous chapter. In conjunction with the STM Studio, a real-time variable monitoring and visualization tool from ST Microelectronics, it provides a fully functional testing interface for the module management unit. Using this tool, we were able to dynamically change the contents of variables, which granted an efficient and safe way to control the balancing procedure and conduct the required experiments. An overview of the STM Studio visualization, during an experiment is presented in the following figure:

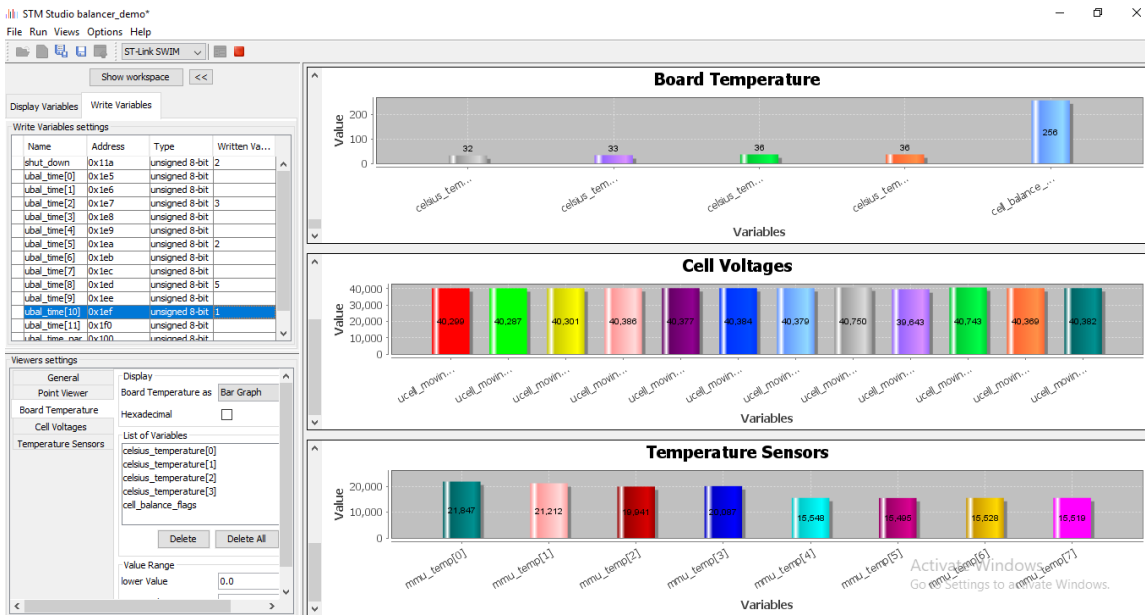


Figure 7.10 ST Visual Studio Graphical User Interface (GUI)

The values of certain variables of interest are displayed on the right side of the figure, in the form of bar graphs, which enables an easy real-time monitoring of the system. On the upper left, we can see the full memory map, in which we can change any desired variable value. This way we can for example, enable or disable balancing switches in the commanded balancing mode, change the cell overvoltage or undervoltage threshold or switch between the different balancing modes.

7.2.2 Commanded Balancing

For the commanded balancing experiments, the battery module was connected to the module management unit without any charge imbalances. Then the balancing circuit was manually activated, through the STM Studio, for a specific number of cells. The cell voltage waveforms for each cell are presented in Figure 7.11. The board temperature was also measured throughout these experiments, in order to monitor the thermal performance of the board.

7 | Experimental Results

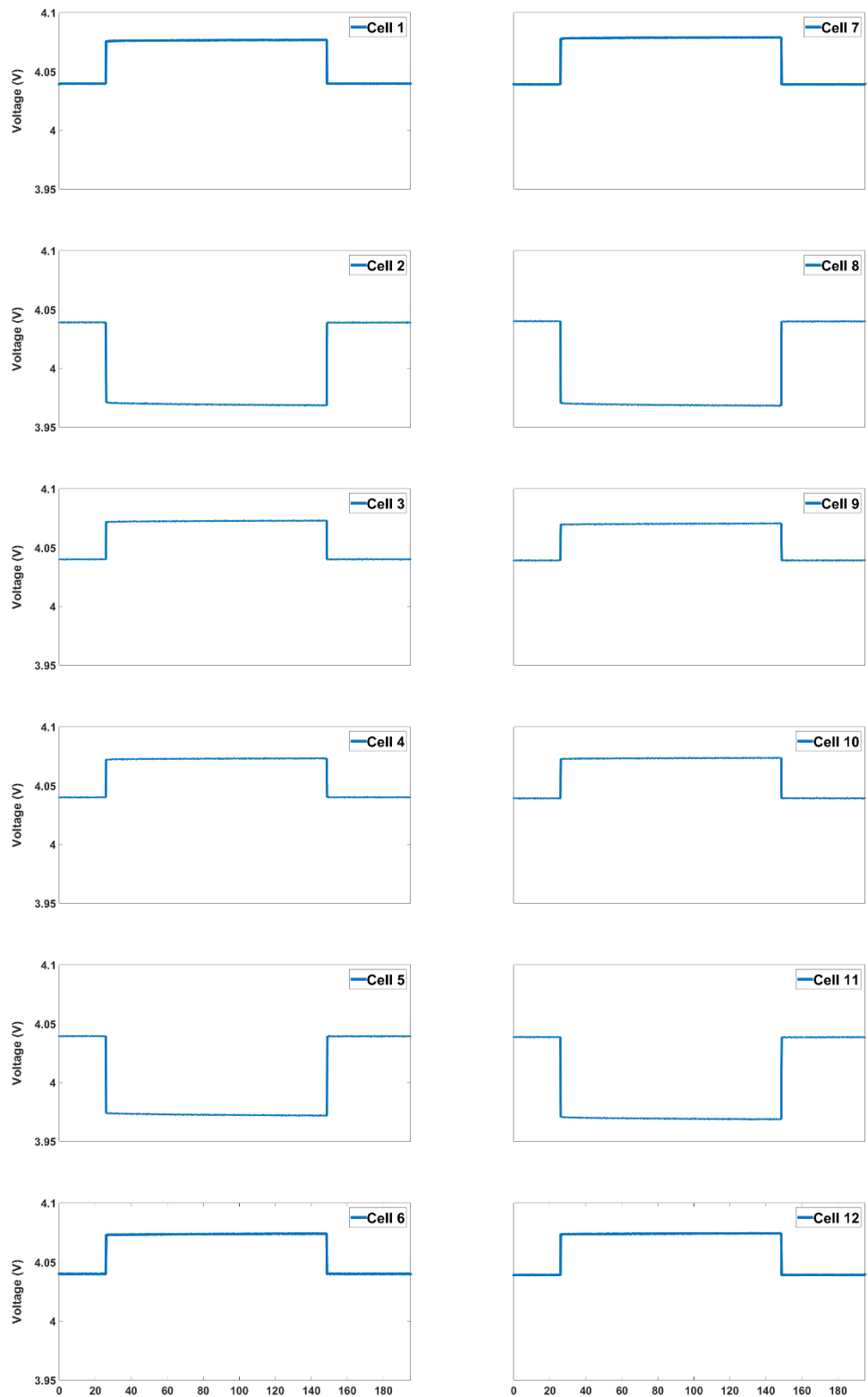


Figure 7.11 Commanded Balancing Experiment – Individual Cell Voltages

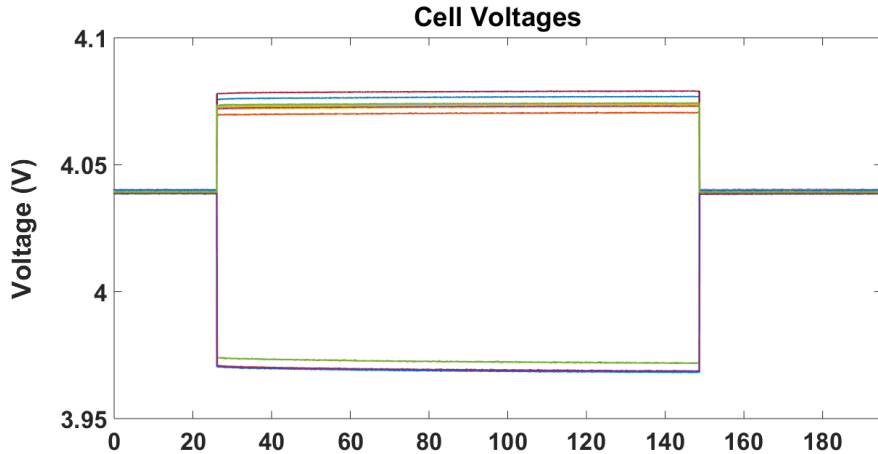


Figure 7.12 Commanded Balancing Experiment – Cell Voltages

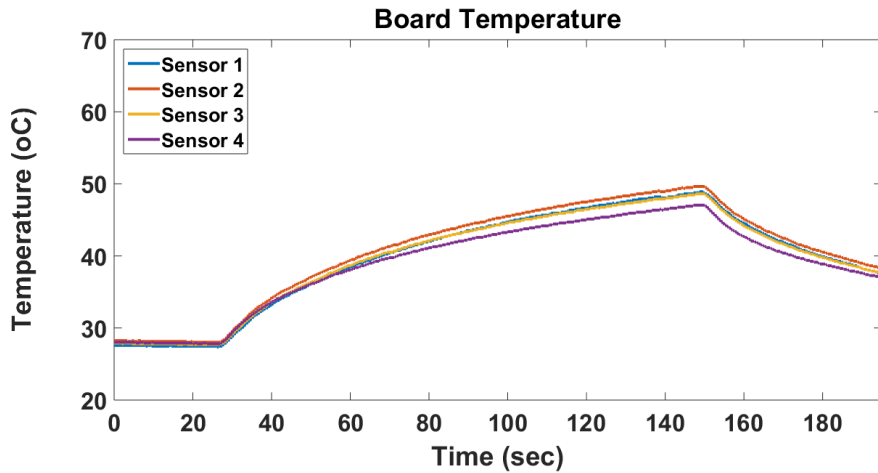


Figure 7.13 Commanded Balancing Experiment – Board Temperature

The balancing circuits for cells 2, 5, 8 and 11, in respect to the bottom of the cell stack, were activated for two minutes in this experiment, as illustrated in figure 7.12. These cells were selected due to their proximity to the board temperature sensors. As we expected, a uniform voltage drop is produced in each cell during the balancing activation, since the cells discharge with an equal balancing current. In figure 7.13, we can observe the rise in board temperature during the balancing cycle due to the heat dissipation of the balancing resistors.

7.2.3 Autonomous Balancing

For this phase of the experiments, certain cells of the battery module were externally discharged, introducing small charge imbalances, in order to test the effectiveness of the autonomous balancing algorithm. The cell voltage waveforms for each cell are presented in Figure 7.14.

7 | Experimental Results

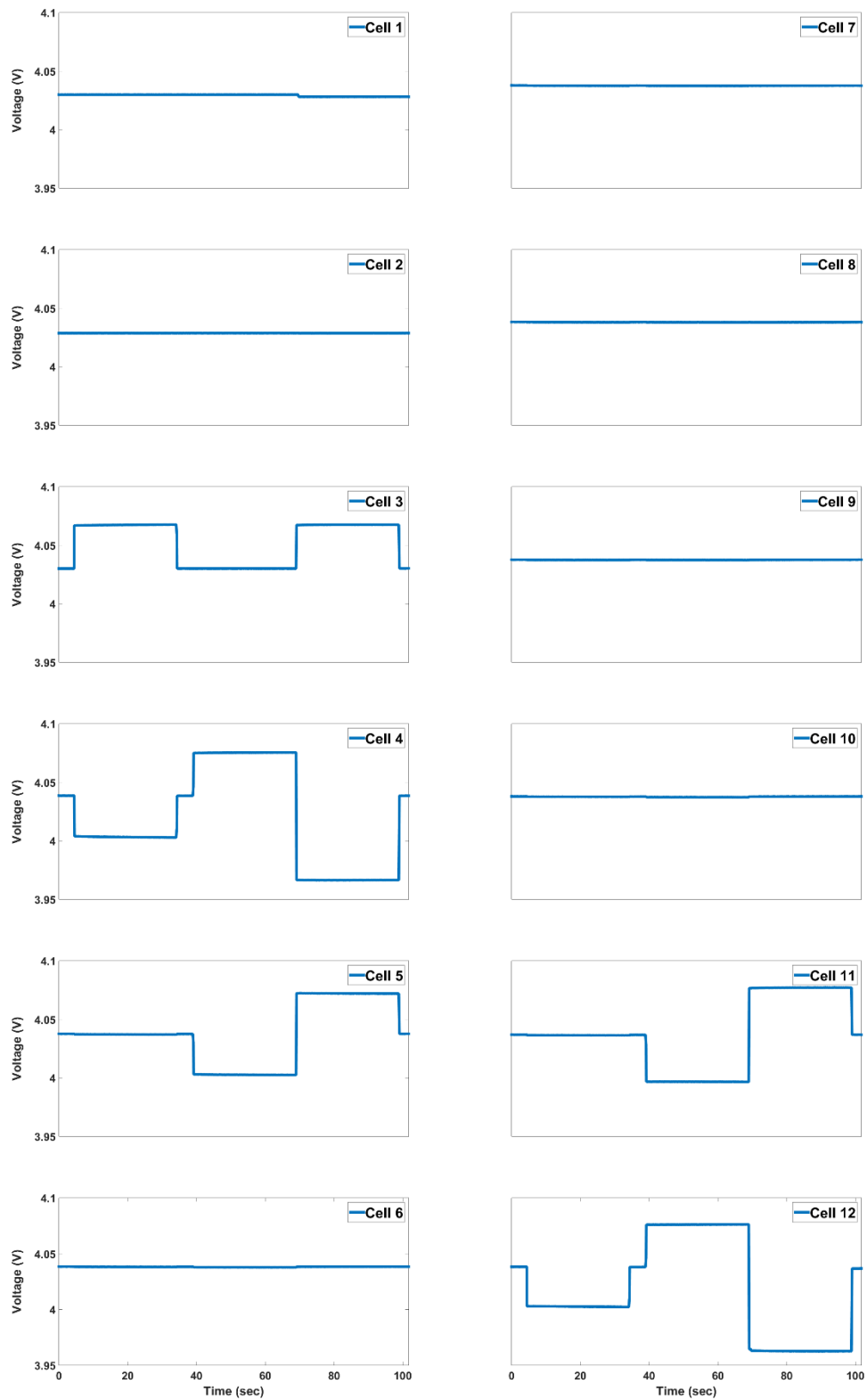


Figure 7.14 Autonomous Balancing Algorithm - Individual Cell Voltages

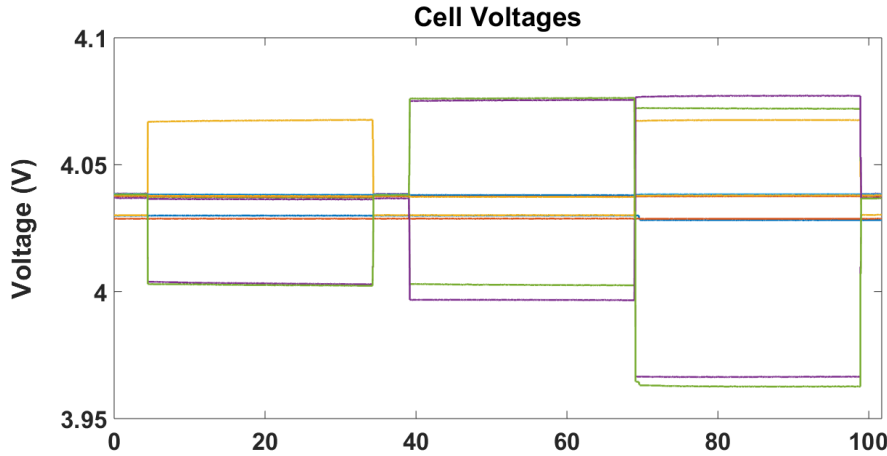


Figure 7.15 Autonomous Balancing Algorithm - Cell Voltages

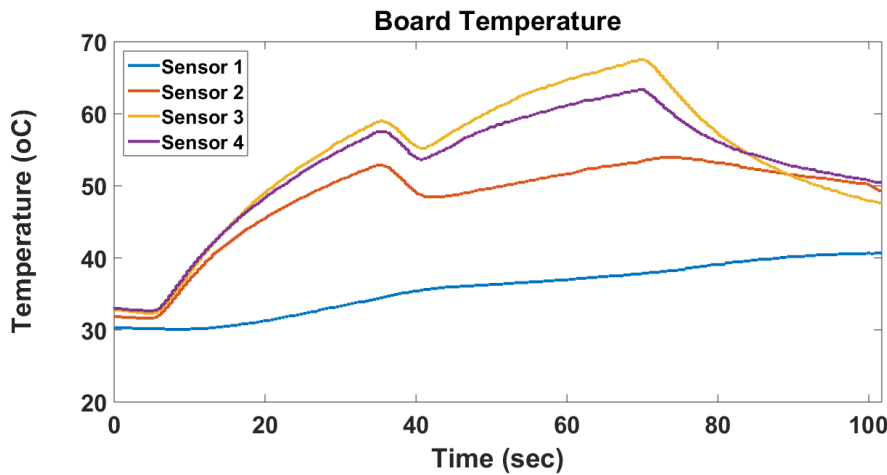


Figure 7.16 Autonomous Balancing Algorithm - Board Temperature

In figure 7.15 we can see the balancing cycles determined by the autonomous algorithm. As we expected, the cells with the lowest voltage were not selected for balancing, while the overcharged cells were discharged for 30 seconds, depending on whether or not they met the imbalance threshold. Furthermore, we may observe that the selected cells differ from cycle to cycle which indicates that the algorithm is sensitive to small voltage deviations. Nevertheless, the voltage drops in the balanced cells are once again uniform, which is expected due to the equal balancing currents.

The board heat dissipation distribution is different from the commanded balancing experiment. As illustrated in figure 7.16, the board areas with active balancing circuits present a significant rise in temperature in respect to areas where the balancing circuits are inactive.

8 Conclusions and Future Work

The thesis purpose was to design and develop a battery management system for lithium ion cells, suitable for automotive applications. The system's architecture has been designed, based on a variety of different approaches and implementations, to satisfy the specific needs of our system. The basic component of this architecture, the module management unit, has been furtherly studied, elaborately designed, implemented and tested. We can safely conclude that with the experimental evaluation of the module management unit the thesis purpose has been fulfilled, since all the major functional requirements have been verified to work as intended.

The system adopts a distributed battery management system architecture with an isolated CAN-bus. It consists of a master control unit, referred as the battery management unit, and several slave units, equal to the battery modules that need to be monitored, referred as module management units. This master-slave topology increases the system's flexibility, as each slave unit can be considered as a standalone system. The overall architecture is independent of the total number of cells in the battery pack as well as of the battery pack structure and topology, since each module management unit is capable of monitoring up to 12 series connected cells, and its is small enough to be integrated in a battery module.

The testing procedure and experimental results of the module management unit provided a proof of concept for our system's design. The implemented passive balancing technique, has been tested using two separate algorithms and its function has been successfully verified. The commanded balancing algorithm performed the balancing cycles for externally selected cells, while the autonomous balancing algorithm performed the balancing cycles based on the monitoring data that it gathered. This highlights the main advantages of the selected architecture, which is the computational flexibility and the increased functional capabilities of the module management unit.

From the knowledge acquired throughout the project there are certain points that can be furtherly evaluated. One example is the implementation of a larger scale experimental setup, where multiple module management units would be used to monitor a bigger number of cells. This would allow the evaluation of the performance of the communication bus and it would provide more ways to investigate the distributed computational approach that we aim with this design. Furthermore, more elaborate balancing algorithms could be implemented, using cell SoC and SoH estimations, to increase the balancing performance and efficiency.

The elaborate design of the battery management unit is still an open concept. We should point out that most of its functionalities can be achieved using a general microcontroller or an ECU. Since the detailed design of the unit does not affect directly any of the system's requirements or its overall functionality, we will assume that its design can vary in each application, based on its specific needs, without any impact on the system's performance.

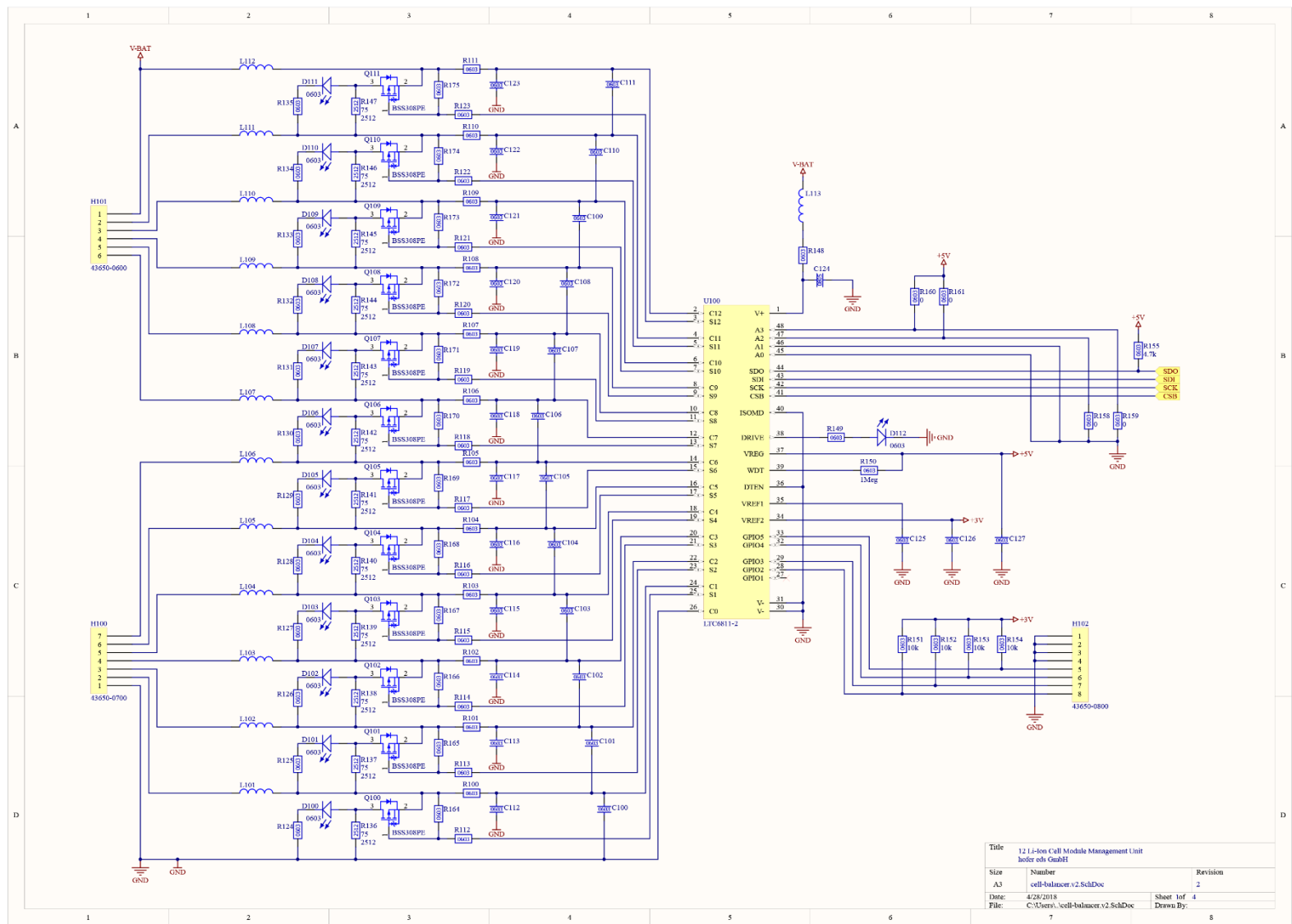
References

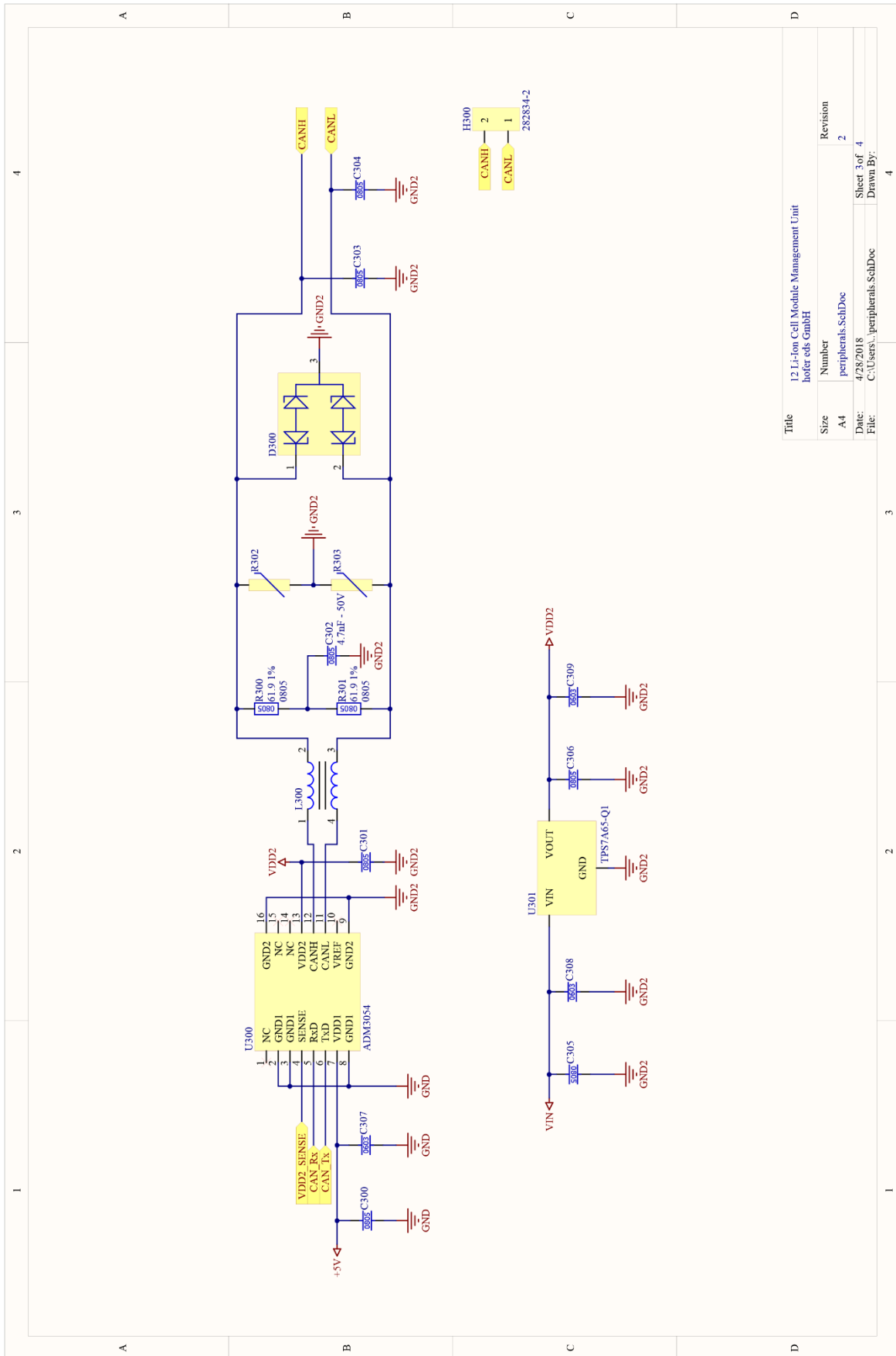
- [1] D. Linden and T. B. Reddy, *Handbook of Batteries*, 3rd Edition, McGraw - Hill, 1995.
- [2] Y. Wu, *Lithium-Ion Batteries: Fundamentals and Applications*, CRC Press , 2015.
- [3] J. M. B. Systems, *Our Guide to Batteries*, Johnson Matthey Battery Systems, 2015.
- [4] H. Budde-Meiwes, J. Muennix, J. Kowal and D. U. Sauer, "A review of current automotive battery technology and future prospects," *Proceedings of the Institution of Mechanical Engineers Part D*, no. 227, pp. 761-776, 2013.
- [5] A. Khaligh and Z. Li, "Battery, Ultracapacitor, Fuel Cell, and Hybrid Energy Storage Systems for Electric, Hybrid Electric, Fuel Cell, and Plug-In Hybrid Electric Vehicles: State of the Art," *IEEE Transactions on Vehicular Technology*, vol. 59, no. 6, pp. 2806 - 2814, 2010.
- [6] B. Scrosati, J. Garche and W. Tillmetz, *Advances in Battery Technologies for Electric Vehicles*, Woodhead Publishing, 2015.
- [7] J. Jiang and C. Zhang, *Fundamentals and Applications of Lithium-ion Batteries in Electric Drive Vehicles*, John Wiley & Sons, 2015.
- [8] W. C. Lee, D. Drury and P. Mellor, "Comparison of passive cell balancing and active cell balancing for automotive batteries," in *IEEE Vehicle Power and Propulsion Conference*, Chicago, 2011.
- [9] J. Douglas, "Battery management for high-power battery stacks," *CAN Newsletter*, pp. 34 - 38, 4 2010.
- [10] Linear Technology, *LTC6811-1/LTC6811-2 Multicell Battery Monitors*.
- [11] ST Microelectronics, *STM8AF526x/8x/Ax Automotive 8-bit MCU, with up to 128 Kbyte Flash, data EEPROM, 10-bit ADC, timers, LIN, CAN, USART, SPI, I2C, 3 to 5.5 V*.
- [12] Linear Technology, *LT8302, Micropower No-Opto Isolated Flyback Converter with 65V/3.6A Switch*.
- [13] Linear Technology, *LT3990/LT3990-3.3/LT3990-5 62V, 350mA Step-Down Regulator with 2.5uA Quiescent Current and Integrated Diodes*.
- [14] Analog Devices, *ADM3054 5 kV rms Signal Isolated High Speed CAN Transceiver with Bus Protection*.
- [15] T. Hubing, "PCB EMC design guidelines: a brief annotated list," in *IEEE Symposium on Electromagnetic Compatibility*, Boston, 2003.

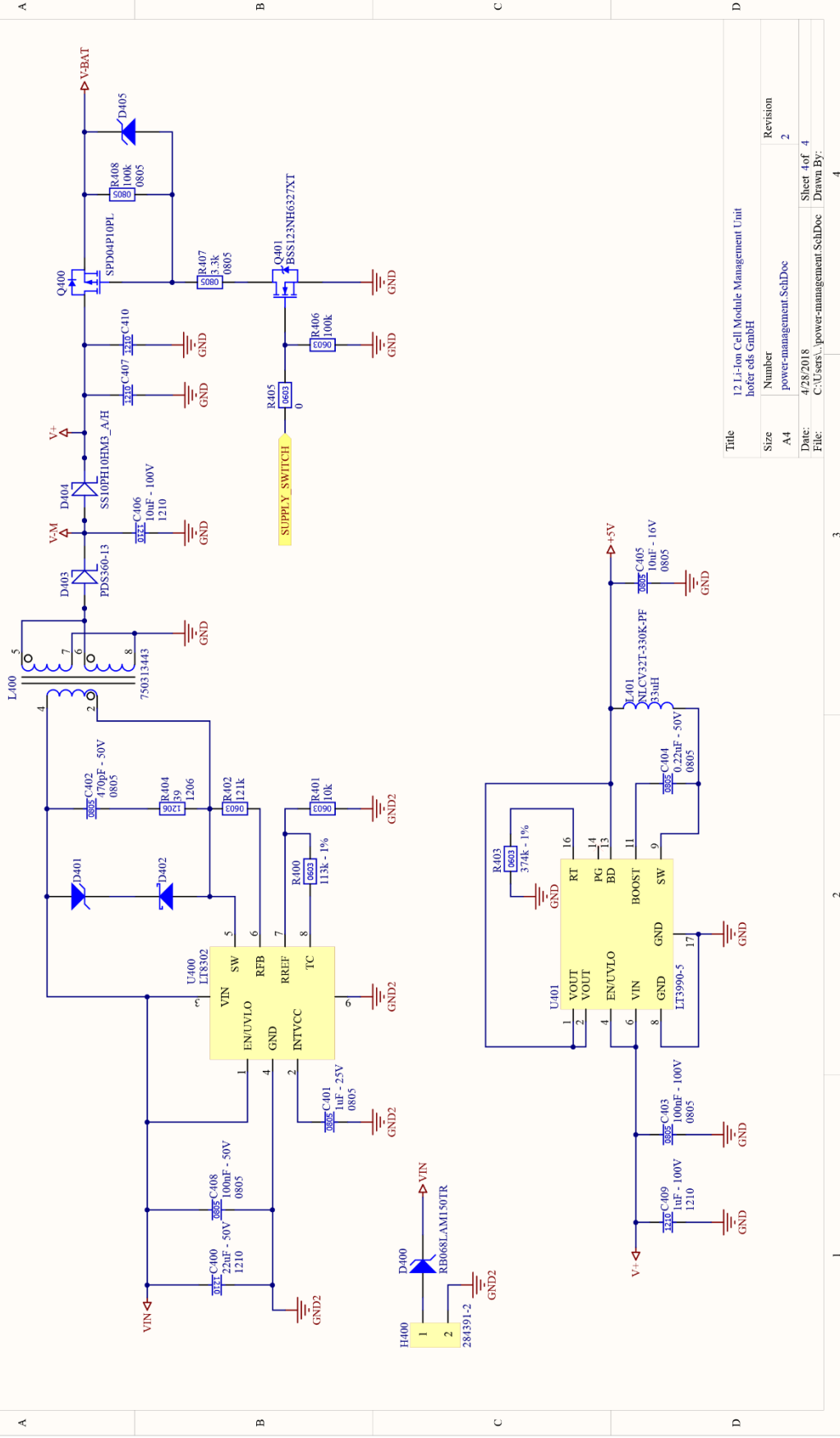
- [16] J. Warner, *The Handbook of Lithium-Ion Battery Pack Design, Chemistry, Components, Types and Terminology*, 1st Edition, Elsevier Science, 2015.
- [17] T. P. J. Crompton, *Battery Reference Book*, 3rd Edition, 2000: Newnes.
- [18] S. Dhameja, *Electric Vehicle Battery Systems*, Newnes, 2001.
- [19] A. Emadi, *Advanced Electric Drive Vehicles*, 2017: CRC Press.
- [20] J. Larminie and J. Lowry, *Electric Vehicle Technology Explained*, 2nd Edition, Wiley, 2012.
- [21] G. Pistoia, *Lithium-Ion Batteries: Advances and Applications*, Newnes, 2013.
- [22] P. Miller, "State of the art and future developments in lithium-ion battery packs for passenger car applications," *Johnson Matthey Technology Rev.*, vol. 1, no. 59, pp. 4-13, 2015.
- [23] M. Zheng, B. Qi and H. Wu, "A Li-ion battery management system based on CAN-bus for electric vehicle," in *3rd IEEE Conference on Industrial Electronics and Applications*, Singapore, 2008.
- [24] M. Brandl, H. Gall, M. Wenger, V. Lorentz, M. Giegerich and F. Baronti, "Batteries and battery management systems for electric vehicles," in *Design, Automation & Test in Europe Conference & Exhibition (DATE)*, Dresden, 2012.
- [25] H. Zhu, Z. Wu, W. Dalong and S. Jiayao, "Design and Implementation of Distributed Battery Management System," *Advanced Materials Research*, Vols. 608-609, pp. 1039-1042, 2012.
- [26] M. Hammer, U. Steininger, L. Wech and M. Lienkamp, "Development of Safe Energy Storage System for Small Electric Vehicles," in *COFAT*, Munich, 2014.
- [27] F. Baronti, G. Fantechi, E. Leonardi, R. Roncella and R. Saletti, "Hierarchical platform for monitoring, managing and charge balancing of LiPo batteries," in *IEEE Vehicle Power and Propulsion Conference*, Chicago, 2011.
- [28] L. Lua, X. Hana, J. Lia, J. Huab and M. Ouyang, "A review on the key issues for lithium-ion battery management in electric vehicles," *Journal of Power Sources*, vol. 226, pp. 272-288, 2013.
- [29] Z. Jiea, J. Sun and Y. Ma, "The System Architecture Design about Test Platform of Battery Management System," *Advanced Materials Research*, vol. 645, pp. 217-220, 2013.
- [30] M. Klein, "Viewing the Battery Management System from Many Lenses," in *2011 PHM Conference, Battery Management System Workshop*, Montreal, 2011.
- [31] M. Schneider, S. Ilgin and N. Jegenhorst, "Automotive battery monitoring by wireless cell sensors," in *IEEE International Instrumentation and Measurement Technology Conference Proceedings*, Graz, 2012.

- [32] F. V. Conte, "Battery and battery management for hybrid electric vehicles: A review," *e & i Elektrotechnik und Informationstechnik*, vol. 123, no. 10, pp. 424-431, 2006.
- [33] R.-E. Habiballah, O. Unnati, F. Baronti and M.-Y. Chow, "Battery Management System: An Overview of Its Application in the Smart Grid and Electric Vehicles," *IEEE Industrial Electronics Magazine*, vol. 7, no. 2, pp. 4 - 16, 2013.
- [34] R. Hu, "Battery Management System For Electric Vehicle Applications," University of Windsor, 2011.
- [35] B. M. B. d. Santos, "Battery Management System applied to Projecto FST's EV prototype," *Tecnico Lisboa*, 2014.
- [36] X. Chen, "Requirements and Concepts for Future Automotive Electronic Architectures from the view of Integrated Safety," *Universitat Karlsruhe*, 2008.
- [37] M. E. V. Team, "A Guide to Understanding Battery Specifications," 2008.
- [38] J. Munson, "How to structure a battery management system," *POWER Supplement*, 2011.
- [39] Intersil, *Implementing Inter-Module Communications in EV Battery Systems*, Intersil, 2015.
- [40] Linear Technology, "Maximizing Cell Monitoring Accurace and Data Integrity," *Power Electronics Europe*, pp. 25 - 28, 2016.
- [41] A. Νικόλαος, *Σχεδιασμός και κατασκευή Ενεργού Συστήματος Διαχείρισης Μπαταριών Ηλεκτρικού Οχήματος*, Θεσσαλονίκη: Αριστοτέλειο Πανεπιστήμιο Θεσσαλονίκης, 2016.

Appendix A Module Management Unit Schematics







Appendix B Microcontroller Software

main.c

```
1. /* Includes ----- */ #
2. include "stm8s.h"
3. define SECOND(7500 u) static uint8_t balance_type = 0;
4. static uint16_t current_time = 0;
5. void main(void) {
6.     CLK_init();
7.     GPIO_init();
8.     ADC2_init();
9.     SPI_init();
10.    ltc_init();
11.    TIM2_init();
12.    while (1) {
13.        current_time = TIM2_GetCounter();
14.        power_supply_monitor();
15.        if ((current_time % (SECOND / 100)) == 0) {
16.            ltc_monitor_cells();
17.        }
18.        if ((current_time % (SECOND / 10)) == 0) {
19.            cell_monitoring();
20.        }
21.        if ((current_time % (SECOND / 2)) == 0) {
22.            cell_management();
23.            measure_temperature();
24.        }
25.        if ((current_time % SECOND) == 0) {
26.            if (balance_type != 0) {
27.                GPIO_WriteHigh(GPIOE, GPIO_PIN_3);
28.            } else {
29.                GPIO_WriteLow(GPIOE, GPIO_PIN_3);
30.            }
31.            cell_balance();
32.            GPIO_WriteReverse(GPIOA, GPIO_PIN_3);
33.        }
34.    }
35. }
36. void CLK_init(void) {
37.     CLK_DeInit();
38.     CLK_HSECmd(DISABLE);
39.     CLK_HSICmd(DISABLE);
40.     CLK_HSICmd(ENABLE);
41.     while (CLK_GetFlagStatus(CLK_FLAG_HSIRDY) == FALSE);
42.     CLK_ClockSwitchCmd(ENABLE);
43.     CLK_HSIPrescalerConfig(CLK_PRESCALER_HSIDIV1);
44.     CLK_SYSCLKConfig(CLK_PRESCALER_CPUDIV1);
45.     CLK_ClockSwitchConfig(CLK_SWITCHMODE_AUTO, CLK_SOURCE_HSI, DISABLE, CLK_CURRENTCLOC
KSTATE_ENABLE);
46.     CLK_PeripheralClockConfig(CLK_PERIPHERAL_SPI, ENABLE);
47.     CLK_PeripheralClockConfig(CLK_PERIPHERAL_I2C, DISABLE);
48.     CLK_PeripheralClockConfig(CLK_PERIPHERAL_ADC, ENABLE);
49.     CLK_PeripheralClockConfig(CLK_PERIPHERAL_AWU, DISABLE);
50.     CLK_PeripheralClockConfig(CLK_PERIPHERAL_UART1, DISABLE);
51.     CLK_PeripheralClockConfig(CLK_PERIPHERAL_TIMER1, DISABLE);
52.     CLK_PeripheralClockConfig(CLK_PERIPHERAL_TIMER2, ENABLE);
53.     CLK_PeripheralClockConfig(CLK_PERIPHERAL_TIMER4, DISABLE);
54. }
55. void GPIO_init(void) { /* De-Initialize GPIO Ports */ }
```

```

56.     GPIO_DeInit(GPIOA);
57.     GPIO_DeInit(GPIOB);
58.     GPIO_DeInit(GPIOC);
59.     GPIO_DeInit(GPIOD);
60.     GPIO_DeInit(GPIOE); /* Initialize SS Pin */
61.     GPIO_Init(GPIOE, GPIO_PIN_5, GPIO_MODE_OUT_PP_HIGH_FAST); /* Initialize SCK-MISO-
MOSI Pins */
62.     GPIO_Init(GPIOC, GPIO_PIN_5, GPIO_MODE_OUT_PP_HIGH_FAST);
63.     GPIO_Init(GPIOC, GPIO_PIN_6, GPIO_MODE_OUT_PP_HIGH_FAST);
64.     GPIO_Init(GPIOC, GPIO_PIN_7, GPIO_MODE_OUT_PP_HIGH_FAST); /* Initialize ADC2 Channe
l Pins */
65.     GPIO_Init(GPIOB, GPIO_PIN_2, GPIO_MODE_IN_FL_NO_IT);
66.     GPIO_Init(GPIOB, GPIO_PIN_3, GPIO_MODE_IN_FL_NO_IT);
67.     GPIO_Init(GPIOB, GPIO_PIN_4, GPIO_MODE_IN_FL_NO_IT);
68.     GPIO_Init(GPIOB, GPIO_PIN_5, GPIO_MODE_IN_FL_NO_IT);
69.     GPIO_Init(GPIOB, GPIO_PIN_6, GPIO_MODE_IN_FL_NO_IT);
70.     GPIO_Init(GPIOB, GPIO_PIN_7, GPIO_MODE_IN_FL_NO_IT);
71.     GPIO_Init(GPIOB, GPIO_PIN_2, GPIO_MODE_IN_FL_NO_IT); /* Power Supply Switch Control
Signal */
72.     GPIO_Init(GPIOC, GPIO_PIN_1, GPIO_MODE_OUT_PP_LOW_FAST); /* Initialize Status LED *
/
73.     GPIO_Init(GPIOD, GPIO_PIN_3, GPIO_MODE_OUT_PP_LOW_FAST);
74.     GPIO_Init(GPIOA, GPIO_PIN_3, GPIO_MODE_OUT_PP_LOW_FAST);
75.     GPIO_Init(GPIOE, GPIO_PIN_3, GPIO_MODE_OUT_PP_LOW_FAST);
76. }
77. void SPI_init(void) { /* De-Initialize SPI Interface */
78.     SPI_DeInit(); /* Initialize SPI in Master mode */
79.     SPI_Init(SPI_FIRSTBIT_MSB, SPI_BAUDRATEPRESCALER_8, SPI_MODE_MASTER, SPI_CLOCKPOLAR
ITY_HIGH, SPI_CLOCKPHASE_2EDGE, SPI_DATADIRECTION_2LINES_FULLDUPLEX, SPI NSS_SOFT, (uint
t8_t) 0x07); /* Wait for Initialization */
80.     Delay(0xff); /* Enable the SPI*/
81.     SPI_Cmd(ENABLE);
82. }
83. void ADC2_init(void) {
84.     ADC2_DeInit();
85.     ADC2_Init(ADC2_CONVERSIONMODE_SINGLE, ADC2_CHANNEL_2, ADC2_PRESSEL_FCPU_D2, \ADC2_E
XTTRIG_TIM, DISABLE, ADC2_ALIGN_RIGHT, ADC2_SCHMITTTRIG_CHANNEL4, \DISABLE);
86.     ADC2_Cmd(ENABLE);
87. }
88. void TIM2_init(void) {
89.     TIM2_DeInit();
90.     TIM2_TimeBaseInit(TIM2_PRESCALER_2048, 15000);
91.     TIM2_Cmd(ENABLE);
92. }
93. uint8_t get_balance_type() {
94.     return balance_type;
95. }
96. void Delay(uint16_t nCount) { /* Decrement nCount value */
97.     while (nCount != 0) {
98.         nCount--;
99.     }
100.    }#
101.    ifdef USE_FULL_ASSERT
102.        /** * @brief Reports the name of the source file and the source line number *
where the assert_param error has occurred. * @param file: pointer to the source fil
e name * @param line: assert_param error line source number * @retval None */
103.        void assert_failed(uint8_t * file, uint32_t line) {
104.            /* User can add his own implementation to report the file name and line numb
er, ex: printf("Wrong parameters value: file %s on line %d\r\n", file, line) */
105.            /* Infinite loop */
106.            while (1) {}

```

```
107.      }#
108.      endif
```

bms_util.c

```
1. #
2. include "stm8s.h" /*----- Global Constants -----*/ /*
   - Cell Voltage Deviation Threshold Value -----*/ #
3. define BALANCE_THRESHOLD(50 u) /* Value in (100uV) */ /*
   - uController ADC Reference Voltage -----
   */ # define uC_ADC_REF_VOLTAGE(50000 u) /* Value in (100uV) */ /*
   - Temperature Sensor Resistor Divider Fixed Resistance Value -----
   */ # define BOARD_NTC_R_REF(10000 u) /* Value in (Ohm) */ /* Board Temperature Sensor
   Resistance LUT */ static
4. const uint16_t BOARD_NTC_LUT_RES[26] = {
5.     26444, 21493, 17586, 14481, 11998, 10000, 8355, 7004, 5891, 4972, 4211, 3579, 3053,
6.     2613, 2244, 1934, 1672, 1451, 1263, 1103, 966, 849, 748, 661, 586, 521
7. }; /* Board Temperature Sensor Temperature LUT */
8. static
9. const uint16_t BOARD_NTC_LUT_TEMP[26] = {
10.    0, 5, 10, 15, 20, 25, 30, 35, 40, 45, 50, 55, 60, 65, 70, 75, 80, 85, 90, 95, 100,
11.   105, 110, 115, 120, 125
12. };
13. static uint8_t ubal_time[CELL_NUMBER];
14. static uint8_t ubal_history[CELL_NUMBER];
15. static uint8_t ubal_time_par = 5;
16. static uint8_t power_supply_fail_counter = 0;
17. static uint8_t cell_uv_counter[CELL_NUMBER] = {
18.     0, 0, 0, 0, 0, 0, 0, 0, 0, 0, 0, 0
19. };
20. static uint8_t cell_ov_counter[CELL_NUMBER] = {
21.     0, 0, 0, 0, 0, 0, 0, 0, 0, 0, 0, 0
22. };
23. static uint8_t shut_down = 0;
24. static uint8_t sample_count = 1;
25. static uint8_t fail = 0;
26. static uint8_t cell_imbalance_counter[CELL_NUMBER] = {
27.     0, 0, 0, 0, 0, 0, 0, 0, 0, 0, 0, 0
28. };
29. static uint16_t cell_balance_counter[CELL_NUMBER] = {
30.     0, 0, 0, 0, 0, 0, 0, 0, 0, 0, 0, 0
31. };
32. static uint16_t cell_balance_flags;
33. static uint16_t ucell_uv;
34. static uint16_t ucell_ov;
35. static uint16_t ucell_min;
36. static uint16_t min_index;
37. static uint16_t board_temp[4];
38. static uint16_t mmu_temp[8];
39. static uint16_t celsius_temperature[4];
40. static uint16_t ucell_moving_average[CELL_NUMBER];
41. static uint32_t ucell_voltage_samples_sum[CELL_NUMBER];
42. /**
   * @brief Returns the current value of @param (cell_balance_flags). * @param Non
   * e * @retval (uint16_t) cell_balance_flags */
43. uint16_t get_balance_flags() {
44.     return cell_balance_flags;
45. }
46. /**
   * @brief Increments the value of @param (cell_balance_counter[index]) * @par
   * am (uint8_t) index, indicates the array element to be incremented * @retval None *
   */
```

```

45. void increment_balance_counter(uint8_t index) {
46.     cell_balance_counter[index]++;
47. }
48. /**
49.  * @brief Returns the current value of @param (board_temp[index]) * @param (uint8_t) index, indicates the array element to be returned * @retval (uint16_t) board_temp[index]
50. */
51. uint16_t get_board_temp(uint8_t index) {
52.     return board_temp[index];
53. }
54. /**
55.  * @brief Routine which triggers the cell voltage & status measurements * @param None * @retval None */
56. void ltc_monitor_cells() {
57.     ltc_measure_registers(CELL_VOLTAGE);
58.     Delay(0xffff);
59.     ltc_measure_registers(STATUS);
60.     Delay(0xffff);
61.     calculate_moving_average();
62. }
63. /**
64.  * @brief Routine which triggers the cell & board temperature measurements * @param None * @retval None */
65. void measure_temperature() {
66.     ltc_measure_registers(GPIO);
67.     Delay(0xffff);
68.     temp_adc_conversion();
69.     temperature_conversion();
70. }
71. /**
72.  * @brief Routine which monitors the power supply rail, and controls the power supply selection switch * @param None * @retval None */
73. void power_supply_monitor() {
74.     uint16_t supply_rail_ADC;
75.     uint16_t supply_rail;
76.     ADC2_Init(ADC2_CONVERSIONMODE_SINGLE, ADC2_CHANNEL_2, ADC2_PRESSEL_FCPU_D2, \ADC2_EXTTRIG_TIM, DISABLE, ADC2_ALIGN_RIGHT, ADC2_SCHMITTRIG_CHANNEL4, \DISABLE);
77.     ADC2_StartConversion();
78.     while (ADC2_GetFlagStatus() == RESET) {}
79.     supply_rail_ADC = ADC2_GetConversionValue();
80.     supply_rail = supply_rail_ADC * 5;
81.     if (supply_rail < 2700) {
82.         power_supply_fail_counter++;
83.     } else {
84.         power_supply_fail_counter = 0;
85.     }
86.     if (shut_down == 0) {
87.         if (power_supply_fail_counter > 3) {
88.             fail = 1;
89.         }
90.         if (supply_rail > 2700) {
91.             fail = 0;
92.         }
93.     } else {
94.         fail = 0;
95.     }
96.     if (fail == 1) {
97.         GPIO_WriteHigh(GPIOC, GPIO_PIN_1);
98.         GPIO_WriteHigh(GPIOD, GPIO_PIN_3);
99.     } else {
100.        GPIO_WriteLow(GPIOC, GPIO_PIN_1);
101.        GPIO_WriteLow(GPIOD, GPIO_PIN_3);
102.    }
103. }

```

```

99.    /** * @brief Routine which monitors the cell status flags and detects UV and OV c
 100.       onditions,           finds the cell with the minimum average voltage and detects cell
 101.       imbalances * @param None * @retval None */
 102.       void cell_monitoring() {
 103.           uint8_t cell_index;
 104.           uint16_t uv_registers;
 105.           uint16_t ov_registers;
 106.           UCELL_MIN = 50000;
 107.           min_index = 0;
 108.           uv_registers = get_uv_registers();
 109.           ov_registers = get_ov_registers();
 110.           for (cell_index = 0; cell_index < CELL_NUMBER; cell_index++) {
 111.               if ((uv_registers & (0x01 << cell_index)) != 0) {
 112.                   cell_uv_counter[cell_index]++;
 113.               } else {
 114.                   cell_uv_counter[cell_index] = 0;
 115.               }
 116.               if ((ov_registers & (0x01 << cell_index)) != 0) {
 117.                   cell_ov_counter[cell_index]++;
 118.               } else {
 119.                   cell_ov_counter[cell_index] = 0;
 120.               }
 121.               if (get_balance_flags() == 0) {
 122.                   for (cell_index = 0; cell_index < CELL_NUMBER; cell_index++) {
 123.                       if (ucell_moving_average[cell_index] < UCELL_MIN) {
 124.                           UCELL_MIN = ucell_moving_average[cell_index];
 125.                           min_index = cell_index;
 126.                       }
 127.                   for (cell_index = 0; cell_index < CELL_NUMBER; cell_index++) {
 128.                       if (cell_index != min_index) {
 129.                           if ((ucell_moving_average[cell_index] - UCELL_MIN) > BALANCE
 130.                               _THRESHOLD) {
 131.                               cell_imbalance_counter[cell_index]++;
 132.                           } else {
 133.                               cell_imbalance_counter[cell_index] = 0;
 134.                           }
 135.                       }
 136.                   }
 137.               }
 138.           /** * @brief Routine which sets the UV and OV flags, and controls the bal
 139.               ancing procedure           by setting/resetting the cell balance flags * @param None
 140.               * @retval None */
 141.           void cell_management() {
 142.               uint8_t cell_index;
 143.               uint8_t current_balance_type;
 144.               current_balance_type = get_balance_type();
 145.               for (cell_index = 0; cell_index < CELL_NUMBER; cell_index++) {
 146.                   if (cell_uv_counter[cell_index] > 30) {
 147.                       UCELL_UV |= (0x01 << cell_index);
 148.                       cell_balance_flags &= ~(0x01 << cell_index);
 149.                   } else {
 150.                       UCELL_UV &= ~(0x01 << cell_index);
 151.                   }
 152.                   if (cell_ov_counter[cell_index] > 30) {
 153.                       UCELL_OV |= (0x01 << cell_index);
 154.                   } else {
 155.                       UCELL_OV &= ~(0x01 << cell_index);
 156.                   }
 157.               }
 158.           }

```

```

155.         }
156.         switch (current_balance_type) {
157.             case 2:
158.                 {
159.                     if (get_balance_flags() == 0) {
160.                         for (cell_index = 0; cell_index < CELL_NUMBER; cell_index++)
161.                             x++);
162.                         if (cell_imbalance_counter[cell_index] > 50) {
163.                             UBAL_TIME[cell_index] = 1;
164.                         } else {
165.                             UBAL_TIME[cell_index] = 0;
166.                         }
167.                     }
168.                     for (cell_index = 0; cell_index < CELL_NUMBER; cell_index++)
169.                 {
170.                     if (UBAL_TIME[cell_index] > 0) {
171.                         if (UBAL_TIME[cell_index] <= UBAL_TIME_PAR) {
172.                             cell_balance_flags |= (0x01 << cell_index);
173.                             cell_imbalance_counter[cell_index] = 0;
174.                         } else if (UBAL_TIME[cell_index] == 0) {
175.                             cell_balance_flags &= ~(0x01 << cell_index);
176.                             cell_balance_counter[cell_index] = 0;
177.                         }
178.                         if (cell_balance_counter[cell_index] > (UBAL_TIME[cell_index] * MINUTES)) {
179.                             cell_balance_flags &= ~(0x01 << cell_index);
180.                             cell_balance_counter[cell_index] = 0;
181.                         }
182.                     }
183.                     break;
184.                 }
185.             case 1:
186.                 {
187.                     for (cell_index = 0; cell_index < CELL_NUMBER; cell_index++)
188.                     {
189.                         if (UBAL_TIME[cell_index] > 0) {
190.                             if (UBAL_TIME[cell_index] <= UBAL_TIME_PAR) {
191.                                 if (UBAL_TIME[cell_index] != UBAL_history[cell_index]) {
192.                                     cell_balance_flags |= (0x01 << cell_index);
193.                                 }
194.                                 if (cell_balance_counter[cell_index] > (UBAL_TIME[cell_index] * MINUTES)) {
195.                                     cell_balance_flags &= ~(0x01 << cell_index);
196.                                     cell_balance_counter[cell_index] = 0;
197.                                 }
198.                                 UBAL_history[cell_index] = UBAL_TIME[cell_index];
199.                             } else if (UBAL_TIME[cell_index] == 0) {
200.                                 cell_balance_flags &= ~(0x01 << cell_index);
201.                                 cell_balance_counter[cell_index] = 0;
202.                             }
203.                         }
204.                         break;
205.                     }
206.                 case 0:
207.                     {

```

```

208.             for (cell_index = 0; cell_index < CELL_NUMBER; cell_index++)
209.             {
210.                 cell_balance_flags &= ~(0x01 << cell_index);
211.                 cell_balance_counter[cell_index] = 0;
212.             }
213.         }
214.     }
215. }
216. /** * @brief Routine which performs ADC conversions for the board temperature sensor readings * @param None * @retval None */
217. void temp_adc_conversion() {
218.     uint8_t index;
219.     ADC2_Init(ADC2_CONVERSIONMODE_SINGLE, ADC2_CHANNEL_4, ADC2_PRESSEL_FCPU_D2, \ADC2_EXTTRIG_TIM, DISABLE, ADC2_ALIGN_RIGHT, ADC2_SCHMITTRIG_CHANNEL4, \DISABLE);
220.     while (ADC2_GetFlagStatus() == RESET) {}
221.     board_temp[0] = ADC2_GetConversionValue();
222.     ADC2_Init(ADC2_CONVERSIONMODE_SINGLE, ADC2_CHANNEL_5, ADC2_PRESSEL_FCPU_D2, \ADC2_EXTTRIG_TIM, DISABLE, ADC2_ALIGN_RIGHT, ADC2_SCHMITTRIG_CHANNEL4, \DISABLE);
223.     ADC2_StartConversion();
224.     while (ADC2_GetFlagStatus() == RESET) {}
225.     board_temp[1] = ADC2_GetConversionValue();
226.     ADC2_Init(ADC2_CONVERSIONMODE_SINGLE, ADC2_CHANNEL_6, ADC2_PRESSEL_FCPU_D2, \ADC2_EXTTRIG_TIM, DISABLE, ADC2_ALIGN_RIGHT, ADC2_SCHMITTRIG_CHANNEL4, \DISABLE);
227.     ADC2_StartConversion();
228.     while (ADC2_GetFlagStatus() == RESET) {}
229.     board_temp[2] = ADC2_GetConversionValue();
230.     ADC2_Init(ADC2_CONVERSIONMODE_SINGLE, ADC2_CHANNEL_7, ADC2_PRESSEL_FCPU_D2, \ADC2_EXTTRIG_TIM, DISABLE, ADC2_ALIGN_RIGHT, ADC2_SCHMITTRIG_CHANNEL4, \DISABLE);
231.     ADC2_StartConversion();
232.     while (ADC2_GetFlagStatus() == RESET) {}
233.     board_temp[3] = ADC2_GetConversionValue();
234. }
235. /** * @brief Routine which converts the board temperature sensor voltage readings to temperature values in degrees Celsius * @param None * @retval None */
236. void temperature_conversion() {
237.     uint8_t index;
238.     uint32_t temp_voltage;
239.     uint32_t voltage_divider_num;
240.     uint32_t voltage_divider_denom;
241.     uint16_t board_ntc_resistance[4];
242.     for (index = 0; index < 4; index++) {
243.         MMU_TEMP[index + 4] = get_uCellTemp(index);
244.         MMU_TEMP[index] = get_BOARD_TEMP(index);
245.     }
246.     for (index = 0; index < 4; index++) {
247.         temp_voltage = ((uint32_t)(MMU_TEMP[index]) * uC_ADC_REF_VOLTAGE);
248.         MMU_TEMP[index] = (uint16_t)(temp_voltage / (1023 u));
249.         voltage_divider_num = ((uint32_t)(MMU_TEMP[index]) * BOARD_NTC_R_REF);
250.         voltage_divider_denom = uC_ADC_REF_VOLTAGE - MMU_TEMP[index];
251.         board_ntc_resistance[index] = (uint16_t)(voltage_divider_num / voltage_divider_denom);
252.     }
253.     convert_resistance_to_temperature(board_ntc_resistance);
254. }

```

```

255.         /** * @brief Routine which translates the board temperature sensor
   resistance value to temperature using linear interpolation * @param None * @re
   tval None */
256.     void convert_resistance_to_temperature(uint16_t R_ntc[]) {
257.         uint8_t lut_index;
258.         uint8_t lut_row_index = 0;
259.         uint8_t ntc_index;
260.         uint16_t numerator;
261.         uint16_t denominator;
262.         for (ntc_index = 0; ntc_index < 4; ntc_index++) {
263.             for (lut_index = 0; lut_index < 26; lut_index++) {
264.                 if (BOARD_NTC_LUT_RES[lut_index] > R_ntc[ntc_index] && BOARD_NTC
   _LUT_RES[lut_index + 1] <= R_ntc[ntc_index]) {
265.                     lut_row_index = lut_index; /*save the found interpolation st
   art point and exit loop*/
266.                     break;
267.                 }
268.             }
269.             numerator = (BOARD_NTC_LUT_RES[lut_row_index] - R_ntc[ntc_index]);
270.             numerator = numerator * (BOARD_NTC_LUT_TEMP[lut_row_index + 1] - BOA
   RD_NTC_LUT_TEMP[lut_row_index]);
271.             denominator = BOARD_NTC_LUT_RES[lut_row_index] - BOARD_NTC_LUT_RES[1
   ut_row_index + 1];
272.             celsius_temperature[ntc_index] = (BOARD_NTC_LUT_TEMP[lut_row_index])
   + (numerator / denominator);
273.         }
274.     }
275.     /** * @brief Routine which calculates the moving average of the
   measured cell voltages every 10 data samples * @param None * @retval None */
276.     void calculate_moving_average(void) {
277.         uint8_t index;
278.         for (index = 0; index < 12; index++) {
279.             if (sample_count == 1) {
280.                 ucell_voltage_samples_sum[index] = get_uCell_data(index);
281.             } else {
282.                 ucell_voltage_samples_sum[index] = ucell_voltage_samples_sum[index]
   + (uint32_t)(get_uCell_data(index));
283.             }
284.         }
285.         sample_count++;
286.         if (sample_count == 11) {
287.             for (cell_index = 0; cell_index < CELL_NUMBER; cell_index++) {
288.                 ucell_moving_average[cell_index] = (uint16_t)(ucell_voltage_samples_
   sum[cell_index] / (sample_count - 1));
289.             }
290.             sample_count = 1;
291.         }
292.     }

```

cdd_ltc6811.c

```
1. #
2. include "cdd_ltc6811.h" /*----- Static Variables -----*/
3. static uint8_t cfgr_data[6];
4. static uint16_t adcv_cfg;
5. static uint16_t adaux_cfg;
6. static uint16_t adstat_cfg;
7. static uint16_t ucell[CELL_NUMBER];
8. static uint16_t ucell_temp[4];
9. static uint16_t ucell_uv_registers;
10. static uint16_t ucell_ov_registers;
11. static uint8_t command_data[12];
12. static uint8_t ltc_register_group[8];
13. static uint16_t gpio_voltage_adc[6];
14. static uint16_t status_voltage_adc[6];
15. static uint16_t calc_PEC;
16. static double UV_THRESHOLD = 3;
17. static double OV_THRESHOLD = 4.2; /*----- Static Constants -----*/
18. static
19. const uint16_t PEC_Table[16] = {
20.     0x0000, 0x4599, 0x4EAB, 0x0B32, 0x58CF, 0x1D56, 0x1664, 0x53FD, 0x7407, 0x319E, 0x3
    AAC, 0x7F35, 0x2CC8, 0x6951, 0x6263, 0x27FA
21. }; /*----- CFGR Default Values -----*/
22. struct LTC_CFGR_PARAMETERS cfgr_default = {
23.     REFON_ENABLED, DTEN_DISABLED, DEFAULT, PD_OFF, 0x0000, 0x0000, 0x0000, 0x00
24. }; /*----- LTC ADC Configuration Values -----*/
25. struct LTC_ADC_PARAMETERS adc_default = {
26.     NORMAL, DCP_ENABLED, ALL_CELLS, ALL_GPIO, ALL
27. };
28. struct LTC_CFGR_PARAMETERS cfgr_current = {
29.     REFON_ENABLED, DTEN_DISABLED, DEFAULT, PD_OFF, 0x0000, 0x0000, 0x0000, 0x00
30. };
31. /** * @brief Returns the current value of @param (ucell[index]). * @param (uint8_t)
    index, indicates the array element to be returned * @retval (uint16_t) ucell[index]
   */
32. uint16_t get_ucell_data(uint8_t index) {
33.     return ucell[index];
34. }
35. /** * @brief Returns the current value of @param (ucell_temp[index]). * @param
    (uint8_t) index, indicates the array element to be returned * @retval (uint16_t) ucell
   _temp[index] */
36. uint16_t get_ucell_temp(uint8_t index) {
37.     return ucell_temp[index];
38. }
39. /** * @brief Returns the current value of @param (ucell_uv_registers). * @param
    None * @retval (uint16_t) ucell_uv_registers */
40. uint16_t get_uv_registers() {
41.     return ucell_uv_registers;
42. }
43. /** * @brief Returns the current value of @param (ucell_ov_registers). * @param
    None * @retval (uint16_t) ucell_ov_registers */
44. uint16_t get_ov_registers() {
45.     return ucell_ov_registers;
46. }
47. /** * @brief Creates the ADC configuration data based on the given adc parameters
   . * @param (LTC_ADC_PARAMETERS) ADC_config - contains the configuration bits * @retv
   al None */
48. void ltc_adc_config(struct LTC_ADC_PARAMETERS ADC_config) {
49.     adcv_cfg = 0x0000 | (((uint16_t)(ADC_config.mode << 7)) | ((uint16_t)(ADC_config
    .dcp)) | ((uint16_t)(ADC_config.ch)));
```

```

50.     adaux_cfg = 0x0000 | ((uint16_t)(ADC_config.mode << 7) | ((uint16_t)(ADC_config
51.         .chg)));
52.     adstat_cfg = 0x0000 | ((uint16_t)(ADC_config.mode << 7) | ((uint16_t)(ADC_config
53.         .chst)));
54.     /**
55.      * @brief Creates the CFGR data based on the given parameters. * @param (LTC
56.      _CFGGR_PARAMETERS) cfgr_config - contains the configuration bits * @retval None */
57.     void ltc_cfgr_config(struct LTC_CFGGR_PARAMETERS cfgr_config) {
58.         cfgr_data[0] = (uint8_t) cfgr_config.adchopt + (uint8_t) cfgr_config.dten + (uin
59.             t8_t) cfgr_config.refon + (uint8_t) cfgr_config.gpiox;
60.         cfgr_data[1] = (uint8_t) cfgr_config.vuv;
61.         cfgr_data[2] = (uint8_t)(cfgr_config.vuv >> 8) | (uint8_t)(cfgr_config.vov << 4
62.             );
63.         cfgr_data[3] = (uint8_t)(cfgr_config.vov >> 4);
64.         cfgr_data[4] = (uint8_t)(cfgr_config.dcc);
65.         cfgr_data[5] = (uint8_t)(cfgr_config.dcc >> 8) | (uint8_t)(cfgr_config.dcto <<
66.             4);
67.     }
68.     /**
69.      * @brief Initializes the CFGR and ADC registers of the LTC6811 * @param Non
70.      e * @retval None */
71.     void ltc_init(void) {
72.         uint8_t cell_index;
73.         set_uv_threshold(UV_THRESHOLD);
74.         set_ov_threshold(OV_THRESHOLD);
75.         cfgr_current = cfgr_default;
76.         ltc_cfgr_config(cfgr_current);
77.         ltc_adc_config(adc_default);
78.         ltc_write_command(WRCFGA, cfgr_data);
79.         Delay(0xffff);
80.     }
81.     /**
82.      * @brief Controls the activation of the external balancing FETs * @param No
83.      ne * @retval None */
84.     void cell_balance() {
85.         uint8_t cell_index;
86.         uint16_t current_balance_flags;
87.         current_balance_flags = get_balance_flags();
88.         for (cell_index = 0; cell_index < 12; cell_index++) {
89.             if ((current_balance_flags & (0x01 << cell_index)) != 0) {
90.                 increment_balance_counter(cell_index);
91.             }
92.         }
93.         cfgr_current.DCC = current_balance_flags;
94.         ltc_cfgr_config(cfgr_current);
95.         ltc_write_command(WRCFGA, cfgr_data);
96.         Delay(0xffff);
97.     }
98.     /**
99.      * @brief Function that initiates the LTC6811 register group data read-
100.      out * @param (ADC_SELECT) adc_input - indicates which LTC6811 register group to be me
asured * @retval None */
101.    void ltc_measure_registers(ADC_SELECT adc_input) {
102.        switch (adc_input) {
103.            case CELL_VOLTAGE:
104.                {
105.                    ltc_cell_measure();
106.                    break;
107.                }
108.            case GPIO:
109.                {
110.                    ltc_gpio_measure();
111.                    break;
112.                }

```

```

101.         case STATUS:
102.             {
103.                 ltc_status_measure();
104.                 break;
105.             }
106.         }
107.     }
108.     /** * @brief Routine that initiates cell voltage ADC, reads out the cell v
   oltage registers           and decodes the cell voltage register data to actual cell v
   oltage values * @param None * @retval None */
109.     void ltc_cell_measure(void) {
110.         ltc_poll_command(PLADC);
111.         ltc_adc_command(ADCV, adcv_cfg);
112.         ltc_poll_command(PLADC);
113.         ltc_read_command(RDCVA, ltc_register_group);
114.         decode_register_data(ltc_register_group, ucell, A);
115.         ltc_read_command(RDCVB, ltc_register_group);
116.         decode_register_data(ltc_register_group, ucell, B);
117.         ltc_read_command(RDCVC, ltc_register_group);
118.         decode_register_data(ltc_register_group, ucell, C);
119.         ltc_read_command(RDCVD, ltc_register_group);
120.         decode_register_data(ltc_register_group, ucell, D);
121.     }
122.     /** * @brief Routine that initiates GPIO ADC, reads out the GPIO registers
   and decodes the GPIO register data to voltage measurements * @param None
   * @retval None */
123.     void ltc_gpio_measure(void) {
124.         ltc_poll_command(PLADC);
125.         ltc_adc_command(ADAX, adaux_cfg);
126.         ltc_poll_command(PLADC);
127.         ltc_read_command(RDAUXA, ltc_register_group);
128.         decode_register_data(ltc_register_group, gpio_voltage_adc, A);
129.         ltc_read_command(RDAUXB, ltc_register_group);
130.         decode_register_data(ltc_register_group, gpio_voltage_adc, B);
131.         memcpy(ucell_temp, gpio_voltage_adc + 1, 4 * sizeof(uint16_t));
132.     }
133.     /** * @brief Routine that initiates the LTC6811 status ADC, reads out the
   status registers           and decodes the status register data * @param None * @r
   etval None */
134.     void ltc_status_measure(void) {
135.         ltc_poll_command(PLADC);
136.         ltc_adc_command(ADSTAT, ADSTAT_CFG);
137.         ltc_poll_command(PLADC);
138.         ltc_read_command(RDSTATA, ltc_register_group);
139.         decode_register_data(ltc_register_group, status_voltage_adc, A);
140.         ltc_read_command(RDSTATB, ltc_register_group);
141.         decode_register_data(ltc_register_group, status_voltage_adc, B);
142.         decode_uv_ov_flags(status_voltage_adc);
143.     }
144.     /** * @brief Decodes the 16-bit adc voltage measurement data from the 8-
   bit LTC6811 registers * @param (uint8_t) register_data[]          - LTC6811 raw regi
   ster data           (uint16_t) adc_data[]           - 16-
   bit adc voltage measurement           (REGISTER_GROUP_ID) register_group - LTC6811 re
   gister group * @retval None */
145.     void decode_register_data(uint8_t register_data[], uint16_t adc_data[], REGISTER
   _GROUP_ID register_group) {
146.         uint8_t adc_index;
147.         uint8_t register_index;
148.         register_index = 0;
149.         for (adc_index = register_group; adc_index < register_group + 3; adc_ind
ex++) {

```

```

150.                 adc_data[adc_index] = (uint16_t)(register_data[register_index]) + ((  

151.                     uint16_t)(register_data[register_index + 1] << 8));  

152.                 register_index = register_index + 2;  

153.             }  

154.         /** * @brief Translates the decoded 16-  

   bit status register data and stores the          UV and OV flags in a single 16-  

   bit variable * @param (uint16_t) register_data[] - LTC6811 decoded status register d  

   ata * @retval None */  

155.     void decode_uv_ov_flags(uint16_t register_data[]) {  

156.         uint8_t status_register_flags[3];  

157.         uint8_t uv_flags[3];  

158.         uint8_t ov_flags[3];  

159.         int i;  

160.         status_register_flags[0] = (uint8_t)(register_data[4]);  

161.         status_register_flags[1] = (uint8_t)(register_data[4] >> 8);  

162.         status_register_flags[2] = (uint8_t)(register_data[5]);  

163.         for (i = 0; i < 3; i++) {  

164.             uv_flags[i] = 0x00 | (0x01 & status_register_flags[i]);  

165.             uv_flags[i] = uv_flags[i] | ((0x04 & status_register_flags[i]) >> 1)  

166. ;  

167.             uv_flags[i] = uv_flags[i] | ((0x10 & status_register_flags[i]) >> 2)  

168. ;  

169.             uv_flags[i] = uv_flags[i] | ((0x40 & status_register_flags[i]) >> 3)  

170.         }  

171.         ucell_uv_registers = (uint16_t)((uint8_t)(uv_flags[0] | (uv_flags[1] <<  

172.             4)) | ((uint16_t)(uv_flags[2] << 8)));  

173.         for (i = 0; i < 3; i++) {  

174.             ov_flags[i] = 0x00 | ((0x02 & status_register_flags[i]) >> 1);  

175.             ov_flags[i] = ov_flags[i] | ((0x08 & status_register_flags[i]) >> 2)  

176. ;  

177.             ov_flags[i] = ov_flags[i] | ((0x20 & status_register_flags[i]) >> 3)  

178. ;  

179.             ov_flags[i] = ov_flags[i] | ((0x80 & status_register_flags[i]) >> 4)  

180.         }  

181.         ucell_ov_registers = (uint16_t)((uint8_t)(ov_flags[0] | (ov_flags[1] <<  

182.             4)) | ((uint16_t)(ov_flags[2] << 8)));  

183.     }  

184.     /** * @brief Routine that forms the command that writes data on the LTC6811  

   registers * @param (LTC_CC) code - LTC6811 command code          (uint8_t)dat  

   a[] - data to be transferred to the LTC6811 * @retval None */  

185.     void ltc_write_command(LTC_CC code, uint8_t data[]) {  

186.         command_data[0] = (uint8_t)(code >> 8);  

187.         command_data[1] = (uint8_t)(code);  

188.         calc_PEC = calculate_PEC(command_data, 2);  

189.         command_data[2] = (uint8_t)(calc_PEC >> 8);  

190.         command_data[3] = (uint8_t)(calc_PEC);  

191.         memcpy(command_data + 4, data, spi_data_length);  

192.         calc_PEC = calculate_PEC(data, 6);  

193.         command_data[10] = (uint8_t)(calc_PEC >> 8);  

194.         command_data[11] = (uint8_t)(calc_PEC);  

195.         ltc_spi_write(command_data);  

196.     }  

197.     /** * @brief Routine that forms the command that reads data from the LTC6811  

   registers * @param (LTC_CC) code - LTC6811 command code          (uint8_t)rx_data[] - data read back from the LTC6811 registers * @retval None */  

198.     void ltc_read_command(LTC_CC code, uint8_t rx_data[]) {  

199.         command_data[0] = (uint8_t)(code >> 8);  

200.         command_data[1] = (uint8_t)(code);  


```

```

195.         calc_PEC = calculate_PEC(command_data, 2);
196.         command_data[2] = (uint8_t)(calc_PEC >> 8);
197.         command_data[3] = (uint8_t)(calc_PEC);
198.         ltc_spi_write_read(command_data, rx_data);
199.     }
200.     /** * @brief Routine that forms the command that triggers an ADC conversion on the LTC6811 * @param (LTC_CC) code - LTC6811 command code (uint16_t)config - ADC configuration bits * @retval None */
201.     void ltc_adc_command(LTC_CC code, uint16_t config) {
202.         code = (uint16_t)(code | config);
203.         command_data[0] = (uint8_t)(code >> 8);
204.         command_data[1] = (uint8_t)(code);
205.         calc_PEC = calculate_PEC(command_data, 2);
206.         command_data[2] = (uint8_t)(calc_PEC >> 8);
207.         command_data[3] = (uint8_t)(calc_PEC);
208.         ltc_spi_write(command_data);
209.     }
210.     /** * @brief Routine that forms the command that polls the LTC6811 ADC converter status * @param (LTC_CC) code - LTC6811 command code * @retval None */
211.     void ltc_poll_command(LTC_CC code) {
212.         command_data[0] = (uint8_t)(code >> 8);
213.         command_data[1] = (uint8_t)(code);
214.         calc_PEC = calculate_PEC(command_data, 2);
215.         command_data[2] = (uint8_t)(calc_PEC >> 8);
216.         command_data[3] = (uint8_t)(calc_PEC);
217.         ltc_spi_poll(command_data);
218.     }
219.     /** * @brief Function that calculates the UV threshold value to be written in the LTC6811 CFGR registers * @param (double) uv_threshold - UV threshold value in Volts * @retval None */
220.     void set_uv_threshold(double uv_threshold) {
221.         cfgr_default.VUV = (uint16_t)((uv_threshold - 0.0016) / 0.0016);
222.         cfgr_current.VUV = (uint16_t)((uv_threshold - 0.0016) / 0.0016);
223.     }
224.     /** * @brief Function that calculates the OV threshold value to be written in the LTC6811 CFGR registers * @param (double) ov_threshold - OV threshold value in Volts * @retval None */
225.     void set_ov_threshold(double ov_threshold) {
226.         cfgr_default.VOV = (uint16_t)(ov_threshold / 0.0016);
227.         cfgr_current.VOV = (uint16_t)(ov_threshold / 0.0016);
228.     }
229.     /** * @brief Function that calculates the PEC value for the input data * @param (uint8_t) data[] - Data Input (uint8_t) data_length - Data Input Length * @retval (uint16_t)(PEC<<1) - Calculated PEC value */
230.     uint16_t calculate_PEC(uint8_t data[], uint8_t data_length) {
231.         uint16_t PEC = 0x10;
232.         int i;
233.         for (i = 0; i < data_length; i++) {
234.             PEC = PEC ^ ((uint16_t) data[i] << 7); // Align and apply data byte
235.             PEC = (PEC << 4) ^ PEC_Table[(PEC >> 11) & 0xF]; // Apply CRC 4-bits at a time, 2 rounds
236.             PEC = (PEC << 4) ^ PEC_Table[(PEC >> 11) & 0xF];
237.         }
238.         return (PEC << 1);
239.     }

```

ltc_spi_com.c

```
1.  #
2.  include "cdd_ltc6811.h"
3.  /** * @brief Routine that writes data on the SPI bus * @param (uint8_t) spi_tx_
   data[] - Data to be transmitted * @retval None */
4. void ltc_spi_write(uint8_t spi_tx_data[]) {
5.     int Tx_Counter = 0;
6.     while (SPI_GetFlagStatus(SPI_FLAG_BSY) != RESET) {}
7.     GPIO_WriteLow(GPIOE, GPIO_PIN_5);
8.     while (Tx_Counter < SPI_DATA_LENGTH + 4) {
9.         while (SPI_GetFlagStatus(SPI_FLAG_TXE) == RESET) {}
10.        SPI_SendData(spi_tx_data[Tx_Counter]);
11.        Tx_Counter++;
12.    }
13.    while (SPI_GetFlagStatus(SPI_FLAG_BSY) != RESET) {}
14.    GPIO_WriteHigh(GPIOE, GPIO_PIN_5);
15. }
16. /** * @brief Routine that writes and reads data from the SPI bus * @param (uint
   8_t) spi_tx_data[] - Data to be transmitted (uint8_t) spi_rx_data[] - Data to
   be received * @retval None */
17. void ltc_spi_write_read(uint8_t spi_tx_data[], uint8_t spi_rx_data[]) {
18.     uint8_t spi_rx_bus_data[12];
19.     int Tx_Counter = 0;
20.     while (SPI_GetFlagStatus(SPI_FLAG_BSY) != RESET) {}
21.     GPIO_WriteLow(GPIOE, GPIO_PIN_5);
22.     while (SPI_GetFlagStatus(SPI_FLAG_TXE) == RESET) {}
23.     SPI_SendData(spi_tx_data[Tx_Counter]);
24.     Tx_Counter++;
25.     while (Tx_Counter < SPI_DATA_LENGTH + 3) {
26.         while (SPI_GetFlagStatus(SPI_FLAG_TXE) == RESET) {}
27.         if (Tx_Counter < 4) {
28.             SPI_SendData(spi_tx_data[Tx_Counter]);
29.         } else {
30.             SPI_SendData(0xFF);
31.         }
32.         while (SPI_GetFlagStatus(SPI_FLAG_RXNE) == RESET) {}
33.         spi_rx_bus_data[Tx_Counter - 1] = SPI_ReceiveData();
34.         Tx_Counter++;
35.     }
36.     while (SPI_GetFlagStatus(SPI_FLAG_RXNE) == RESET) {}
37.     spi_rx_bus_data[Tx_Counter - 1] = SPI_ReceiveData();
38.     while (SPI_GetFlagStatus(SPI_FLAG_BSY) != RESET) {}
39.     GPIO_WriteHigh(GPIOE, GPIO_PIN_5);
40.     memcpy(spi_rx_data, spi_rx_bus_data + 4, SPI_DATA_LENGTH * sizeof(uint8_t));
41. }
42. /** * @brief Routine that waits for the LTC6811 ADC end of conversion * @param
   (uint8_t) spi_tx_data[] - Data to be transmitted * @retval None */
43. void ltc_spi_poll(uint8_t spi_tx_data[]) {
44.     uint8_t spi_rx_poll_status;
45.     int Tx_Counter = 0;
46.     spi_rx_poll_status = 0x00;
47.     while (SPI_GetFlagStatus(SPI_FLAG_BSY) != RESET) {}
48.     GPIO_WriteLow(GPIOE, GPIO_PIN_5);
49.     while (SPI_GetFlagStatus(SPI_FLAG_TXE) == RESET) {}
50.     SPI_SendData(spi_tx_data[Tx_Counter]);
51.     Tx_Counter++;
52.     while (spi_rx_poll_status != 0xff) {
53.         while (SPI_GetFlagStatus(SPI_FLAG_TXE) == RESET) {}
54.         if (Tx_Counter < 4) {
55.             SPI_SendData(spi_tx_data[Tx_Counter]);
```

```
56.     } else {
57.         SPI_SendData(0xFF);
58.     }
59.     while (SPI_GetFlagStatus(SPI_FLAG_RXNE) == RESET) {}
60.     spi_rx_poll_status = SPI_ReceiveData();
61.     Tx_Counter++;
62. }
63. while (SPI_GetFlagStatus(SPI_FLAG_RXNE) == RESET) {}
64. spi_rx_poll_status = SPI_ReceiveData();
65. while (SPI_GetFlagStatus(SPI_FLAG_BSY) != RESET) {}
66. GPIO_WriteHigh(GPIOE, GPIO_PIN_5);
67. }
```